REPAIR OF IMPACT-DAMAGED PRESTRESSED CONCRETE BRIDGE GIRDER USING GLASS FRP REBAR

by

MARIA ANGELES DE LA FLOR MONTERO

Presented to the Faculty of the Graduate School of
The University of Texas at Arlington in Partial Fulfillment
of the Requirements
for the Degree of

MASTER OF SCIENCE IN CIVIL ENGINEERING

THE UNIVERSITY OF TEXAS AT ARLINGTON
December 2015

Copyright © by María Ángeles De La Flor Montero 2015

All Rights Reserved

Acknowledgements

I would like to extend my sincere and deepest gratitude to my advisor Dr. Nur Yazdani, for his guidance and constant support through the completion of my degree. I thank him for bearing with my faults and helping me to finish this research work. I am also honored to have had the opportunity to take his courses. He gives his classes with care and detail, allowing the distance students to follow the courses as if they were present.

I am grateful to Dr. Seyedali Abolmaali and Dr. Seyed Mohammad Razavi for readily accepting to serve in my thesis committee as well as for their extraordinary courses I had the honor to be enrolled in. Their courses have helped me to develop this investigation.

I am also thankful to the Civil and Environmental Engineering staff for helping me in every administrative step during the completion of my Degree at the University of Texas at Arlington.

I would like to express my gratitude to Trinity Infrastructure LLC for allowing me to conduct this research. Special thanks to Francisco David Berrocal Ruiz and Leonardo Le for their help and support. I would not have been able to develop this thesis without their help.

Additionally, I thank to my parents, my brothers and sister for their support, love and encouragement during all these years of study. Finally I am grateful to my loving husband, Francisco, for all his unconditional love during these years, for his support and patience during this research work.

August 11, 2015

Abstract

REPAIR OF IMPACT-DAMAGED PRESTRESSED

CONCRETE BRIDGE GIRDER USING

GLASS FRP REBAR

María Ángeles De La Flor Montero

The University of Texas at Arlington, 2015

Supervising Professor: Nur Yazdani

Overpass girders are risked by the impact of the traffic, over height vehicle, travelling under the structure, creating a hazard for the drivers over and under the bridge.

When a bridge girder is damaged the repair solution adopted has to meet the following criteria:

- Safety. The repaired structure has to provide a minimum level of service to guarantee the safety of the traffic during the life of the structure.
- Repair time: The repair time has to be minimized to limit risks and inconveniences for the traffic.
- Economy. The adopted solution has not only to fulfill the previous requirements, but also has to be the most economical.

Nowadays a lot of construction projects have to confront this kind of issue. The Lyndon B. Johnson (LBJ) Express construction project had to solve this problem. The LBJ project is located on I-635 and I-35 in North Dallas, Texas. The bridge number 54 of the LBJ project was hit by a truck, causing severe damage on one of its girders. The incident caused loss of concrete and exposed several strands. The solution adopted for the engineers was install fiber glass rebar and fill with repair mortar.

This study models the damaged girder before and after the repair to analyze its structural behavior. The data obtained by this model have been compared to the data obtained by the field test. The ABAQUS software has been used to model the girder.

The objectives of this study are provide a better understanding of the structural behavior and propose adequate modeling techniques of beams repaired with GFRP rebar. The proposed techniques will help to establish adequate repair procedures and to anticipate the structural behavior of damaged girders prior to the repair process

Table of Contents

List of Illustrations

List of Tables

Chapter 1

INTRODUCTION

1.1.- Introduction

Concrete bridge repair has been an issue to be confronted by engineers almost from the beginning of their activity. The damage suffered by the structure may have different origins. They may be due to fire, to a poor design or construction, the passage of time or just the impact of vehicles. The assessment of damage is important in deciding the most suitable repair system in every situation. The types of repair can range from making the in situ repair with minimal disruption or inconvenience to traffic until the demolition of all or part of the structure and its reconstruction.

One of the most common problems any structure has to face today is the impact caused by vehicles that exceed the clearance for which they are designed. The Lyndon B. Johnson (LBJ) Express construction project had to solve this problem. The bridge number 54 of the LBJ project was hit by a truck, causing severe damage on one of its girders. The incident caused loss of concrete and exposed several strands.

1.2.- Project Background

The LBJ Freeway is a partial loop of 37 miles (59.55 km) located in Dallas, Texas. It travels along the north Dallas area, starting southeast of the city at an intersection with I-20 and ending at its meeting with SH 121 at the north entrance to the Dallas-Fort Worth International Airport (Wikipedia, 2015).

In 2011 a remodeling of the highway in the stretch running between I-35 and US 75 began. This project will create a new section of tollway with four lanes each way. These four lanes added to the eight lanes of the freeway and the 3 lanes of the frontage road will confront the volume of traffic that flows through this segment daily.

Figure 1-1 LBJ Express Project Area

This is a major project approximately 13 miles (20.92 km) long, with a large number of bridges and overpasses where about 7000 beams will be used and with a deadline of less than 5 years. Because of these features the work schedule has been critical to meet the project deadline. One of the most important factors to meet this schedule has been traffic control since all the construction work has been developed diverting the traffic flowing through this area.

Keeping the traffic flowing caused the coexistence of new routes with old layout or temporary plot. It was during one of these phases of coexistence when the accident that damaged the structure number 54 occurred. The overpass had been completed while the lower trace was still the old route. This situation caused the structure to temporally have a lower clearance than the one it is finally design for and motivated the accident.

Bridge number 54 is located on Preston road over the LBJ express freeway in North Dallas. It is formed by 3 spans with different number of girder in each one. The

span number 1 is the southernmost of the structure and the northernmost is the span number 3. The girders used are prestressed with depressed strands. For spans 1 and 2 the girders are type "Tx46" girder and for span 3 are type "Tx28" girder.

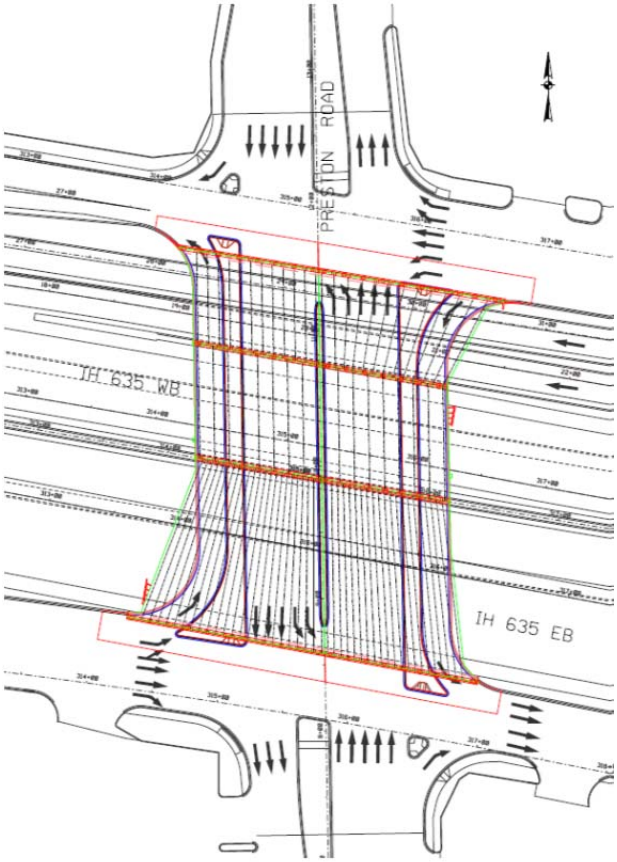

Figure 1-2 Preston Road Bridge, Bridge 54

The girder damaged by the truck was the last girder of the second span in the westbound direction. The impact caused damage along the bottom flange losing concrete and exposing several strands decreasing the strength of the beam.

Figure 1-3 Damaged Girder

The solution taken by the constructors consisted of the following steps:

- Remove the loss concrete,
- Chip the existing beam to provide a rough surface,
- Drill to place number 4 transverse and longitudinal fiberglass rebar,
- Apply bonding agent, and
- Fill with BASF LA40 repair mortar.

1.3.- Research Significance

Determining the most appropriate solution to perform the repair of prestressed elements is a complicated task that requires a comprehensive study.

Among the most used repair systems the repairs carried out using Fiber Reinforced Polymer (FRP) are the most common. These systems include benefits like cost efficiency, performance time and high section strengthening. The Glass Fiber

Reinforced Polymer (GFRP) system was adopted as a solution to repair the bridge number 54 of the LBJ Freeway.

The fact that they are increasingly common has increased the number of researches or studies on the use of these systems in bridge repair application. However, most of these researches investigate the behavior of a particular FRP system: the Carbon Fiber Reinforced Polymer (CFRP).

Chapter 2 of this thesis, literature review, includes an analysis of the studies found related to the use of FRP systems and its application to bridge repair. Although most of them are focused on the use of CFRP, the number of investigations about the use of GFRP systems has increased in the last years.

These investigations are focused mainly in the use of GFRP for bridge deck reinforcement and in the durability of GFRP systems. The topics studied in these researches are varied and include the application of GFRP not only to bridge repair but also to strengthen other sections such as square columns or railroad crossties.

The number of studies related to the use of GFRP for bridge girder repair is low. Therefore this thesis is important since it studies a use of GFRP less investigated. This research work establishes a finite element model to analyze the behavior of a prestressed concrete beam repaired with GFRP. This analysis is conducted by using a finite element program, ABAQUS, to later compare the results with the data from the field test.

Most of the researches described in Chapter 2 obtain the results based on scale models or imposing a given type of impact. In this case the damaged beam is part of a real structure in service, it is not an isolated element, hit by a truck causing a particular structural damage. This is another reason that makes this thesis necessary since none of the researches found represents the actual structural behavior of the girder.

1.4.- Objective Of The Study

The main objective of this research is to provide a better understanding of modeling the behavior of beams repaired with GFRP rebar. To achieve this objective, the girder has been modeled before and after the repair.

The tasks to be completed are:

- Modeling by finite element software the girder at each phase.
- Analyze the results obtained by the theoretical model and compare them to the field test data.
- Establish conclusions about the relationship between the actual behavior of beams repaired with GFRP and the theoretical behavior.

1.5.- Thesis Organization

This thesis has been organized as follows:

Chapter 1 describes general aspects of the thesis as well as the need for this study.

Chapter 2 reviews the literature and references available. It provides a description of the regulations and guidelines that can be found for bridge repair. It also defines and describes the different types of FRP systems. Finally it includes the studies and researches related to FRP systems that have been found and the software that will be used to perform this thesis.

Chapter 3 includes the description of the original girder, the description of the damage, and the description of the repair solution adopted by the company.

Chapter 4 describes the results of the tests carried out in the field. It shows the strains measured by the strain gauges during the two phases of the field test.

Chapter 5 explains the 3D model generated using ABAQUS. It includes all the data needed to model the two phases of the field test.

Chapter 6 exhibits the results obtained from ABAQUS. It compares these results with the field test data summarized in Chapter 4.

Chapter 7 establishes the study's conclusions based on Chapter 6.

Appendix A provides the bridge drawings.

Appendix B includes the tables of the strain measured in the field test.

Finally, at the end of this research work it is included a list of references used to develop this thesis.

Chapter 2

LITERATURE REVIEW

This literature review is divided in four parts. The first part consist of the review of the last normative and guidelines that can be used for repairing prestressed concrete girders. The second part defines and describes the types of Fiber Reinforced Polymer (FRP) systems. The third part analyzes numerous thesis, studies and dissertations that have been published during the last years. Finally the fourth part describes the finite element software that is used for the development of this thesis.

2.1.- Normative And Guidelines For Repair Prestressed Concrete Girders

The normative and guidelines for bridges repair found are listed below:

- AASHTO LRFD Bridge Design Specifications (AASHTO, 2012), including the "Guide Specifications for Design of Bonded FRP System for Repair and Strengthening of Concrete Bridge Elements."
- NCHRP REPORT 654, "Evaluation and Repair Procedures for Precast/Prestressed Concrete Girders with Longitudinal Cracking in the Web," (Tadros, Badie, & Tuan, 2010).
- NCHRP REPORT 655, "Recommended Guide Specification for the Design of Externally Bonded FRP Systems for Repair and Strengthening of Concrete Bridge Elements," (Zureick, Ellingwood, Nowak, Mertz, & Triantafillou, 2010).
- NCHRP 20-07/task 307, "Updated Research for Collision Damage and Repair of Prestressed Concrete Beams," (Harries, Kasan, Miller, & Brinkman, 2012).

The Guide Specifications for Design of Bonded FRP Systems supplements the AASHTO LRFD Bridge Design Specifications. According to AASHTO, (2012)

> "These guide specifications are intended for the repair and strengthening of reinforced and pre-stressed highway bridge structures using externally bonded fiber-reinforced polymer (FRP) composite systems."

The objective of the NCHRP REPORT 654 is to establish a guide to help the technical team to decide whether to accept, fix or remove the girder with longitudinal web cracking. This manual also includes criteria for acceptance of materials and repair methods for beams with end zone cracking. Depending on the crack width the guide recommends different types of repair systems. Table 2-1 summarizes the four criteria set:

Table 2-1 NCHRP REPORT 654 Criterion (Tadros, Badie, & Tuan, 2010)

CRITERION	CRACK WIDTH, in (mm)	RECOMMENDED SOLUTION
FIRST	0 - 0.012 (0 - 0.3)	Not Repair
SECOND	0.012 - 0.025 (0.3 - 0.06)	Cracks be filled with a cementitious packing material and then covered with a water resistant surface sealant.
THIRD	0.025 - 0.050 (0.06 - 0.13)	Epoxy injection for cracks wider than 0.025 in (0.06 mm) and cementitious packing material for cracks narrower than 0.025 in (0.06 mm)
FOURTH	Greater than 0.050 (0.13)	Rejection unless it can be shown by detailed analysis that structural capacity and long term durability are not compromised

The lack of specifications nationally recognized for the use of externally bonded FRP systems has hindered the use of these systems for the repair and strengthening of bridges. The NCHRP REPORT 655 has as a goal to establish specifications that help the engineer to use these systems for the repair and strengthening of prestressed or

reinforced concrete structures. This report includes the use of thermoset polymers reinforced by carbon, glass or aramid fibers. In addition to six illustrative examples the guide provides the formulation needed to calculate bending, shear, axial, torsion and their combinations.

Finally the NCHRP 20-07/task 307 is not an official publication of the National Cooperative Highway Research Program (NCHRP). However it was prepared as part of NCHRP Project 20-07, task 307 (Harries, Kasan, Miller, & Brinkman, 2012). This report aims to establish a foundation to help engineers in the repair of prestressed beams providing the necessary criteria to decide whether to repair in situ or remove the damaged item. This guide updates de NCHRP REPORT 280, 1985. Nine repair techniques are described including the following:

- Externally Bonded Carbon Fiber Reinforced Polymer (EB-CFRP)
- Externally Bonded Post-Tensioned Carbon Fiber Reinforced Polymer (bPT-CFRP)
- Post-Tensioned Steel (PT-steel)
- Internal Strand Splicing

Based on the loss of strands Table 2-2 is set to provide a guide for classifying the prestressed concrete girder damage.

Table 2 -2 Damage Classification for Prestressed Concrete Girders (Harries, Kasan, Miller, & Brinkman, 2012)

		Strand loss	Camber
MINOR	Concrete with shallow spalls, nicks and cracks, scrapes and some efflorescence, rust or water stains. Damage does not affect member capacity. Repairs are for aesthetic and preventative purpose only (NCHRP 280)	No exposed strands.	No effect of girder camber.
MODERATE	Larger cracks and sufficient spalling or loss of concrete to expose strands. Damage does not affect member capacity. Repairs are intended to prevent further deterioration (NCHRP 280)	Exposed strands. No severed strands.	No effect of girder camber.
SEVERE I	Damage affects member capacity but may not be critical - being sufficiently minor or not located at a critical section along the span [2.5]. Repairs to prevent further deterioration are warranted although structural repair is typically not required.	Less than 5% strand loss.	Partial loss of camber.
SEVERE II	Damage requires structural repair that can be affected using a non-prestressed/post-tensioned method. This may be considered as repair to affect the STRENGTH (or ultimate) limit state.	Strand loss greater than 5%.	Complete loss of camber.
SEVERE III	Decompression of the tensile soffit has resulted [2.6.1.2]. Damage requires structural repair involving replacement of prestressing force through new prestress or port-tensioning. This may be considered as repair to affect the SERVICE limit state in addition to the STRENGTH limit state.	Strand loss exceeding 20%. In longer and heavily loaded sections, decompression may not occur until close to 30% strand loss.	Vertical deflection less than 0.5%.
SEVERE IV	Damage is too extensive. Repair is not practical and the element must be replaced.	Strand loss greater than 35%.	Vertical deflection greater than 0.5%.

Once the type of damage has been defined the manual provides several flow charts based on the type of damage and beams with the solution that can be taken.

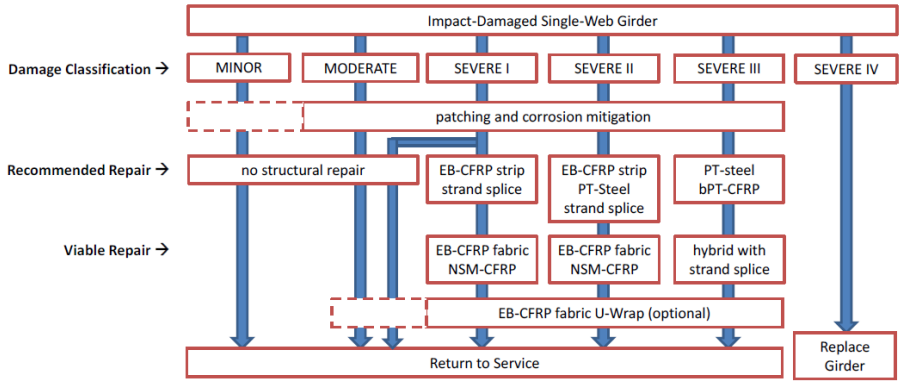

Figure 2-1 Repair Selection Flow Chart For Prestressed Concrete Single-Web Girders (Harries, Kasan, Miller, & Brinkman, 2012)

Therefore the AASHTO 2012 along with the different NCHRP reports form a good basis for carrying out the repair of damaged structures.

2.2.- Fiber Reinforced Polymers (FRP)

Two are the main components of Fiber Reinforced Polymer (FRP): polymers and fibers. Masuelli (2013, p. 3) defines FRP as

> "Fiber-reinforced polymer (FRP), also Fiber-reinforced plastic, is a composite material made of a polymer matrix reinforced with fibers."

The polymers used are vinylester or polyester thermosetting plastic, epoxy and phenol formaldehyde resins. Among the most common fibers are glass, carbon, aramid and basalt (Masuelli, 2013).

FRP reinforcements are easy to install, lightweighted and exhibit high tensile strength, which facilitates handling and accelerates the construction or repair. Other advantages of their use are their good long-term performance and low cost (Zureick, Ellingwood, Nowak, Mertz, & Triantafillou, 2010). These characteristics have made the use of FRP systems more common in civil engineering.

However there are also disadvantages to consider when these systems are used. They have brittle failure, poor shear resistance, poor resistance to fire and high temperatures, loose strength upon bending and they are susceptible to stress-rupture effects (Masuelli, 2013).

Because the fibers take a largest amount of volume and they resist the greater proportion of the load, the fibers are the main component on a fiber reinforced composite material. For this reason it is important to make a proper selection of the type of fiber, fiber length, volume occupied inside the compound and fiber orientation (Mallick, 2008).

Nanni, Luca, & Zadeh (2014) describe the types of fibers more common as follows:

- Carbon. It exhibits modulus and strength three times higher than glass fiber and also it is ten times more expansive. The type of carbon fiber more used in civil engineering is the carbon fiber made from polyacrylonitrile (PAN). PAN-based carbon fiber is characterized by high modulus and high strength. Other kind of carbon fiber that can be found are the carbon fiber made from rayon, used to generate low modulus carbon fiber, and pitch, it has higher modulus than PAN but lower strength.

Figure 2-2 Carbon Fiber Rebar

- Glass. It has good thermal and electrical insulation properties. The main types of glass fiber are three:
    - Electrical (E-glass). It has high mechanical properties, low predisposition to moisture and high electrical insulating properties.
    - Alkali-Resistance (AR-glass). It resists very well the alkali attack.

- High- Strength (S-glass). It is more expensive than E- glass making it less preferable despite it has a higher modulus and tensile strength.

Figure 2-3 Glass Fiber Rebar

- Aramid. It offers high toughness, high impact resistance and good mechanical properties at low density. The most common type of aramid fiber is Kevlar. It is resistant to lubricants, fuels and organic solvents. Its high price limits its use.

Figure 2-4 Aramid Fiber Composite Rebar

- Basalt. It has high elastic modulus and high biosolubility. Basalt fiber is slightly stronger than E-glass, but from an environmental point of view is safer since it is a non-magnetic, non-corrosive and non-toxic material. Also it has very good insulating characteristics and high-heat stability.

Figure 2-5 Basalt Composite Rebar

2.3.- FRP Researches

Nowadays a large number of thesis, dissertations or articles about bridge repair can be found. These studies investigate the structural behavior and the advantages or disadvantages of a particular bridge repair system, including the use of FRP.

Between the types of FRP systems used for construction the most common is the CFRP. The CFRP investigations that have been developed are not only large in number but also they are varied. The topics vary from establishing recommendations for bridge repair using CFRP to studying the strengthening of prestressed concrete girder with CFRP.

Another type of FRP that is used for repair is the GFRP. GFRP is used especially for bridge decks due to its good durability and corrosion properties. Although the number of investigations about the use of GFRP to repair bridge girder is low in recent years the number of investigations about other uses of GFRP has increased. These investigations have focused not only in the use of GFRP in bridge deck but also they studied its application in other structural members.

2.3.1.- CFRP Researches

Some of the CFRP researches develop design guidelines and recommendations in order to carry out the repair of the elements damaged either by vehicle impact or not.

Hutchinson (1999) demonstrates how the use of externally bonded CFRP sheets is an effective solution for improving the shear strength of prestressed concrete I-girders. With the information obtained this dissertation establishes recommendations and guidance for using CFRP sheets.

Pantelides, Reaveley, & Burningham (2010) provide a guide repair of bridge girders using FRP. The girders considered in this study are either reinforced or

prestressed concrete girders suffering from shear o flexural strength deficiencies related to end cracking or to vehicular collision.

Hasenlamp, Badie, Hanna, & Tadros (2012) establish criteria for repair materials and methods for prestressed concrete girders with end zone cracking caused by prestress release.

Rosenboom, Miller, & Rizkalla (n.d.) come through with a shear design model that describes precisely the shear behavior of a section repaired with CFRP.

Not all studies on CFRP set guidelines to follow, but most of them provide conclusions that help future bridge repairs.

Cha (2001) demonstrates how the use of carbon fiber composites strengthened the prestressed concrete beams up to 86% for high-strength concrete and 58% for normal strength concrete. Therefore the greatest increases in strength are obtained for high-strength concrete.

Klaiber, Wipf, & Kempers (2003) based on the laboratory and field tests, they infer that the use of CFRP for repair prestressed concrete girder is feasible when about 15% of the strands are severed.

Green & Boyd (2005) conclude that the CFRP systems can restore up to 90% of the moment capacity loss after a vehicle impact.

Kasan (2012) shows that the prestress structure redevelops the same strength once it has been repaired with CFRP.

Brinkman (2012) studied which of the different types of CFRP is better. He made the comparison between three systems: near surface mounted (NSM), externally bonded (EB), and bonded post-tensioned (BPT). The last system was the most effective restoring the lost capacity.

Many of these researches have been conducted in laboratory using scale elements with a simulated damage to perform better investigations on possible repair solutions. Rosenboom and Kasan are two researchers who have used scale elements.

Rosenboom (2006) tested thirty full-scale prestressed concrete bridge girders, twenty one of them were C-Channels girders. These girders were retrofitted with FRP materials. This dissertation examines not only the repair and strengthening of prestressed girders with FRP materials from an engineering point of view, but also the bond behavior and its relationship with FRP.

Kasan (2009) investigated with twenty two prototype prestressed concrete bridge girders, including spread boxes (SB), AASHTO type I girders (IB), and adjacent boxes (AB), varying degree of damage and CFRP repair techniques. It was concluded that when 25% or more of the strands in a girder no longer contribute to its capacity the best option is to replace it.

Other researchers like Bullock, Barnes, & Schindler (2011) base their results not only in tests performed in the laboratory but also in field investigations. They analyzed the effectiveness of the use of FRP as repair system on the I-565 in Huntsville, Alabama. The structure showed wide cracks as a result of thermal deformations and inadequate reinforcement details. They concluded that the FRP system used was an effective repair solution.

2.3.2.- GFRP Researches

Most of the studies about the use of FRP systems in civil engineering are about the use of CFRP. However, lately the number of investigations about using GFRP has increased.

Two advantages of the use of glass fiber reinforced polymers are their corrosive resistance and their durability.

Abushagur (2004) found that the use of glass fiber reinforced polymer not only creates a corrosion protective layer for steel structures but also improves the flexural capacity of steel sections.

Ragaby (2007), Liu (2011), and Besser (2011) are three authors that investigated about the use of GFRP bars as reinforcement. For Ragaby the use of fiber reinforced polymer as reinforcement for bridge deck slabs is a good solution to the corrosion problems suffered by bridge deck slabs. He studied the fatigue behavior and fatigue life of concrete bridge decks slabs reinforced with glass FRP bars. His results showed that the concrete bridge deck slabs reinforced with glass FRP bars had superior fatigue performance and longer fatigue life.

Huang (2010) and Yan (2005) focused their investigations on the durability of the GFRP. Huang had as objective to achieve a better understanding of the durability behavior and degradation mechanism of GFRP bars in concrete environments. He developed more accurate environmental reduction factors that those given by the design codes. Yan investigated the durability of glass fiber composites as bridge deck reinforcement subject to weathering conditions.

The GFRP has a varied use. It can be used to strengthen railroad crossties, to improve the flexural capacity of steel sections or to repair columns.

Laosiriphong (2000) found that the use of glass fiber reinforced composites wraps increased the durability of railroad crossties. He tested half scale wooden crossties wrapped with GFRC. The glass fiber reinforcement enhanced the flexural rigidity by 44 percent and the shear modulus by 18 percent. Therefore he concluded that railroad crossties are strengthened by wrapping them with GFRPC.

Memon (2002) investigated the use of GFRP sheets to repair square columns. The columns tested were under simulated earthquake loads. The study concludes that the use of GFR sheets can significantly enhance ductility, energy dissipation ability, and moment capacity of deficient square columns.

Smith (2004) investigated the rehabilitation of timber railroad bridges using GFR composite materials. He tested four full scale timber stringers. Two of them were tested to failure in bending and then were repaired with GFRP composite wraps. The other two specimens were tested to failure in shear. He found that all specimens showed significant signs of strength regain. He concluded that the use of GFRP composite materials in the repair, allowed the recovery of 55%-60% of initial strength. Therefore the use of GFRP composite materials for rehabilitation of timber railroad bridges provides a quick and easy to install alternative.

Mahmood (2002) compared the cracking of concrete members reinforced either with Glass FRP or steel. He concluded that there is no difference between the cracks width when using steel or GFRP.

Johnson (2014) conducted an experimental program with twenty four large scale beams reinforced with different types of Glass FRP bars. The study concludes that the bent bar GFRP stirrups tested exhibit acceptable thermal and mechanical properties.

2.4.- Finite Element Modeling

In order to carry out the necessary calculations to study the behavior of damaged items, it is often used the Finite Element Method (FEM). To facilitate this analysis there are different software available to help in the modeling of these elements.

Much of the research mentioned above used this kind of software. Ragaby (2007) used the software ANACAP to model bridge deck slabs. Brinkman (2012) used

XTRACT to obtain the flexural capacity of prestressed I-girders. The software ANSYS can be used to accurately predict the crack patterns and failure modes of FRP strengthened girders (Haque, 2014).

The software used for the development of this thesis is ABAQUS. ABAQUS was created in the late seventies by David Hibbit, Bengt Karlsson, and P. Sorensen. The software is highly sophisticated and allows modelling the behavior of structures under external loads.

One of the advantages of using ABAQUS is that it has an extensive library of materials, including the elastic and elastic-plastic solids, and elements, such as beams or plates. Its most important capabilities or abilities are:

- Analysis of static and dynamic problems.
- Contact between solids modelling.
- Model changes in shape of solids.
- Model phenomena such as buckling or vibrations.

The use of this program will help to obtain a model that reflects the behavior of the prestressed girders before and after the repair.

Chapter 3

CASE DESCRIPTION

This Chapter describes the main characteristics of the problem studied in this thesis. The chapter is divided into three parts. The first part describes the girder damaged by the truck and the bridge where it is located. The second part is the damage description; it includes a description of the area damaged. The last part explains the solution adopted by the company to repair the girder.

3.1.- Girder Description

Bridge number 54 is located on Preston road over the LBJ express freeway. The bridge consists of two different structures, the northbound and the southbound structures.

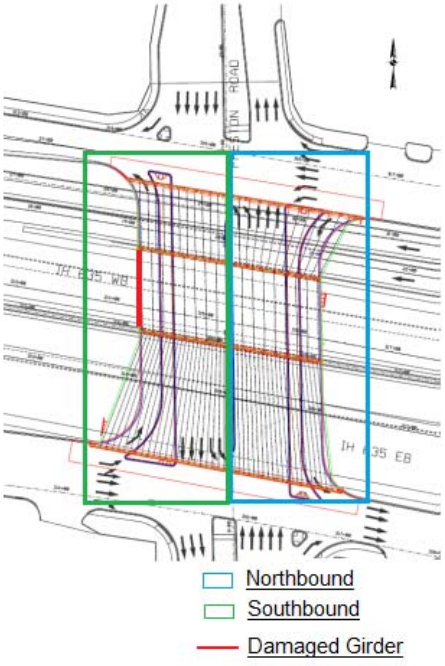

Figure 3-1 Bridge 54 Layout

Both structures have 3 spans with different number of girder in each one. The types of girder used for both structures are prestressed concrete I girders type Tx46 and Tx28.

The southbound structure is formed by 23 prestressed I-girders type Tx46 in the span 1, by 9 prestressed I-girders type Tx46 in the span 2 and 11 prestressed I-girders type Tx28 in the span 3. Figure 3-2 shows the position and the number of the girders according to the drawings.

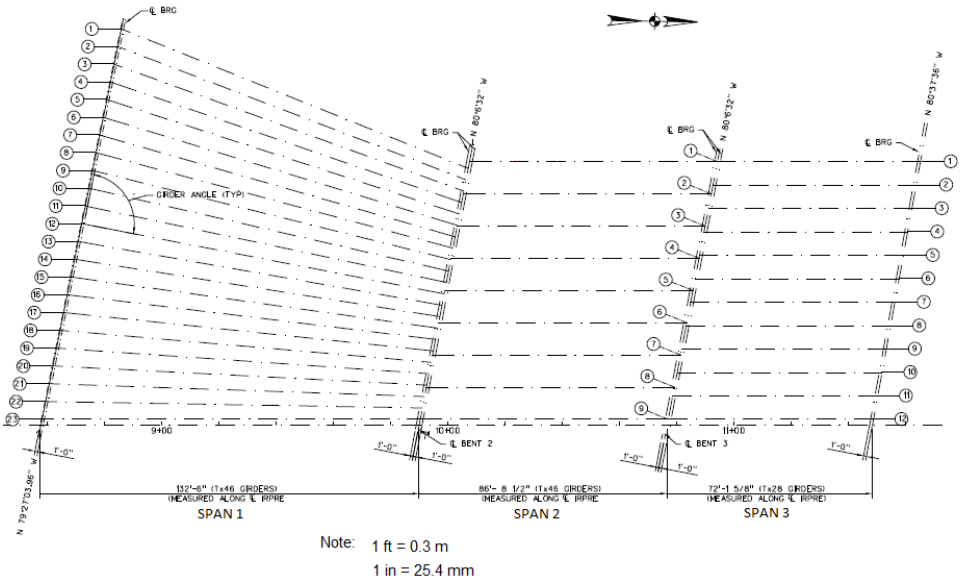

Figure 3-2 Preston Road Southbound Girder Layout

Similarly the northbound structure is formed by 21 prestressed I-girders type Tx46 in the span 1, 9 prestressed I-girders type Tx46 in the span 2 and 13 prestressed I-girders type Tx28 in the span 3, Figure 3-3.

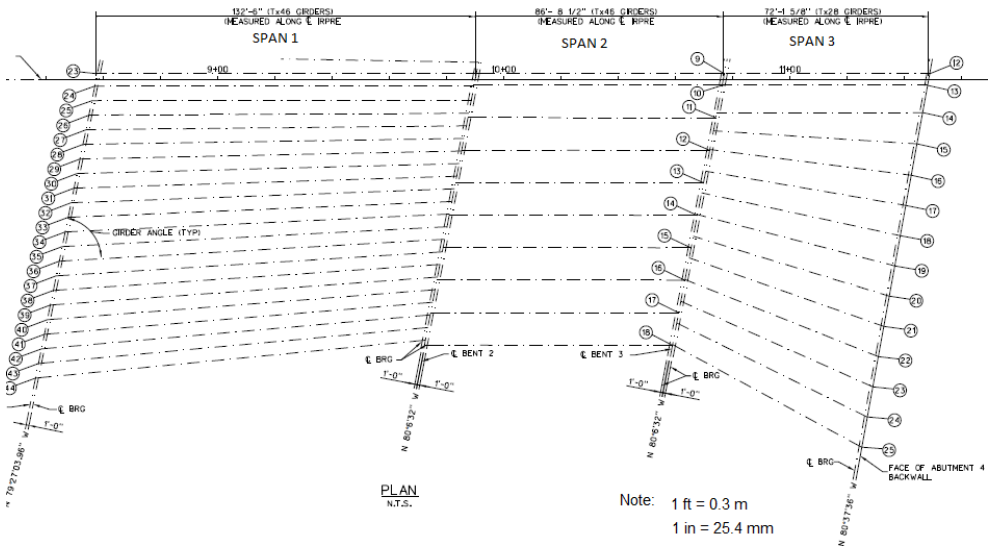

Figure 3-3 Preston Road Northbound Girder Layout

The damaged girder is located in the span 2 of the southbound structure. The span 2 has a total width of 95.5 ft (29.11 m) and its slab is 8 in (203 mm) thick. The spacing between the girders is 11.45 ft (3.5 m). The two overhangs have a width of 3.5 ft (1.07 m) and 2.25 ft (0.69 m), Figure 3-4.

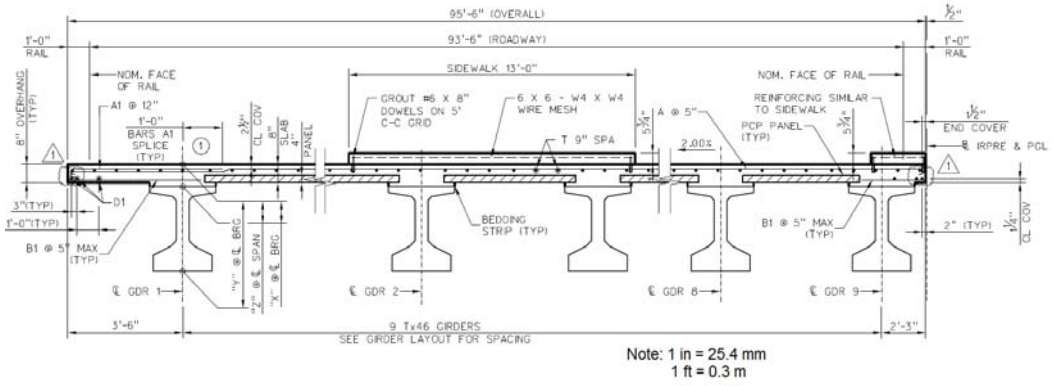

Figure 3-4 Southbound Slab Section

According to the number given in the drawings, the damaged girder is the girder number 1 of the span 2. It is a simple supported beam with a total length of 86.195 ft (26.27 m) and a clear span of 84.667 ft (25.81 m).

The girder number 1 of the span 2, damaged girder, is a prestressed concrete I-girder type Tx46 with 42 low relaxation strands placed according to the strand pattern shown in Figure 3-5.

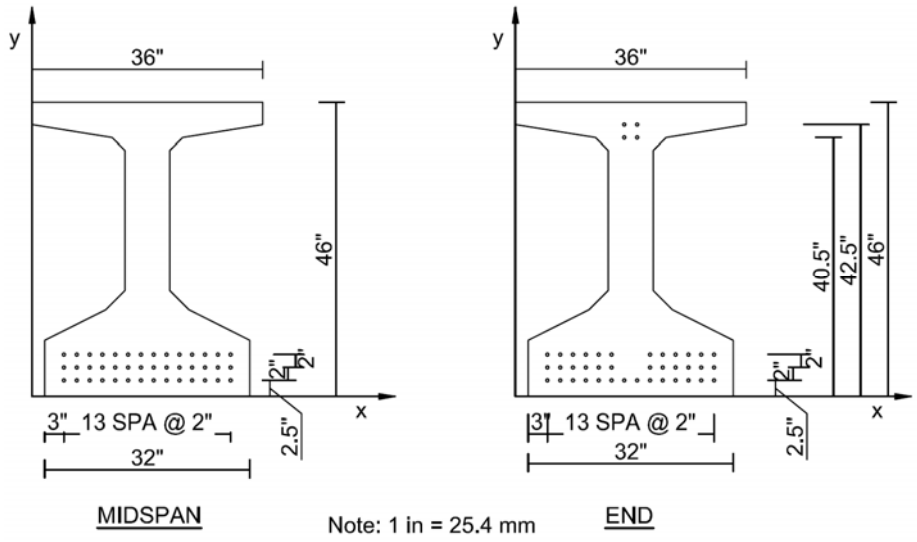

Figure 3-5 Strand Pattern

This is a non-standard pattern, with all strands non debonded and four of them harped. With this strand pattern the eccentricity is 15.6 in (396 mm) at midspan and 12.17 in (309 mm) at end. The strands are grade 270, f_{pu} = 270 ksi (1,861 MPa), with 0.5 in (12.7 mm) diameter. The girder concrete strength is 8,500 psi (58.6 MPa).

The reinforcement is made with a grade 60 steel, f_y = 60 ksi (414 MPa). The bars used were bars number 3, 4, 5 and 6 following the TxDOT standard. The distribution of these bars is shown in Figure 3-6.

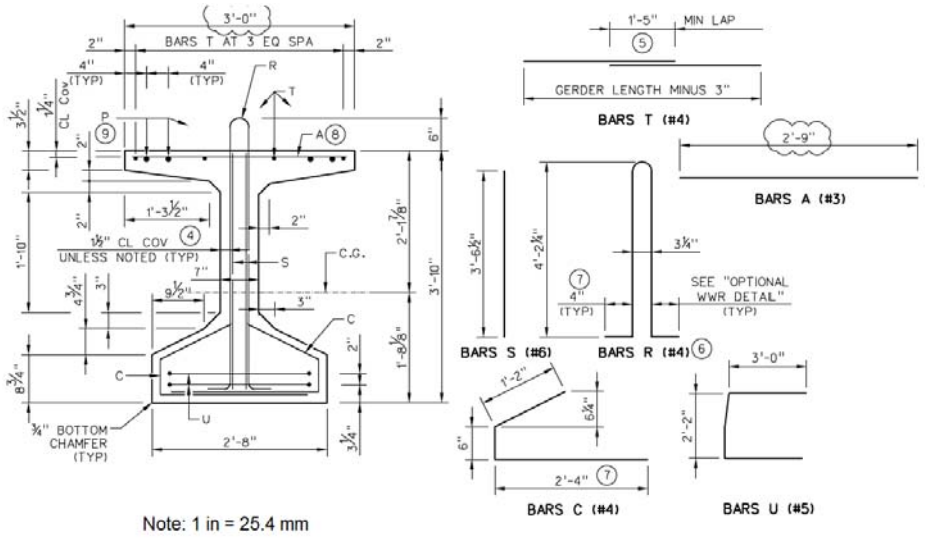

Figure 3-6 Steel Reinforcement

Appendix A of this thesis includes the bridge number 54 drawings.

3.2.- Damage Description

According to the drawings, Figure 3-2, the girder damaged was the girder number 1 of the second span in the southbound structure. The impact caused damage along the bottom flange losing concrete and exposing several strands. The center of the impact was located at 22 ft (6.7 m) from the southernmost support, Figures 3-7 and 3-8.

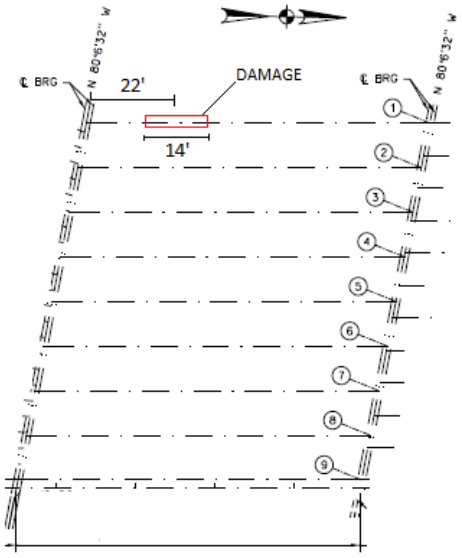

Note: 1 ft = 0.3 m

Figure 3-7 Damage Plan View

Figure 3-8 Damage Location

The total length of the damage was about 14 ft (4.3 m), leaving three strands in the bottom row exposed but none of the strands was severed, Figures 3-9 and 3-10.

Figure 3-9 Damage

Figure 3-10 Strands Bottom Row Exposed

The damaged section is shown in Figure 3-11.

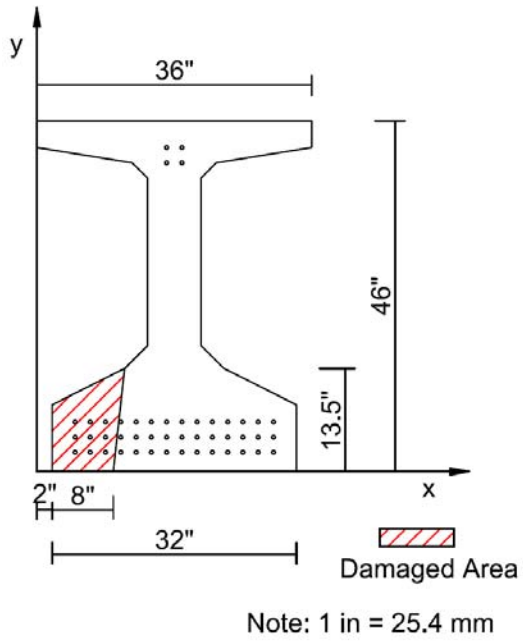

Figure 3-11 Damaged Section

3.3.- Repair Solution Adopted

Based on the damage classification included in NCHRP 20 07, Table 2-2, since the strands were exposed and none of them was severed, the damage can be classified as moderate. Although there was no structural damage an adequate repair was required to prevent further deterioration and the corrosion of the strands.

The solution adopted by the company was based on the use of three different materials. These materials were:

- Bonding agent, EMACO P24. It was used to ensure the bond between the repair mortar and the concrete. It was applied to all concrete, strands surfaces and fiber glass rebar. Table 3-1 shows the technical data given by the manufacturer.

Table 3-1 Bonding Agent. Technical Data

Test Data

PROPERTY	RESULTS	TEST METHOD
Pot life, mixed 150 g, min, at 72° F (22° C)	90	
Working time, min, at 72° F (22° C)	30	
Compressive strength, psi (MPa), 28 days	8,000 (55.2)	ASTM C 109
Flexural strength, psi (MPa), 28 days	1,000 (6.9)	ASTM C 348
Tensile bond strength, 14 days		ACI 503R
Open time, hrs	**Psi (MPa)**	
2	> 200 (1.4)	
9	> 200 (1.4)	
24	> 200 (1.4)	
Slant shear bond, 14 days		ASTM 882
Open time, hrs	**Psi (MPa)**	
2	> 3,000 (20.7)	
9	> 2,500 (17.2)	
24	> 2,000 (13.7)	
Splitting tensile, psi (MPa), 28 days	1,000 (6.9)	ASTM C 496

Test results are averages obtained under laboratory conditions. Expect reasonable variations.

- #4 Fiber Glass Rebar. The use of fiber glass rebar was motivated by its high resistance to corrosion. Also, this kind of solution reduces to the minimum the aesthetic impact of the repair; the use of wrap in a recently built bridge would have produced a higher impact. The rebar were arranged both longitudinally and transversally. The length of the transverse rebar were 8 in (203 mm), embedded 4 in (101 mm) inside the girder section. These bars and the bonding agent were placed to ensure the adherence between the concrete surface and the repair mortar surface. The rebar were spaced at 6 in (152 mm) along the length of the damage and located at 8.5 in (216 mm) from the bottom. The longitudinal rebar were placed along the damage above and below the transverse rebar and they had a length of 14 ft. (4.3 m). These rebar

enhance the flexural capacity of the repair section. They compensate the use of a repair mortar with a nominal strength, $f'_c = 6{,}000\ psi\ (41.4\ MPa)$, lower than the nominal strength of the prestressed girder concrete, $f'_c = 8{,}500\ psi\ (58.6\ MPa)$. The materials properties given by the manufacturer are shown in Table 3-2.

Table 3-2 Fiber Glass Rebar. Technical Data

PULTRALL — V•ROD STANDARD

Revision: May 2011

V-Rod standard straight bars only, does not apply to bent bars

		#2 GFRP V•ROD	#3 GFRP V•ROD	#4 GFRP V•ROD	#5 GFRP V•ROD	#6 GFRP V•ROD	#7 GFRP V•ROD	#8 GFRP V•ROD
Minimum guaranteed tensile strength *	MPa	938	889	941	934	807	816	703
	ksi	136	129	136	135	117	118	102
Nominal tensile modulus	GPa	52,5 ±2,5	53,4 ±2,5	53,6 ±2,5	55,4 ±2,5	56,6 ±2,5	53,5 ±2,5	52,9 ±2,5
	ksi	7609 ±363	7739 ±363	7768 ±363	8029 ±363	8203 ±363	7754 ±363	7667 ±363
Tensile strain	%	1,79	1,66	1,76	1,69	1,43	1,53	1,33
Poisson's ratio	(-)	0,25	0,21	0,26	0,25	0,25	0,25	0,28
Nominal Flexural strength	MPa	1200	1161	1005	930	882	811	776
	ksi	174	168	146	135	128	117	112
Nominal Flexural modulus	GPa	48,8	46,1	46,8	46,8	45,1	44,6	45,1
	ksi	7071	6685	6787	6786	6533	6466	6539
Flexural strain	%	2,46	2,52	2,15	1,99	1,96	1,82	1,72
Nominal Bond strength	MPa	14						
	psi	2029						
Bond dependent coefficient	(-)	0,8						
Longitudinal coefficient of thermal expansion	xE-6/°C	6,2						
	xE-6/°F	3,5						
Transverse coefficient of thermal expansion	xE-6/°C	23,8						
	xE-6/°F	13,2						
Moisture absorption	%	0,65	0,47	0,38	0,25	0,21	0,36	0,17
Glass content	% vol	65						
	% weight	83						
Weight	g/m	95	181	298	488	659	887	1132
	lb/ft	0,064	0,122	0,200	0,328	0,443	0,596	0,761
Effective cross-sectional area (including sand coating) **	mm^2	47,0	95,0	149,0	234,0	302,0	396,0	546,0
	$inch^2$	0,0729	0,1473	0,2310	0,3627	0,4681	0,6138	0,8463
Nominal cross-sectional area	mm^2	31,7	71,3	126,7	197,9	285,0	387,9	506,7
	$inch^2$	0,0491	0,1104	0,1963	0,3068	0,4418	0,6013	0,7854

* the minimum guaranteed tensile strength must not be used to calculate the strength of the bent portion of a bent bar. Instead use the minimum guaranteed tensile strength found in the technical data sheet of bent V-Rod bars.
** Please contact the manufacturer for dowelling applications.
Development and splice lengths are available upon request but should be properly calculated by a design engineer.

Please refer to the bent bar data sheet for designs using bent V-Rod bars.
It is the responsibility of the design engineers to contact the bar manufacturer to get the latest updates of this technical data sheet.

- LA40 Repair mortar. It was applied to cover the strands exposed and the fiber glass rebar, restoring the section to its original shape. According to its manufacturer the LA40 repair mortar is a one component shrinkage-compensated micro concrete. This mortar has been designed for large volume repair. Its technical data are given by Table 3-3.

Table 3-3 Repair Mortar. Technical Data

Test Data

PROPERTY	RESULTS	TEST METHODS
Fresh wet density, lb/ft³ (kg/m³)	142 (2,275)	ASTM C 138
Compressive strength, psi (MPa); 2" (51 mm) cubes		ASTM C 109
1 day	2,500 (17.2)	
7 days	5,000 (34.5)	
28 days	6,000 (41.4)	
Compressive strength, psi (MPa); 3 by 6" (76 by 152 mm) cylinders, at 28 days	5,000 (34.5)	ASTM C 39
Flexural strength, psi (MPa), at 28 days	1,150 (7.9)	ASTM C 348
Slant shear bond strength, psi (MPa), at 28 days	3,000 (20.7)	ASTM C 882, (modified[1])
Splitting tensile strength, psi (MPa), at 28 days	500 (3.4)	ASTM C 496
Drying shrinkage, µstrain, at 28 days	350	ASTM C 157, (unmodified)
Drying shrinkage, µstrain, at 21 days	611	ASTM C 157, (modified)
Freeze/thaw resistance, % RDM[2]	100	ASTM C 666
Coefficient of thermal expansion, in/in/° F (cm/cm/° C)	5.5 x 10^{-6} (9.9 x 10^{-6})	CRD C 39

[1]No bonding agent

[2]RDM = Relative Dynamic Modulus

Results were obtained with a water / powder ratio of 4 qts/80 lb (3.8 L/36 kg) bag or 2.7 qts/55 lb (2.6 L/25 kg) bag.

All application and performance values are typical for the material, but may vary with test methods, conditions, and configurations.

The repair procedure comprised the following steps:

1) Remove the loss concrete.
2) Chip the existing beam to provide a rough surface.
3) Drill to place number 4 fiber glass rebar.
4) Place number 4 fiber glass rebar.
5) Apply bonding agent.
6) Install formwork.
7) Fill with repair mortar.

8) Remove the formwork.

The first and second step had the objective of obtaining a clear surface that allows for the perfect adherence between the parts. Chipped concrete had a minimum depth of 1.5 in (38 mm). Where the area of the strand exposed was greater than 25% of its total cross sectional area, the concrete was chipped back to allow for proper consolidation and bonding of concrete repair material.

Once all the delaminated concrete was removed, the third step was carried out. The holes where the transverse rebar had to be placed were drilled following the sketch of Figure 3-12.

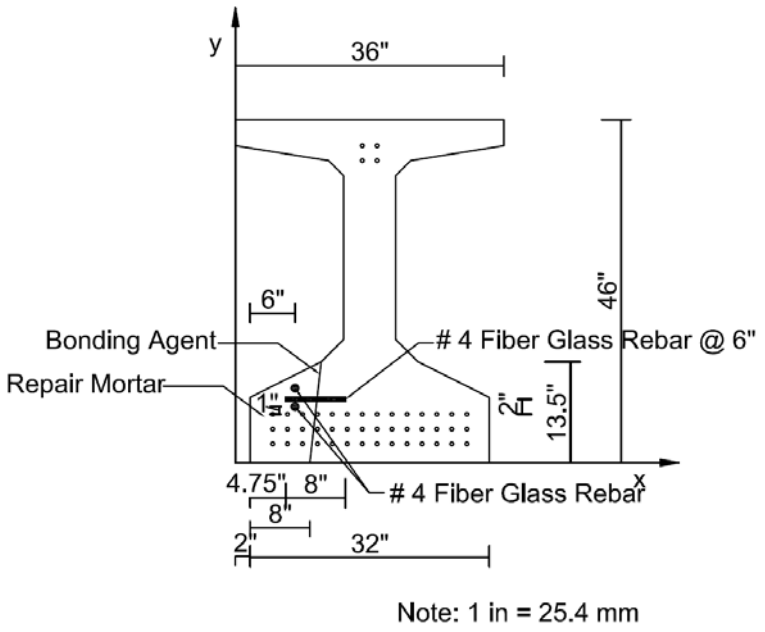

Figure 3-12 Repair Sketch

After drilling the holes and cleaning the strands of all rusty surfaces the fiber glass rebar were placed. Then the bonding agent was applied to all concrete, strands and fiber glass rebar, ensuring the bond between the concrete and the repair mortar.

The next step was the step number 6, the installation of a formwork on the repair section was necessary to ensure the shape of the original girder was restored. Once the formwork was installed the repair mortar was poured.

Finally after twelve hours of curing period the formwork was removed, step 8.

Chapter 4

FIELD TESTING

The field tests performed consisted of monitoring the strains on the damaged girder before and after the repair when subjected to different loading cases. The monitoring was performed in two phases. The first phase monitored the damaged girder using six strain gauges placed on the damaged girder. The second phase was performed once the girder was repaired. To monitor this second phase the same gauges were uses plus one new gauge placed on the repaired section. For each phase a truck was placed in different positions and the associated strains were recorded.

4.1.- Truck Description

The truck used for the test was not the standard truck defined by AASHTO. AASHTO uses a design truck with a total weight of 72,000 lbs (320,272 N). The weight of the truck used for the test was 90,000lbs (400,340 N). This weight is distributed in six axles. Figure 4-1 shows the characteristics of the truck.

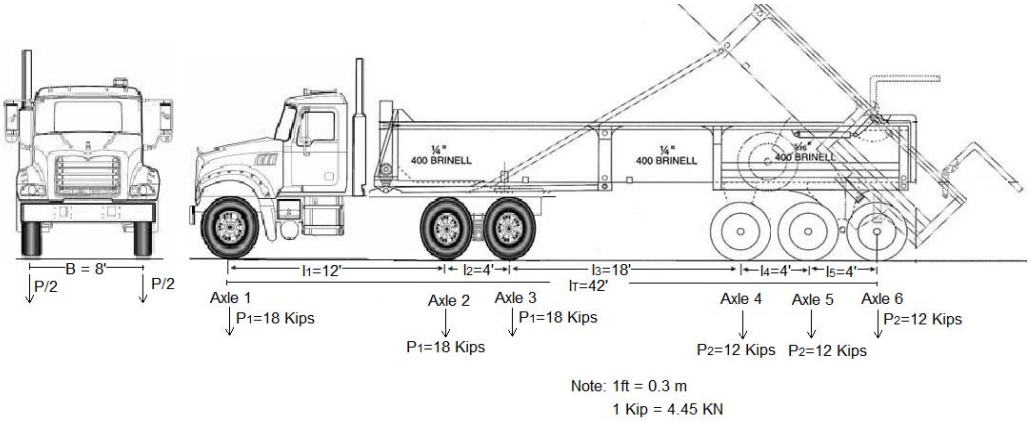

Figure 4-1 Truck Characteristics

The total length of the truck is 42 ft (12.8 m) and its width is 8 ft (2.4 m). The weight transmitted for the three first axles is 18,000 lbs (80,068 N) and for the last three axles 12,000 lbs (53,379 N).

4.2.- Phase 1: Field Test

The first phase of the test consisted of monitoring the damaged girder strains with the truck placed at two different positions. The strains were measured using six strain gauges, enumerated from 1 to 6, placed according to Figure 4-2.

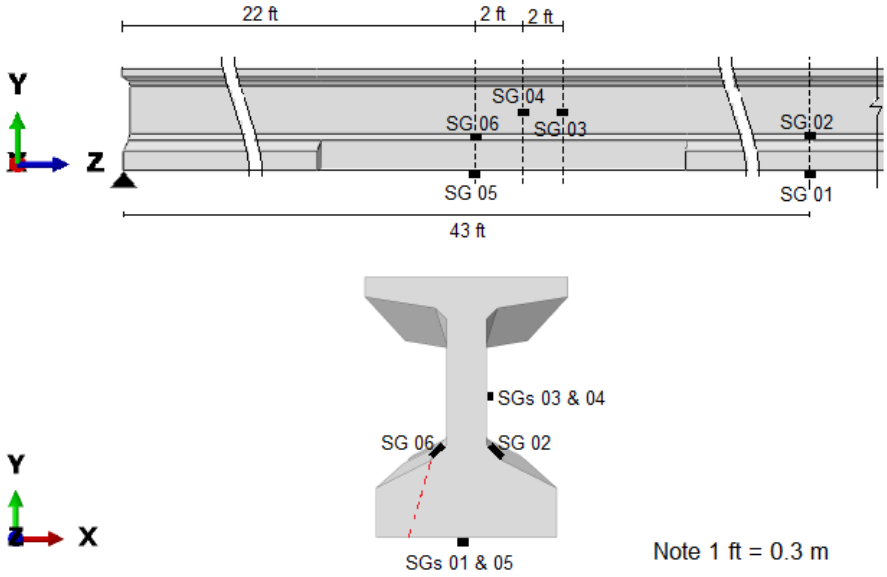

Figure 4-2 Strain Gauges Distribution

Once all gauges were placed the strain test began. The truck positions are described below.

4.2.1.-Truck Positions

The truck was laid on the bridge first over the damaged girder, position 1 and then over the next undamaged girder, position 2.

In the first position, Figure 4-3, the truck was centered on the damage over the damaged girder and stayed in the same position for 650 seconds. The truck was at 3.5 ft (1.07 m) from the barrier.

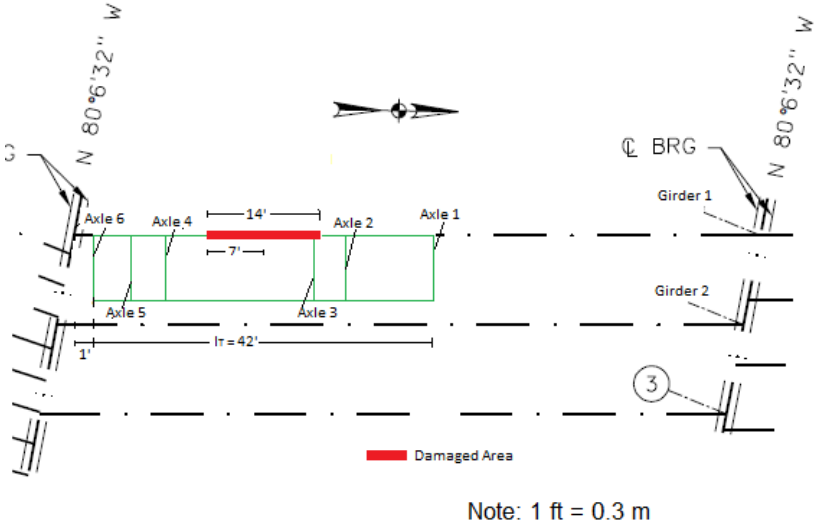

Figure 4-3 Truck Position 1

After 650 seconds the truck was moved to the next undamaged girder, girder 2. The truck remained in this position about 200 seconds. The truck was at 10.95 ft (3.34 m) from the barrier. This position is shown in Figure 4-4.

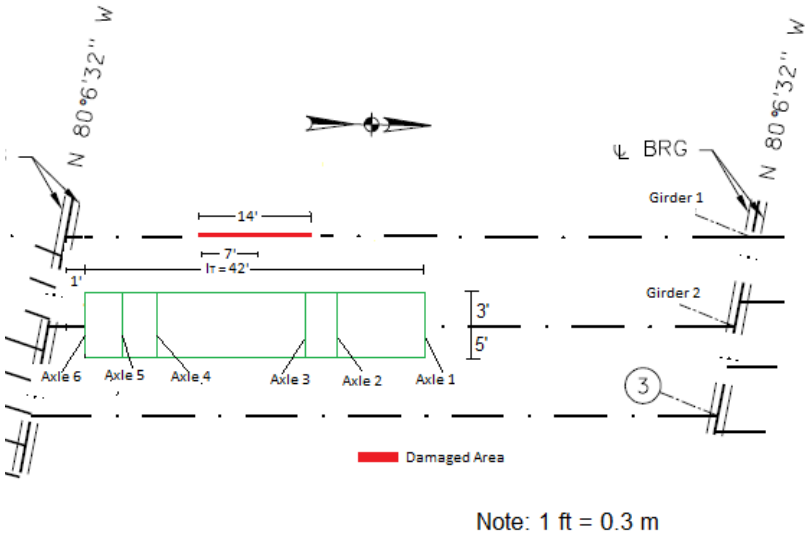

Figure 4-4 Truck Position 2

The data collected by the strain gauges are explained below.

4.2.2.- Phase 1: Experimental Data.

The strains measured by the gauges are represented in Figures 4-5 and 4-6.

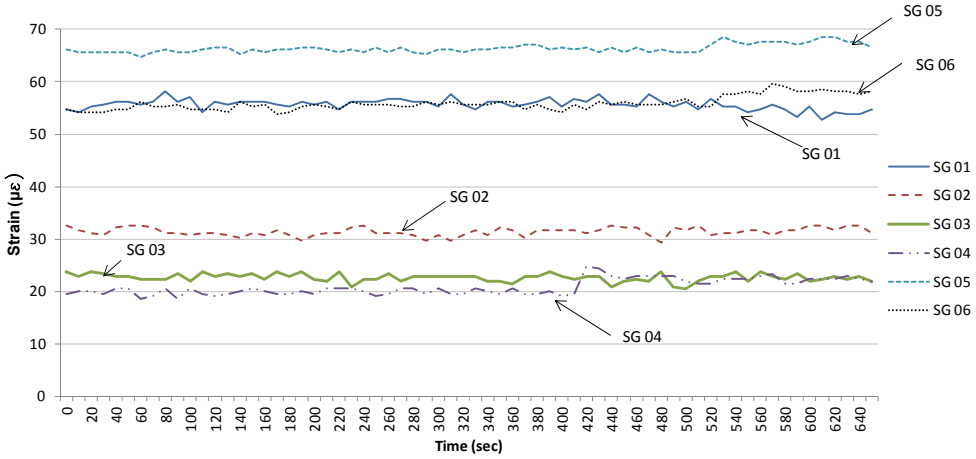

Figure 4-5 Truck Position 1: Strain Measurements

For a better understanding the strain measurements obtain for position 2 are shown in two different graphs.

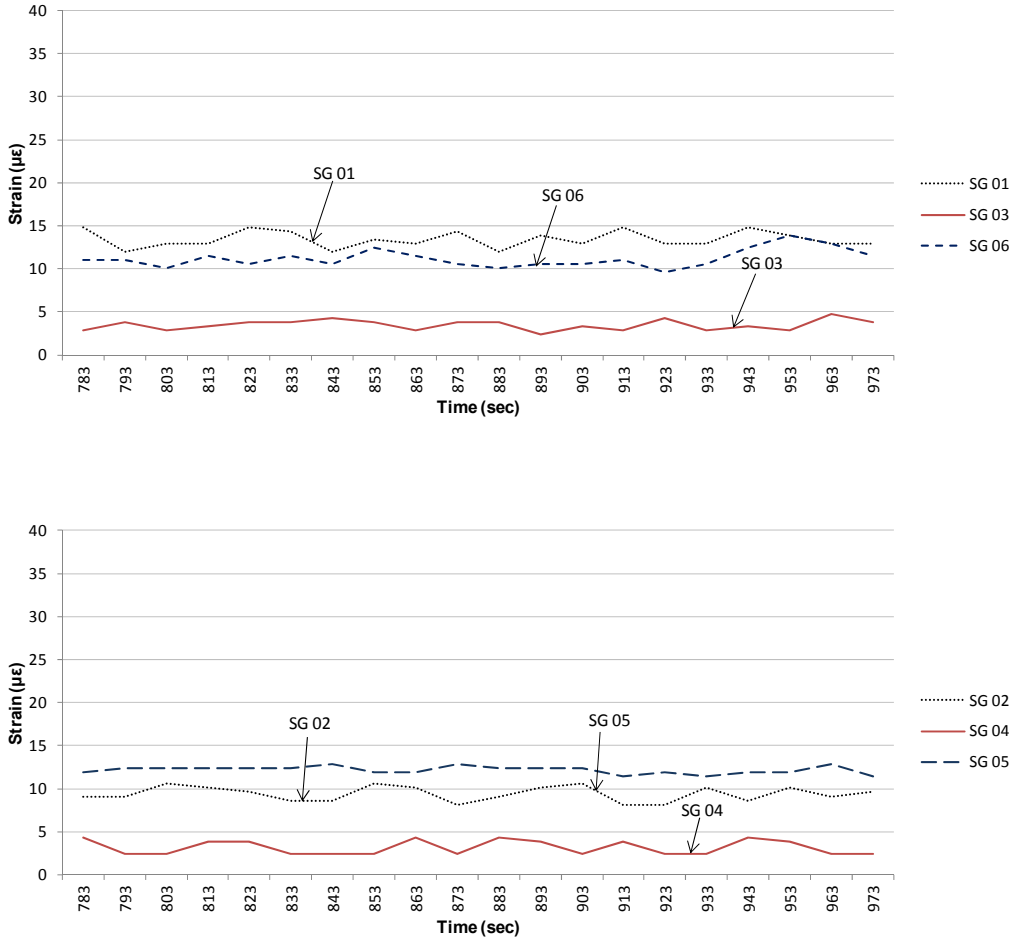

Figure 4-6 Truck Position 2: Strain Measurements

From both figures it can be observed how the strain measured varied from one truck position to another. This is because at position 1 the truck was almost over the damaged girder causing elevated values for the strain. However at position 2 the truck was moved over the next undamaged girder, therefore the strains on the damaged girder were reduced.

On both cases the strains recorded were very small, with values lower than 70 με in all cases. The average values of the strains for truck position 1 are given by Table 4-1.

Table 4-1 Truck Position 1. Average Strain

Average Strain ($\mu\varepsilon$)					
SG 01	SG 02	SG 03	SG 04	SG 05	SG 06
55.67	31.38	22.65	20.83	66.35	55.91

Similarly, Table 4-2 gives the average values for truck position 2.

Table 4-2 Truck Position 2. Average Strain

Average Strain ($\mu\varepsilon$)					
SG 01	SG 02	SG 03	SG 04	SG 05	SG 06
13.46	9.40	3.48	3.12	12.15	11.21

The values of the strains obtained from the field test for this phase are included in Appendix B.

4.3.- Phase 2: Field Test

Once the girder was repaired, the second phase of the field test was performed. On this second phase the strain gauges were placed at the same position that for Phase 1, only one new strain gauge, number 7, was added. This gauge was attached to the bottom of the repaired flange, Figure 4-7

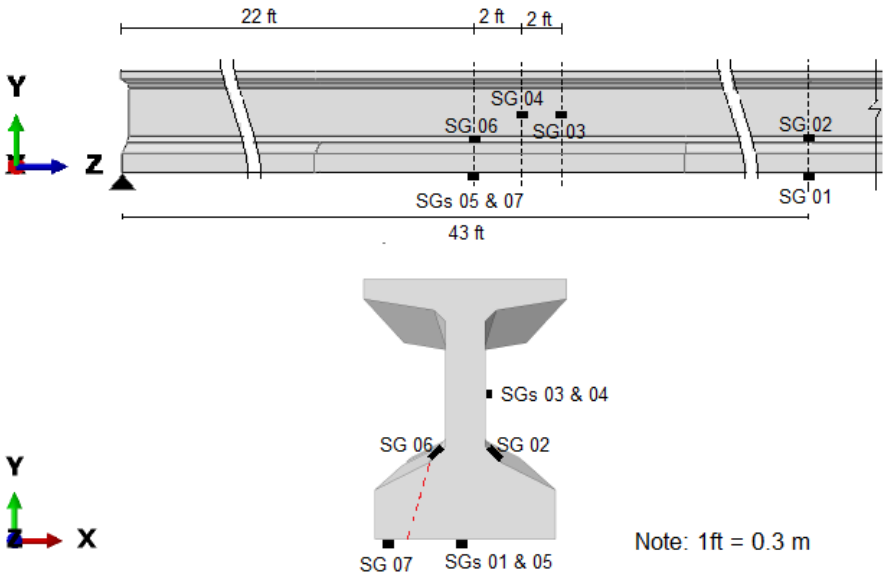

Figure 4-7 Strain Gauges Positions On Repaired Girder.

For this second phase the truck was placed in four different positions as explained below.

4.3.1.- Truck Positions

First the truck was placed at 3.5 ft (1.07 m) from the barrier at the girder end, position 3. At this position the truck was centered over the repaired area and stopped for about 100 seconds.

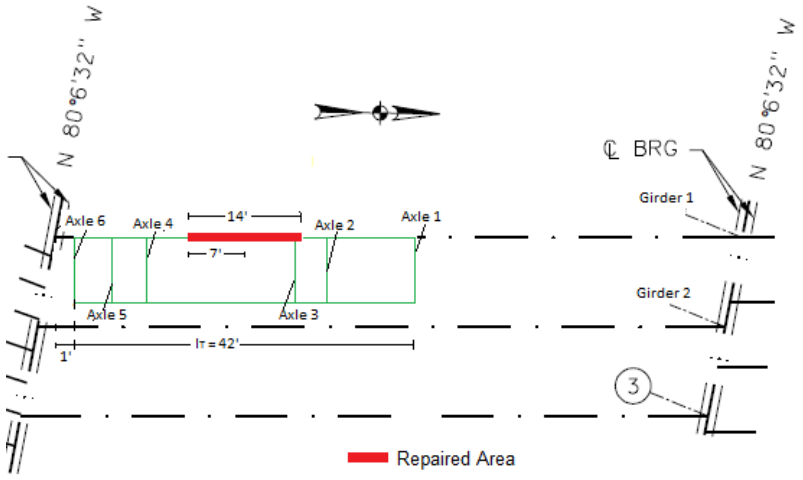

Note: 1 ft = 0.3 m

Figure 4-8 Truck Position 3

After position 3 the truck was moved to midspan at 3.5 ft (1.07 m) from barrier, position 4, and remained at this location for 350 seconds.

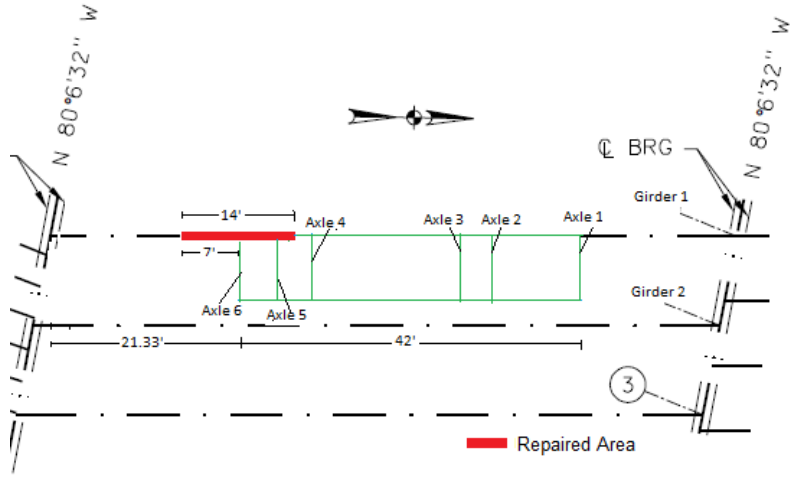

Note: 1 ft = 0.3 m

Figure 4-9 Truck Position 4

The next position, position 5, was at 10.95 ft (3.34 m) from barrier at the end of the girder as shown in Figure 4-10. The truck was on this position for about 220 seconds.

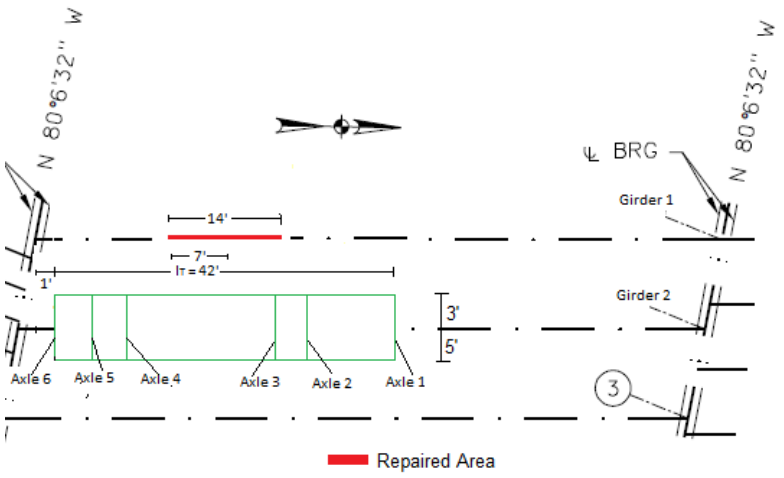

Note: 1 ft = 0.3 m

Figure 4-10 Truck Position 5

Finally the truck moved from position 5 to position 6, at 10.95 ft (3.34 m) from barrier and 21.33 ft (6.5 m) from the southernmost support, Figure 4-11. The truck stopped about 150 seconds.

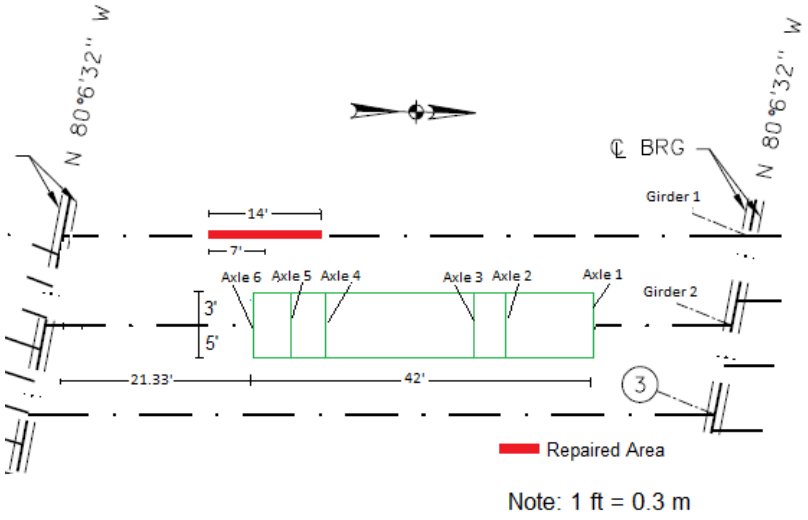

Note: 1 ft = 0.3 m

Figure 4-11 Truck Position 6

The data obtained during this phase of the field test are explained below.

4.3.2.- Phase 2: Experimental Data

The strains measured by strain gauges 1 to 7 for each truck position are shown in Figure 4-12 through Figure 4-15. For a better understanding the strain measurements for each truck position have been shown in two different graphs.

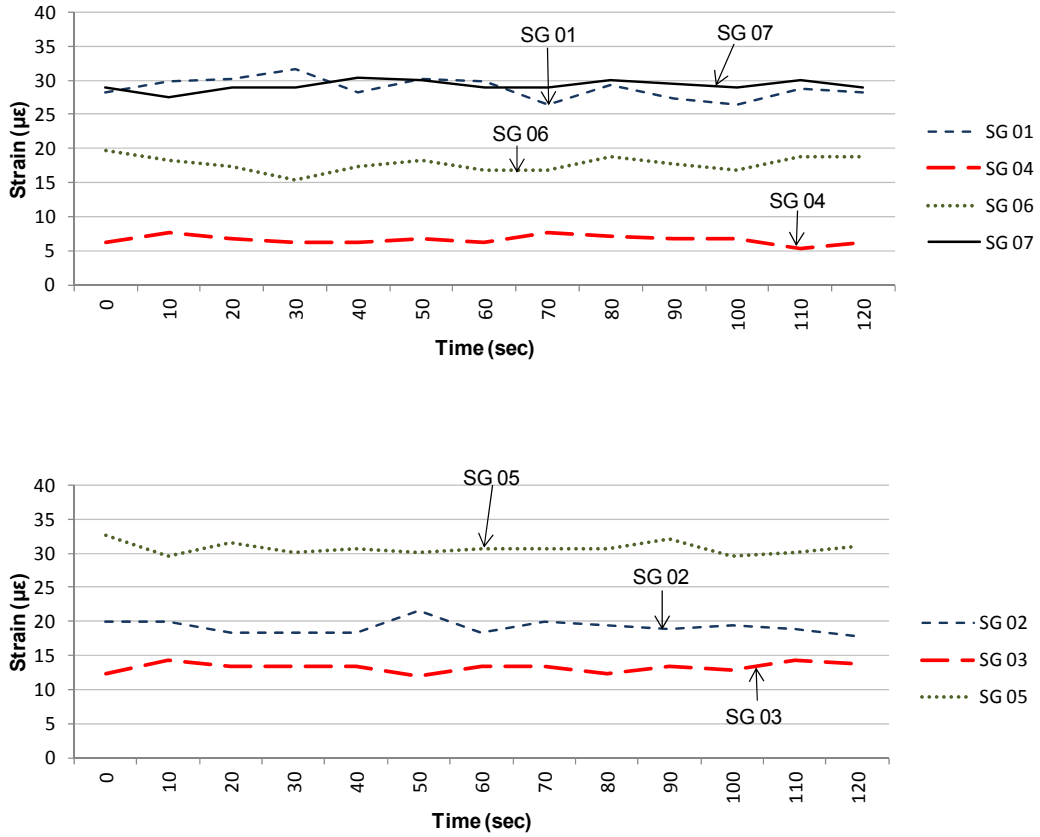

Figure 4-12 Truck Position 3: Strain Measurements

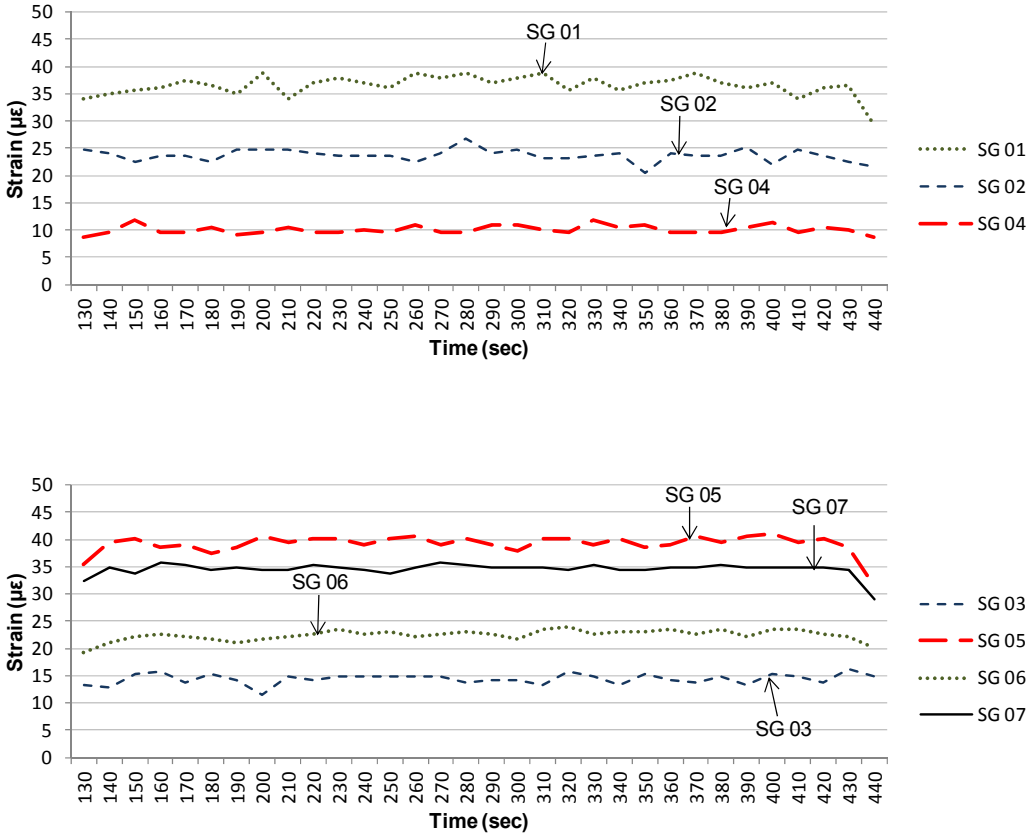

Figure 4-13 Truck Position 4: Strain Measurements

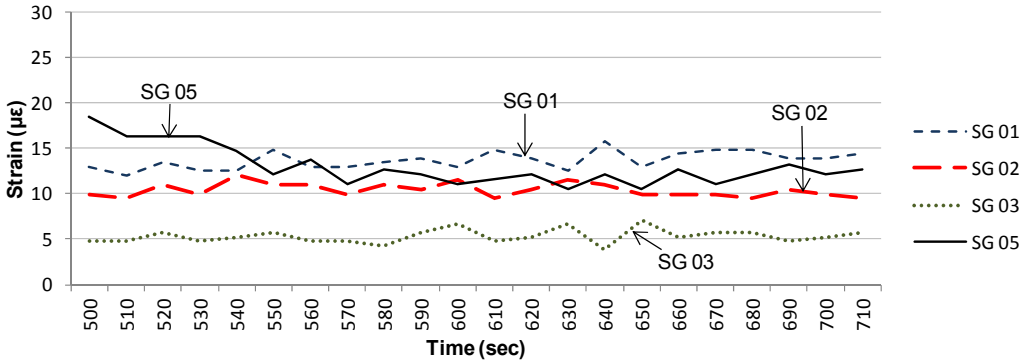

Figure 4-14 Truck Position 5: Strain Measurements I

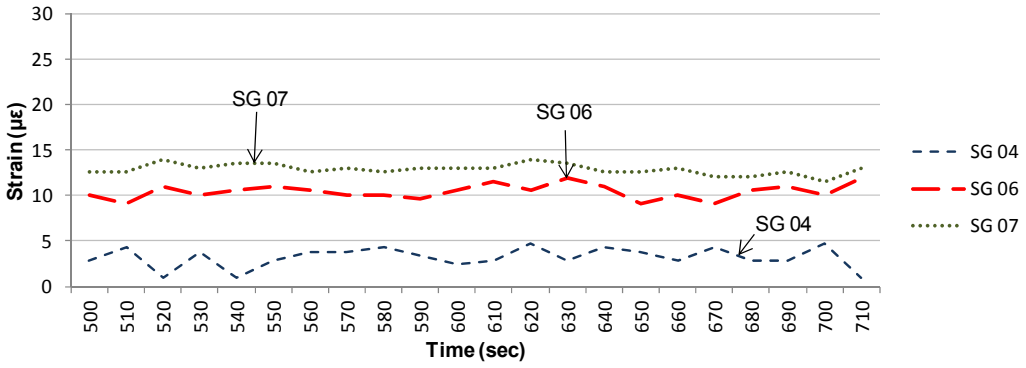

Figure 4-15 Truck Position 5: Strain Measurements II

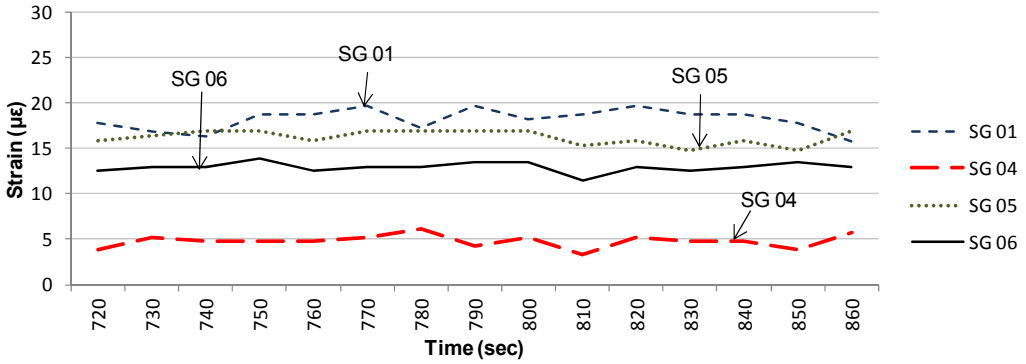

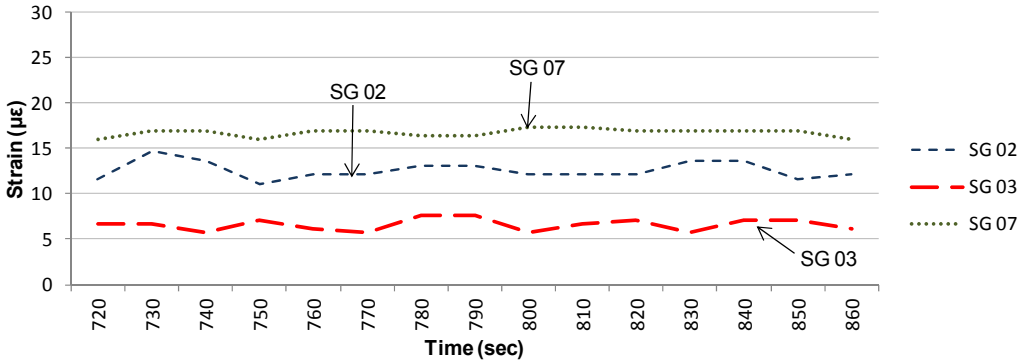

Figure 4-16 Truck Position 6: Strain Measurements

The first thing that can be observed from the graphs is that the strains measured for the damaged girder in Phase 2 are significantly lower than those measured in Phase 1. The higher average strain measured for position 1 was 66.35 με with the strain gauge number 5. For position 3, that it is a similar position than position 1, the higher average strain measured was 30.69 με, Table 4-3, with the same gauge. Similarly for position 5 the average strain measured, Table 4-5, was lower than for position 2. This trend in the data obtained shows that the repair method used increased the capacity of the girder.

The graphs and tables show greater strain values for the positions where the truck was over the damaged girder, position 3 and 4, Tables 4-3 and 4-4.

Table 4-3 Truck Position 3. Average Strain

Average Strain ($\mu\varepsilon$)						
SG 01	SG 02	SG 03	SG 04	SG 05	SG 06	SG 07
28.84	19.19	13.21	6.56	30.69	17.73	29.24

Table 4-4 Truck Position 4. Average Strain

Average Strain ($\mu\varepsilon$)						
SG 01	SG 02	SG 03	SG 04	SG 05	SG 06	SG 07
36.50	23.70	14.38	10.04	39.13	22.41	34.48

From Tables 4-5 and 4-6 it can be observed that the average strain values were reduced due to the movement of the truck to the next undamaged girder.

Table 4-5 Truck Position 5. Average Strain

Average Strain ($\mu\varepsilon$)						
SG 01	SG 02	SG 03	SG 04	SG 05	SG 06	SG 07
13.68	10.43	5.32	3.21	12.98	10.45	12.89

Table 4-6 Truck Position 6. Average Strain

Average Strain (με)						
SG 01	SG 02	SG 03	SG 04	SG 05	SG 06	SG 07
18.18	12.57	6.60	4.80	16.16	12.93	16.71

On all cases the strains were very small, all values were less than 40 με Appendix B includes all the strains measured for each truck position for Phase 2.

Chapter 5

FINITE ELEMENT MODEL

The software used for the development of this thesis is ABAQUS. It has been used to model the two phases of the field test. Therefore, two different models have been computed with their respective loading cases according to the truck position.

5.1.- General Considerations

To work with ABAQUS it is important to be consistent with the units. To facilitate the performance the units used have been inches, in, and pounds, lbs. For both phases the coordinate system used is shown in Figure 5-1.

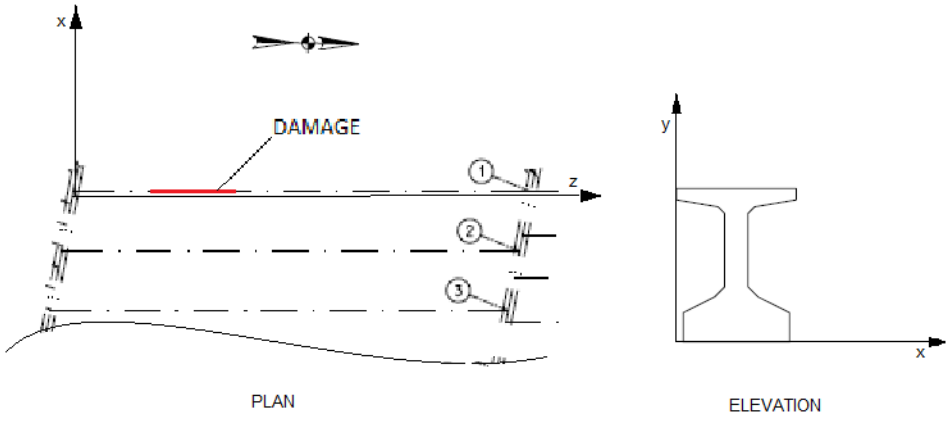

Figure 5-1 Coordinate System

The strain measured in the field test does not include the deformation of the girder once in place and subjected to the self-weight of the rest of the bridge superstructure elements. In order to be able to compare the strains measured in the field tests and the strains obtained with the models developed using ABAQUS, it has been

necessary to compute the model only with dead load and prestress force and then with dead load, prestress force and live load. The strain difference between the two cases is then compared to the strain measured by the gauges.

ABAQUS has eight modules. Different information is imputed in each of the modules. The steps followed to model each phase are:

1) Define the geometry, part module.
2) Define material properties, material module.
3) Join the parts, assembly module.
4) Define the load phases, step module.
5) Define loads and boundary conditions, load module.
6) Define the mesh, mesh module.
7) Run the model, job module.
8) Obtain the results, visualization module.

Points 5-2 and 5-3 describe the steps from one through six for each phase. The last two steps, seven and eight, have been explained on Chapter 6.

5.2.- Phase 1: Damaged Girder Model.

The Phase 1 model has two loading cases corresponding with the truck position 1 and truck position 2 of the field test. Each step followed in the development of the Phase 1 model has been described below.

5.2.1.- Geometry

For this step the part module has been used. In this module the different parts that form the section are introduced. Because of the different materials used, three

different parts have been defined. These parts are the concrete girder section, the concrete slab and haunch section, and the steel reinforcement.

5.2.1.1.- Concrete Girder Section

The concrete girder section has been defined as a 3D deformable extrusion solid. The total length of the girder is 1,016 in (25,806 mm) between supports. This part includes the damaged section. The undamaged section has been defined from z = 0 to z = 180 in (4,572 mm) and from z = 348 in (8,839 mm) to z = 1,016 in (25,806 mm)

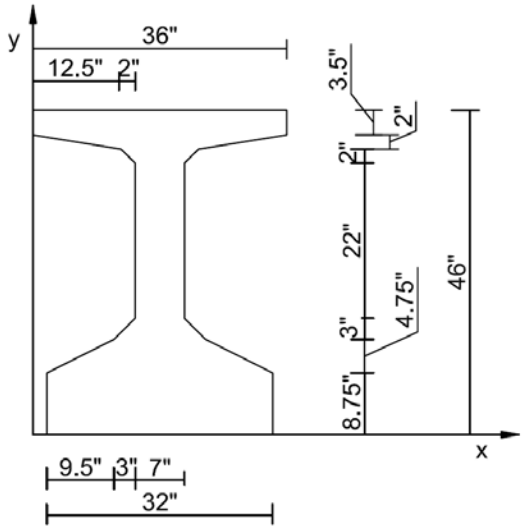

Figure 5-2 Undamaged Section

The damaged section, Figure 5-3, has been introduced between the z coordinates 180 in (4,572 mm) to 348 in (8,839 mm), for a total length of 168 in (4,267 mm).

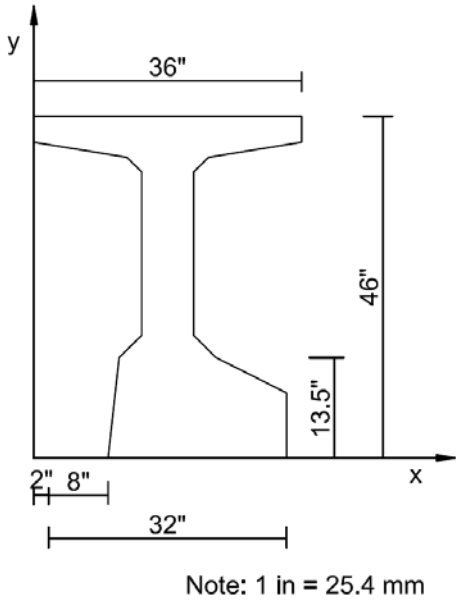

Figure 5-3 Damaged Section

Figure 5-4 gives a final view of the girder section that has been modeled.

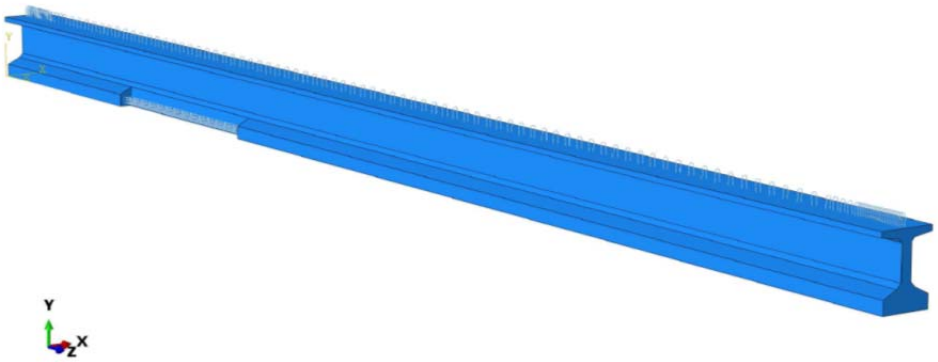

Figure 5-4 ABAQUS. Damaged Girder Model

5.2.1.2.- Concrete Slab Section

This part includes the slab section and the haunch section. Both the haunch and slab section were defined as a 3D deformable extrusion solid.

Following AASHTO LRFD provisions, a slab width equal to the effective flange width have been used in the model. The effective flange width defines the composite section and it has been calculated according to AASHTO 2012. From article 4.6.3.6, AASHTO 2012, the effective flange width, Figure 5-5, of a concrete deck slab is:

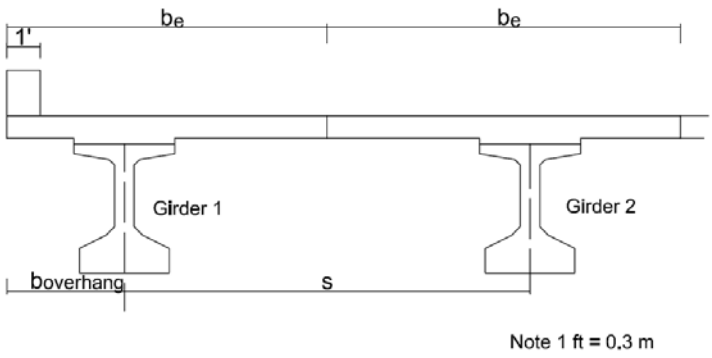

Figure 5-5 Effective Flange Width

For girder 1:

$$b_e = \frac{1}{2}s + b_{overhang} \quad (1)$$

For girder 2:

$$b_e = s \quad (2)$$

Where:

$s = girder\ spancing$

$b_{overhang} = overhang\ width$

For this thesis the case to compute is the case 1. From Equation 1 the effective flange width is:

$$b_e = \frac{1}{2}\,(11.45) + \,3.5 = 9.22\,ft = 110.69\,in\,(2{,}811\,mm)$$

A different width, the transformed width, b_{tr}, has to be considered when designing or analyzing the composite section. Since the slab and the girder have different modulus of elasticity, this width is used to transform the cast-in-place slab into a fictitious slab having the same concrete properties that the prestressed concrete girder. For the case studied in this thesis, this transformed width is not necessary, because the software ABAQUS allows the use of sections with different materials properties. Therefore the section used for the model is defined in Figure 5-6.

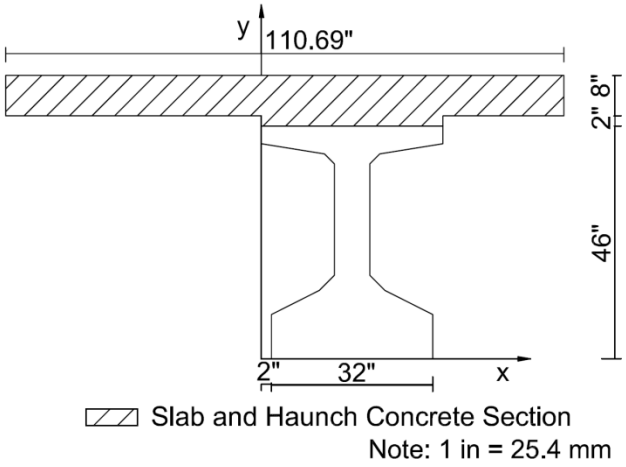

Figure 5-6 Slab and Haunch Concrete Section

The total area, A_T, and height, h_T, of the section defined are:

$$A_T = \,b_e \cdot t_s + \,b_{haunch} \cdot t_{haunch} + A_g \tag{3}$$

$$A_T = 1718.55\,in^2\,(1{,}108{,}739\,mm^2)$$

$$h_T = \,h_g + t_{haunch} + t_s \tag{4}$$

$$h_T = 56\,in\,(1{,}422\,mm)$$

Where:

$b_e = effective\ flange\ width = 110.69\ in\ (2{,}811\ mm)$

$t_s = slab\ depth = 8\ in\ (203\ mm)$

$b_{haunch} = haunch\ width = 36\ in\ (914\ mm)$

$t_{haunch} = haunch\ depth = 2\ in\ (51\ mm)$

$A_g = girder\ Area = 761\ in^2\ (490{,}966\ mm^2)$

$h_g = girder\ height = 46\ in\ (1{,}168\ mm)$

The slab and haunch concrete section was placed above the girder through its total length to obtain the composite section modeled, Figure 5-7.

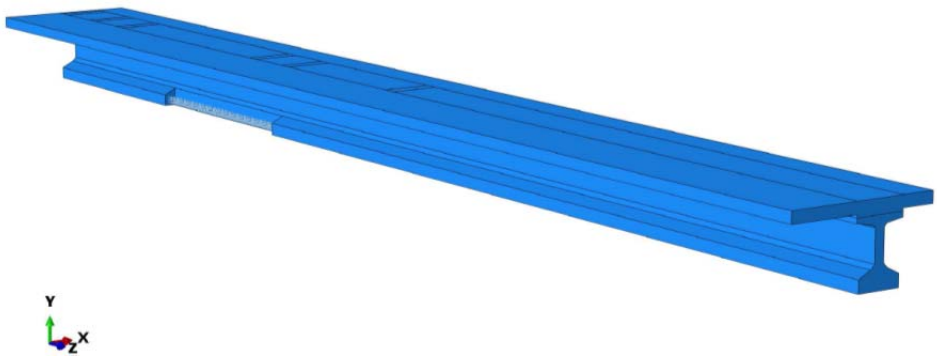

Figure 5-7 ABAQUS. Composite Section Model

5.2.1.3.- Steel Reinforcement

This part includes all the steel reinforcement used in the fabrication of the girder. The bars have been introduced according to the drawings, Figure 3-6, with their respective dimensions. Table 5-1 shows the type of bars introduced and their dimensions.

Table 5-1 Steel Reinforcement

Bars	Type	Nominal Diameter, ϕ, in (mm)	Nominal Area, A_n, in^2 (mm^2)
A	#3	0.375 (9.5)	0.11 (71)
C	#4	0.5 (12.7)	0.20 (129)
R	#4	0.5 (12.7)	0.20 (129)
T	#4	0.5 (12.7)	0.20 (129)

The reinforcement has been defined as a deformable 3D wire with a truss section. Truss sections are only capable of developing axial stresses, therefore they are considered adequate to model the reinforcement behavior. The location of each bar into the model is shown in Figure 5-8.

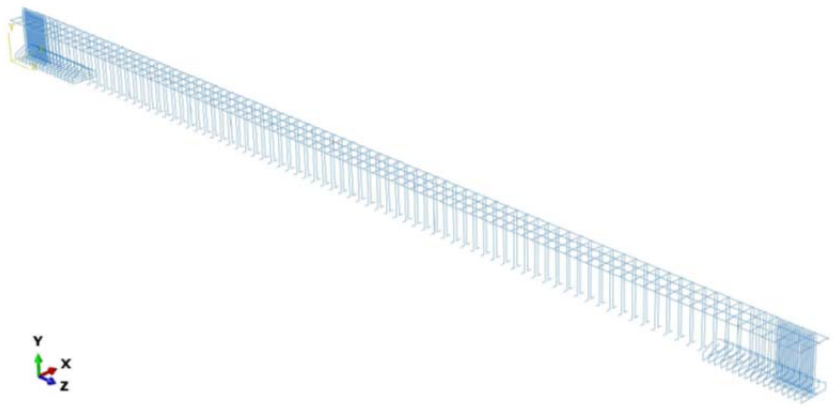

Figure 5-8 ABAQUS Steel Reinforcement

Once all parts were defined the following step was determining the material properties for each part.

5.2.2.- Material Properties

To model the girder it was necessary to define the material properties of each part that forms the beam. These material properties are defined by the stress-strain relationship of each material used.

5.2.2.1.- Concrete Girder Section

For concrete the stress-strain relationship is not linear. The model has to be capable of representing the behavior of concrete in compression and tension. On both cases the concrete has elastic and inelastic behavior. ABAQUS software provides three different models for reinforced concrete elements:

- Smeared crack concrete model: for concrete under monotonic loads.
- Brittle crack concrete model: it is used for reinforced concrete. It assumes linear elastic behavior of concrete in compression and linear elastic concrete up to yield point in tension. Its use is limited to elastic behavior of concrete.
- Concrete damaged plasticity: is the technique that best represents the behavior of the concrete for this study. It considers the inelastic behavior of concrete both in compression and tension.

For the elastic behavior the data needed are the modulus of elasticity and the Poisson's ratio. The modulus of elasticity has been computed using article 5.4.2.4 of AASHTO 2012:

$$E_{cg} = 33{,}000 \cdot k_1 \cdot w_c^{1.5} \sqrt{f'_c} \qquad (5)$$

Where:

$k_1 = 1$

$w_c = concrete\ selfweight = 0.150\ kcf\ (23.8\ K\,N/m^3)$

$$f'_c = concrete\ strength = 8{,}500\ psi\ (58.61\ MPa)$$

$$E_{cg} = 55.893 \cdot 10^5\ psi\ (38{,}537\ MPa)$$

For prestressed concrete AASHTO 2012 gives as Poisson's ratio the following:

$$\nu = 0.2$$

To use the concrete damaged plasticity (CDP) model it is necessary to input different data for the compression and tension behavior. The first data that ABAQUS required when using CDP model is the default parameters. These parameters have been obtained from Kmiecik & Kamiski, (2011). They recommend using the following default parameters values:

- Dilatation angle: 36
- Eccentricity: 0.1
- $f_{b0}/f_{c0} = 1.16$
- k = 0
- Viscosity parameter: 0

After introducing this data, it was necessary to define the stress-strain relationship for both compression and tension. The stress-strain curves are different for each type of concrete; they depend on their concrete strength. In the absence of experimental data to characterize the behavior of the concrete used to fabricate the girder the following model for the stress-strain curve were used.

1) The equation propose by Wight & Macgregor, (2012), for compression
2) The equation given by Wahalathantri, et al. (2011), for tension.

Wight & Macgregor, (2012), give an equation for the compressive behavior of the concrete valid for concrete strength from 2,000 psi (13.8 MPa) to 18,000 psi (124 MPa).

They establish a relationship between the stress, f_c, and the corresponding strain, ε_c. The compressive stress-strain diagram has been obtained from equation:

$$\frac{f_c}{f'_c} = \frac{n\left(\varepsilon_c/\varepsilon_0\right)}{n-1+\left(\varepsilon_c/\varepsilon_0\right)^{nk}} \quad (6)$$

Where:

f'_c = peak stress obtained from a cylinder test

ε_c = strain when f_c reaches f'_c

n = a curve-fitting factor equal to $E_c/(E_c - E'_c)$

E_c = initial tangent modulus (when $\varepsilon_c = 0$)

$E'_c = f'_c/\varepsilon_0$

k = a factor to control the slopes of the ascending and descending branches of the stress-strain curve, taken equal to 1 for $\varepsilon_c/\varepsilon_0$ less than 1 and taken greater than 1 for $\varepsilon_c/\varepsilon_0$ greater than 1.

For normal density concrete:

$$n = 0.8 + \left(\frac{f'_c}{2500}\right) \quad (7)$$

Where f'_c is in psi.

For $\varepsilon_c/\varepsilon_0 \leq 1.0$

$$k = 1$$

For $\varepsilon_c/\varepsilon_0 > 1.0$

$$k = 0.67 + \frac{f'_c}{9000} \geq 1.0\ (psi)$$

In this case:

$$f'_c = 8{,}500\ psi\ (58.6\ MPa)$$

$$E_c = 55.893 \cdot 10^5\ psi\ (38{,}537\ MPa)$$

The compressive stress-strain curve obtained by substituting these values into Equation 6 is given by Table 5-2. Figure 5-9 shows the stress-strain diagram.

Table 5-2 Concrete Girder Section: Compressive Stress-Strain Values

k	ε_c	σ_c psi (MPa)
1	0	0.00 (0)
1	0.00025	1397.26 (9.63)
1	0.0005	2792.06 (19.25)
1	0.00075	4170.64 (28.76)
1	0.001	5495.11 (37.89)
1	0.00125	6693.67 (46.15)
1	0.0015	7662.65 (52.83)
1	0.00175	8290.22 (57.16)
1.6144	0.002	8489.38 (58.53)
1.6144	0.00225	7380.02 (50.88)
1.6144	0.0025	5730.55 (39.51)
1.6144	0.00275	4104.28 (28.3)
1.6144	0.003	2817.21 (19.42)
1.6144	0.00325	1907.93 (13.15)

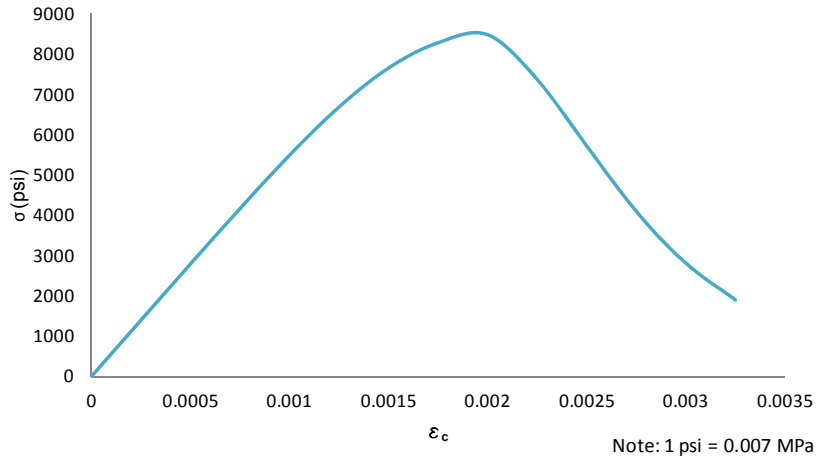

Figure 5-9 Concrete Girder Section. Compressive Stress-Strain Diagram

Elastic behavior has been considered up to $0.5 \cdot \sigma_{cu}$ with $\sigma_{cu} = \max \sigma = f'_c = 8{,}500\ psi\ (58.6\ MPa)$.

The inelastic behavior for compression started at $\sigma = 4{,}250\ psi\ (29.3\ MPa)$. The values of the stresses and their corresponding inelastic strains have been given to model the inelastic behavior of concrete in compression.

To model the tensile behavior of concrete with ABAQUS it has been used the model proposed by Wahalathantri, et al., (2011). Their model is an adaptation for ABAQUS of the tension stiffening model given by Nayal & Rasheed, (2006), Figure 5-10.

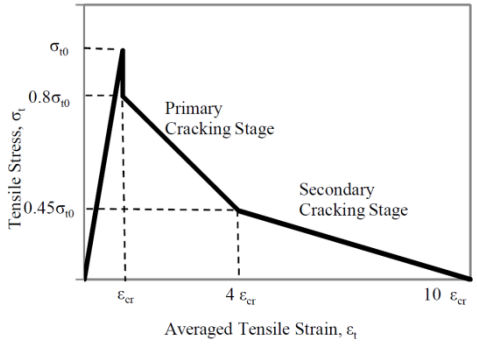

Figure 5-10 Tension Stiffening Model For Concrete (Nayal & Rasheed, 2006)

The modified tension stiffening model used by Wahalathantri, et al., (2011), that has been used for this thesis is shown in Figure 5-11.

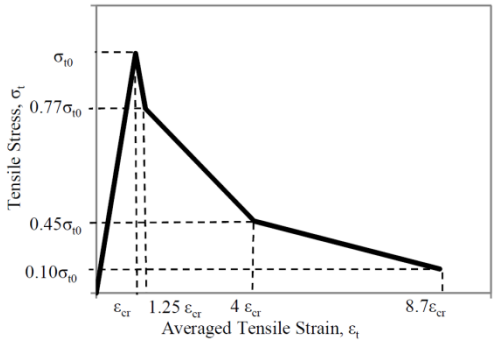

Figure 5-11 Tension Stiffening Model for ABAQUS (Wahalathantri, et al., 2011)

From Figures 5-10 and 5-11 it can be observed that the points that define the different cracking stages are not the same. To model the tensile behavior of concrete for ABAQUS Wahalathantri, et al. (2011), used the values (1.25 ε_{cr}, 0.77 σ_{t0}) and (8.7 ε_{cr}, 0.10 σ_{t0}) instead of (ε_{cr}, 0.8 σ_{t0}) and (10 ε_{cr}, 0) to avoid ABAQUS run time errors.

Applying the modified tension stiffening model for ABAQUS, the tensile behavior of the concrete girder is given by Figure 5-12.

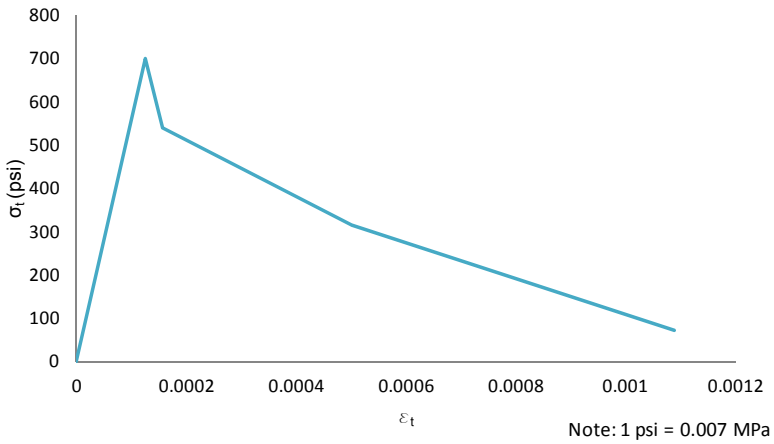

Figure 5-12 Concrete Girder Section. Tensile Stress -Average Tensile Strain Diagram

To obtain this diagram it is required to calculate the values of the tensile stress (σ_t) and the averaged tensile strain (ε_t). The maximum tensile stress is:

$$\sigma_t = \sigma_{t0} = \sigma_{cr} = f_r = 0.24 \cdot \sqrt{f'_c} = 699.71\ psi\ (4.82\ MPa)$$

The maximum tensile strain is:

$$\varepsilon_t = \varepsilon_{cr} = \sigma_{cr}/E_c = 0.00013$$

Knowing the two values given before it was possible to obtain the diagram and therefore the values needed to introduce into ABAQUS to model the tensile behavior of concrete, Table 5-3.

Table 5-3 Concrete Girder Section. Tensile Stress-Strain Values

σ_t, psi (MPa)		ε^{ela}_{cr}	ε^{ine}_{cr}
699.71	(4.82)	1.25E-04	0.00E+00
538.78	(3.71)	9.64E-05	6.01E-05
314.87	(2.17)	5.63E-05	4.44E-04
69.97	(0.48)	1.25E-05	1.08E-03

Finally, to complete the data required to use the concrete damage plasticity model, the damage parameters have to be specified. The damage parameters are two, the compressive damage, d_c, and the tensile parameter, d_t. Both values have been obtained using the equations given by Birtel & Mark, (2006).

The compressive damage is given by:

$$d_c = 1 - \frac{\sigma_c E_c^{-1}}{\varepsilon_c^{pl}(1/b_c - 1) + \sigma_c E_c^{-1}} \tag{8}$$

Where:

$$\varepsilon_c^{pl} = \varepsilon_c - \sigma_c E_c^{-1} \tag{9}$$

$$b_c = 0.7$$

ε_c^{pl} = inelastic compressive strain

ε_c = compressive strain

σ_c = compressive stress

E_c = concrete modulus of elasticity

b_c = constant factor determined experimentally

Evaluating the stresses and strains obtained from the compressive behavior into Equation 8, the values of the compressive damage parameter used in the development of the models with ABAQUS are represented in Figure 5-13.

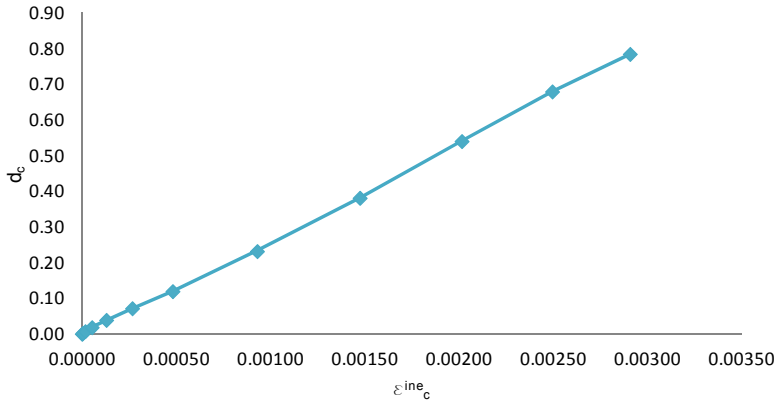

Figure 5-13 Concrete Girder Section. Compressive Inelastic Strain - Compressive Damage Diagram

The tensile damage parameter, d_t, depends on the inelastic strain and an experimentally determined parameter, b_t. The equation to obtain this parameter is:

$$d_t = 1 - \frac{\sigma_t E_c^{-1}}{\varepsilon_t^{pl}(1/b_t - 1) + \sigma_c E_c^{-1}} \tag{10}$$

With:

$$\varepsilon_t^{pl} = \varepsilon_t - \sigma_t E_c^{-1} \tag{11}$$

$$b_t = 0.1$$

ε_t^{pl} = inelastic tensile strain

ε_t = tensile strain

σ_t = tensile stress

E_c = concrete modulus of elasticity

b_t = constant factor determined experimentally

The data introduced into ABAQUS is represented by Figure 5-14.

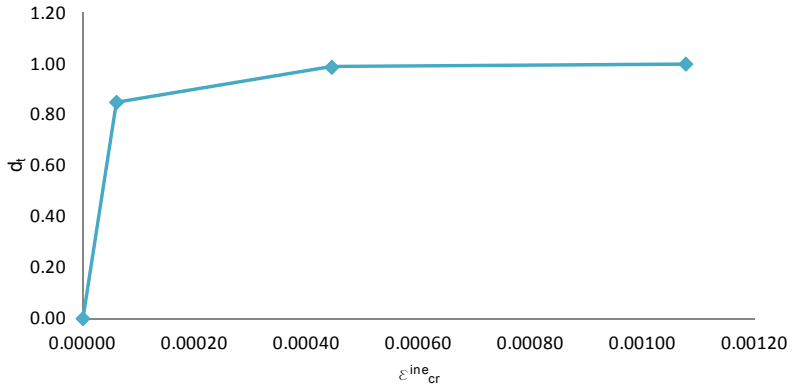

Figure 5-14 Concrete Girder Section. Tensile Inelastic Strain - Tensile Damage Diagram

5.2.2.2.- Concrete Slab Section

The material properties of slab and haunch section were defined following the same model used for the concrete girder section, concrete damaged plasticity model. The data introduced is described below.

For elastic behavior:

- $f'_c = 4000\ psi\ (27.6\ MPa)$
- $E_c = 38.34 \cdot 10^5\ psi\ (26{,}436\ MPa)$.
- $\nu = 0.2$

For concrete damaged plasticity:

Default parameters:

- Dilatation angle: 36

- Eccentricity: 0.1
- $f_{b0}/f_{c0} = 1.16$
- k = 0
- Viscosity parameter: 0

Compressive stress-strain relationship: From Equation 6 the stress-strain relationship is given by Table 5-4 and Figure 5-15.

Table 5-4 Concrete Slab and Haunch Section: Compressive Stress-Strain Values

k	ε_c	σ, psi (MPa)
1	0	0.00 (0.00)
1	0.00025	952.51 (6.57)
1	0.0005	1854.92 (12.79)
1	0.00075	2641.31 (18.21)
1	0.001	3257.66 (22.46)
1	0.00125	3680.06 (25.37)
1	0.0015	3916.87 (27.01)
1	0.00175	3998.69 (27.57)
1.114	0.002	3905.87 (26.93)
1.114	0.00225	3718.49 (25.64)
1.114	0.0025	3486.00 (24.06)
1.114	0.00275	3236.59 (22.32)
1.114	0.003	2988.16 (20.60)
1.114	0.00325	2751.03 (18.97)
1.114	0.0035	2530.39 (17.45)
1.114	0.00375	2328.26 (16.05)
1.114	0.004	2144.81 (14.79)
1.114	0.00425	1979.17 (13.65)
1.114	0.0045	1830.02 (12.62)
1.114	0.00475	1695.82 (11.69)
1.114	0.005	1575.03 (10.86)
1.114	0.00525	1466.19 (10.11)
1.114	0.0055	1367.96 (9.43)
1.114	0.00575	1279.13 (8.82)
1.114	0.006	1198.61 (8.26)
1.114	0.00625	1125.48 (7.76)
1.114	0.0065	1058.88 (7.30)
1.114	0.00675	998.10 (6.88)
1.114	0.007	942.50 (6.50)

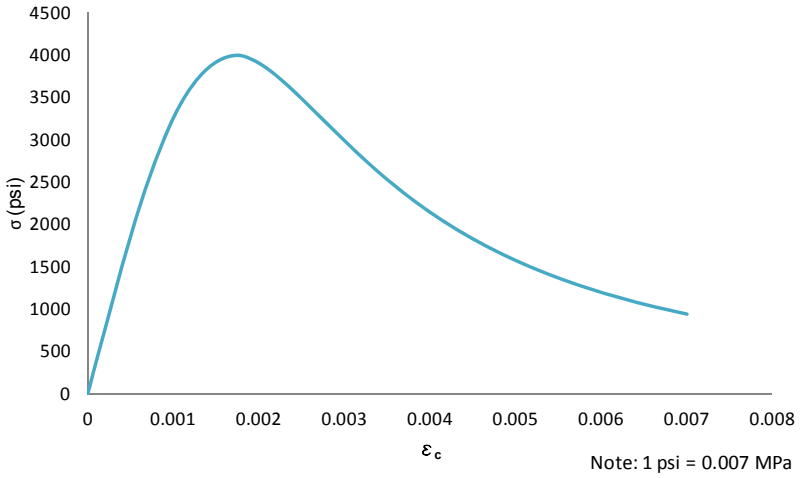

Figure 5-15 Concrete Slab and Haunch Section. Compressive Stress-Strain Diagram

The elastic behavior for compression has been assumed until $0.5 \cdot \sigma_{cu} = 0.5 \cdot f'_c = 0.5 \cdot 4{,}000 = 2{,}000\ psi\ (13.8\ MPa)$.

Using the model proposed by Wahalathantri, et al., (2011), the tensile stress-strain relationship given by Table 5-5, is shown in Figure 5-16.

Table 5-5 Concrete Slab and Haunch Section: Tensile Stress-Strain Values

σ_t, psi (MPa)		ε^{ela}_{cr}	ε^{ine}_{cr}
480.00	(3.31)	1.25E-04	0.00E+00
369.60	(2.55)	9.64E-05	6.01E-05
216.00	(1.49)	5.63E-05	4.44E-04
48.00	(0.33)	1.25E-05	1.08E-03

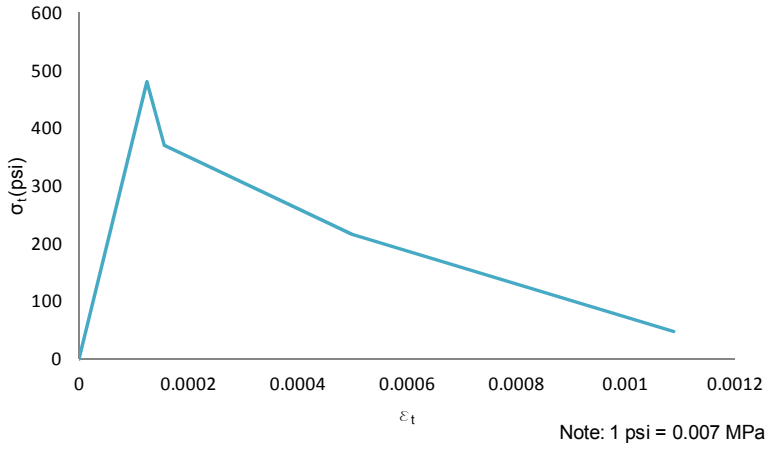

Figure 5-16 Concrete Slab and Haunch Section. Tensile Stress -Average Tensile Strain Diagram

Finally, Figures 5-17 and 5-18 show the damage parameters introduced into ABAQUS obtained from Equation 8 and 10.

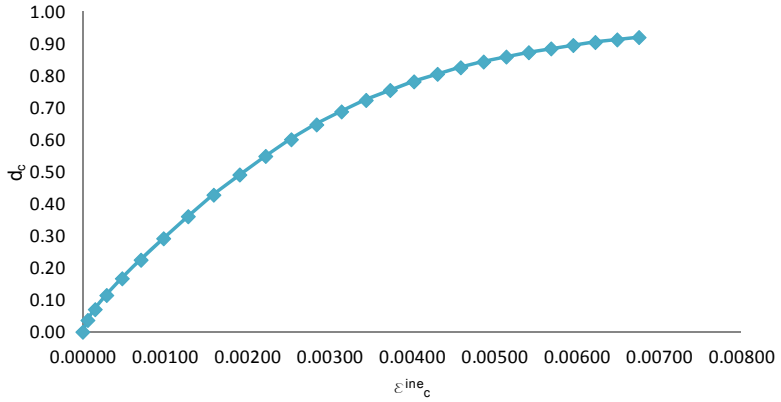

Figure 5-17 Concrete Slab and Haunch Section. Compressive Inelastic Strain - Compressive Damage Diagram

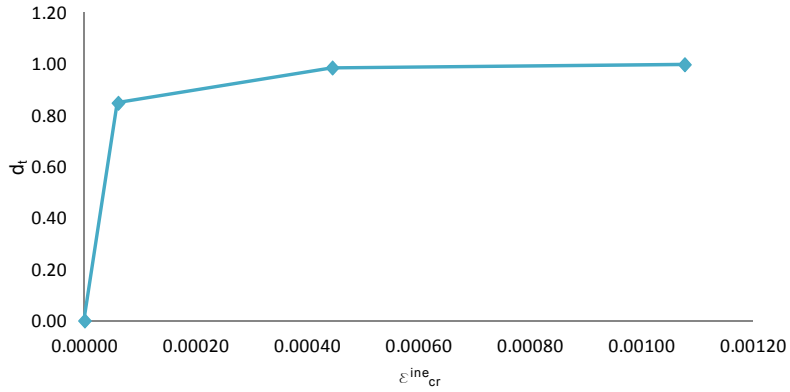

Figure 5-18 Concrete Slab and Haunch Section. Tensile Inelastic Strain - Tensile Damage Diagram

5.2.2.3.- Steel Reinforcement

The steel used for the reinforcement was a grade 60 steel. The behavior considered for the steel reinforcement is represented in the following stress-strain diagram:

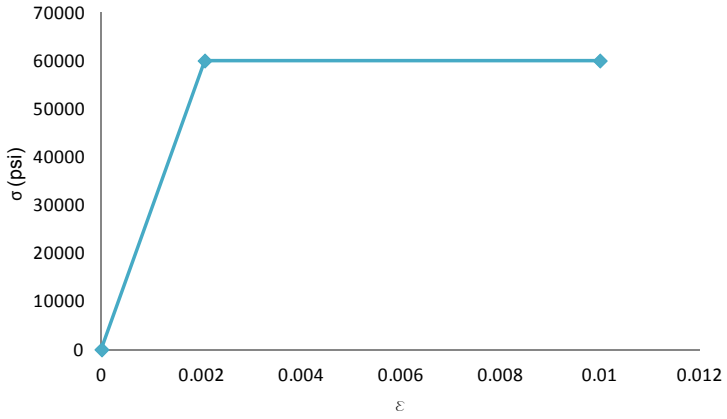

Figure 5-19 Steel Reinforcement. Stress-Strain Diagram

This is an elastic-plastic behavior. For the elastic behavior it has been introduced the following modulus of elasticity and Poisson's ratio.

$$E_s = 29 \cdot 10^6\ psi\ (199{,}948\ MPa)$$

$$\nu = 0.3$$

For the plastic behavior the yield stress considered has been:

$$f_y = 60{,}000\ psi\ (413.7\ MPa)$$

Once all the material properties were defined the following step consisted of assembling the parts to generate the complete girder model.

5.2.3.- Assembly

The assembly module is used to assemble the different parts defined in the model. Before joining the parts, each of them were placed into its final position according to the drawings. Then the parts were joined using the command interaction. For the steel reinforcement the interaction defined was embedment, the bars were embedded into the concrete girder. The union between the girder and the slab and haunch was performed by the type of interaction tie. These two types of interactions constrain the degrees of freedoms of the nodes in contact, and guarantee the compatibility in the deformation of the different elements and, therefore, an adequate stress transmission.

5.2.4.- Step

This module is used to define the type of problem to be solved and the output variables to be obtained.

A new step, step 1, was defined to introduce the loads. The type of problem defined for step 1 was static-general.

The variables selected to be computed were stresses, strains and displacements.

5.2.5.- Load

The loads and boundary conditions were defined into the load module. The girder has been considered as simply supported at both ends. All loads were introduced into step 1.

In order to establish a comparison between the results obtained by the model and the data obtained by the field test, the loads were not factored. Therefore, only one load combination has been considered for each phase, dead load plus live load, DL + LL. The model was not only subjected to dead and live loads but also to the prestress force.

The live load is the load transmitted by the truck used for the field test at each position, Figure 4-1.

For Phase 1 two different loading cases have been studied corresponding to truck position 1 and truck position 2. Both loading cases have the same dead loads and prestress force. However the live load varies according to the truck position. The loading cases computed have been:

1) Dead load + prestressed force + live load for truck position 1.
2) Dead load + prestressed force + live load for truck position 2.

5.2.5.1.- Dead Loads

The dead loads that have been considered are the dead loads from the barrier, the slab, the haunch and the girder. These dead loads have been defined by the self-weight of each part. Their characteristic are:

- Barrier: the type of barrier used was C221. It is a 1 ft wide barrier and its length is the same that the beam, 1,016 in (25,806 mm). According to the drawings from appendix A, the railing weight, w_r, is 495 plf (7,340 N/m).
- Slab: The wide of slab considered is the effective flange, b_e = 110.69 in (2,811 mm). Its depth is 8 in (203 mm) and the concrete weight, w_{cs}, is 150 pcf (23,829 N/m^3).
- Haunch: The haunch has the same width that the top flange of the girder, that is 36 in (914 mm), and its depth is 2 in (51 mm). The weight of the concrete for the haunch is the same that the concrete used for slab, 150 pcf (23,829 N/m^3).
- Girder: According to the drawings the girder weight, w_g, used has been 793 plf (11,760 N/m).

5.2.5.2.- Prestress Force

To obtain the effective prestress force, F_e, for each strand it was necessary to compute the effective stress, f_{pe}, and then multiply this value by the nominal area, A_n, of one strand.

The effective stress has been obtained using AASHTO 2012. The effective stress is the stress that remains after all losses have occurred. According to article 5.9.5.1. from AASHTO 2012, the total loss of prestress is obtained as:

$$\Delta f_{pT} = \Delta f_{pES} + \Delta f_{pLT} \quad (12)$$

Where:

Δf_{pT} = Total loss (ksi)

Δf_{pES} = Sum of all losses or gains due to elastic shortening or extension at the time of application of prestress and/or external loads (ksi)

Δf_{pLT} = Losses due to long-term shrinkage and creep of concrete, and relaxation of the steel (ksi).

The elastic shortening has been obtained from article 5.9.5.2.3 of AASHTO 2012. For pretensioned members the loss due to elastic shortening is:

$$\Delta f_{pES} = \frac{E_P}{E_{ct}} f_{cgp} \tag{13}$$

Where:

E_p = modulus of elasticity of prestressing steel (ksi)

E_{ct} = modulus of elasticity of concrete at transfer or time of load application (ksi)

f_{cgp} = the concrete stress at the center of gravity of prestressing tendons due to the prestressing force immediately after transfer and the self-weight of the member at the section of maximum moment (ksi).

From the commentary section the loss due to elastic shortening in pretensioned member may be determined as follow:

$$\Delta f_{pES} = \frac{A_{ps} \cdot f_{pbt} \cdot (I_g + e_m{}^2 \cdot A_g) - e_m \cdot M_g \cdot A_g}{A_{ps} \cdot (I_g + e_m{}^2 \cdot A_g) + \frac{A_g \cdot I_g \cdot E_{ci}}{E_p}} \tag{14}$$

Where:

A_{ps} = area of prestressing steel (in^2)

A_g = gross area of section (in^2)

E_{ci} = modulus of elasticity of concrete at transfer (ksi)

E_p = modulus of elasticity of prestressing tendons (ksi)

e_m = average prestressing steel eccentricity at midspan (in)

f_{pbt} = stress in prestressing steel immediately prior to transfer (ksi)

I_g = moment of inertia of gross concrete section (in^4)

M_g = midspan moment due to member self-weight (kip-in)

From drawings:

$$A_{ps} = A_n * n_T = 0.153 * 42 = 6.43\ in^2\ (4{,}148\ mm^2)$$

$$A_g = 761\ in^2\ (490{,}966\ \ mm^2)$$

From article 5.4.4.2 of AASHTO 2012:

$$E_p = 28500\ ksi\ (196{,}500\ MPa)$$

From article 5.4.2.4 of AASHTO 2012:

$$E_{ci} = 33{,}000 \cdot K_1 \cdot {w_c}^{1.5}\sqrt{f'_{ci}} \quad (15)$$

Where:

$$k_1 = 1$$

$$w_c = 0.15\ kcf\ (23.8\ \ kN/m^3)$$

$$f'_{ci} = 6.3\ ksi\ (43.4\ MPa)$$

Substituting the values:

$$E_{ci} = 4811.95\ \ ksi\ (33{,}177\ MPa)$$

From Table 5.9.3-1, AASHTO 2012, for low relaxation strands:

$$f_{pbt} = 0.75 * f_{pu} \quad (16)$$

$$f_{pbt} = 0.75 * 270 = 202.5\ ksi\ (1{,}396\ MPa)$$

The moment at midspan due to the self-weight is:

$$M_g = \frac{w*l^2}{8} \quad (17)$$

For $\omega = 793\ plf\ (11{,}760.2\ \ N/m)$ and $l = 84.667\ ft\ (25.81\ m)$

$$M_g = 710.6\ kip.ft = 8526.93\ kip.in\ (937\ kN.m)$$

Finally the loss due to elastic shortening is:

$$\Delta f_{pES} = 14.24\ ksi\ (14.24\ MPa)$$

To obtain the prestress losses due to creep, shrinkage and relaxation, or time dependent losses, AASHTO 2012 provides two different methods. The first method or

approximate method uses an equation to compute the time dependent losses, obtained as an approximation of the refined method for a wide range of standard prestressed concrete I-beam. This method is conservative. The second method is more accurate, it is the refined method. This method provides a better estimate of the time dependent losses. To compute this method it is necessary to provide the time between transfer and deck placement and the time between deck placement and final time. Since there is not enough data for the time between transfer and deck placement for this case, the approximate method given by AASHTO 2012, article 5.9.5.3 has been used. The long term prestress loss, Δf_{pLT}, has been estimated using the following formula:

$$\Delta f_{pLT} = 10 \cdot \frac{f_{pi} \cdot A_{ps}}{A_g} \cdot \gamma_h \cdot \gamma_{st} + 12 \cdot \gamma_h \cdot \gamma_{st} + \Delta f_{pR} \quad (18)$$

In which:

$$\gamma_h = 1.7 - 0.01H \quad (19)$$

$$\gamma_{st} = \frac{5}{1 + f'_{ci}} \quad (20)$$

f_{pi} = prestressing steel immediately prior to transfer (ksi)

$$f_{pi} = 0.75 * f_{pu} = 202.5\ ksi\ (1{,}396\ MPa)$$

H = the average annual ambient relative humidity (%)

$$H = 70\%$$

γ_h = correction factor for relative humidity of ambient air

$$\gamma_h = 1$$

γ_{st} = correction factor for specified concrete strength at time of prestress transfer to the concrete member

$$\gamma_{st} = 0.685$$

Δf_{pR} = an estimate of relaxation loss taken 2.4 ksi for low relaxation strand.

Substituting the values:

$$\Delta f_{pLT} = 11.71 + 8.22 + 2.4 = 22.33\ ksi\ (154\ MPa)$$

Finally the total value of the prestress losses is:

$$\Delta f_{pT} = \Delta f_{pES} + \Delta f_{pLT} \tag{21}$$

$$\Delta f_{pT} = 14.24 + 22.33 = 36.572\ ksi\ (252\ MPa)$$

The effective stress in strand, f_{pe}, is obtained as:

$$f_{pe} = f_{pi} - \Delta f_{pT} \tag{22}$$

$$f_{pe} = 202{,}500 - 36{,}572 = 165{,}928\ psi\ (1{,}144\ MPa)$$

Effective prestress force for each strand:

$$F_e = f_{pe} * A_n \tag{23}$$

$$F_e = 25{,}387\ lbs\ (112{,}927\ N)$$

To reduce the computational cost and because the contribution of prestressing steel to the stiffness of the girder section is minimum (Saiedi, 2007), the prestressing strands have not been included in the ABAQUS model as a part.

The modeling of the prestress strands has been realized introducing in ABAQUS their equivalent forces. These equivalent forces have been obtained using the load-balancing method, Figure 5-20.

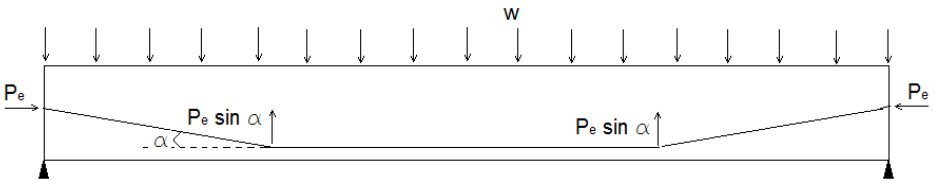

Figure 5-20 Load-Balancing Method

According to this method the prestress force is equivalent to a combination of two forces. These two forces are:

- Compressive axial force, P_e, equal to:

$$P_e = F_e \tag{24}$$

- Vertical force, P_{ev}, applied on the draped points, equal to:

$$P_{ev} = F_e \cdot \sin \alpha \tag{25}$$

Where α is the angle of the depressed strand.

For the girder studied the compressive axial force has been applied at the ends of the girder for each strand. The value of this force is equal to the effective prestress force of the strand.

$$P_e = F_e = \ 25{,}387 \ \ lbs \ (112{,}927 \ N)$$

The vertical force is zero for straight strands and equal to P_{ev} for the depressed strands. This force has been applied at each draped point, located respectively at 5 ft (1.52 m) and 2 in (51 mm) from midspan.

$$P_{ev} = F_e \cdot \sin \alpha = 2{,}042 \ lbs \ (9{,}085 \ N)$$

With:

$$F_e = \ 25{,}387 \ \ lbs \ (112{,}927 \ N)$$

$$\alpha = 0.08 \ rad$$

5.2.5.3.- Live Load: Truck Position 1

The characteristics of the truck used to compute the live load are:

- Total weight, w_T = 90,000 lbs (400,340 N)
- Number of axles, N =6
- Truck width, B = 8 ft (2.44 m)
- Load for axle 1 to 3, P_1 = 18,000 lbs (80,068 N)
- Load for axle 4 to 6, P_2 = 12,000 lbs (53,379 N)
- Total length, l_T = 42 ft (12.8 m)

- Distance between axle 1 and 2, l_1 = 12 ft (3.66 m)
- Distance between axle 2 and 3, l_2 = 4 ft (1.22 m)
- Distance between axle 3 and 4, l_3 = 18 ft (5.49 m)
- Distance between axle 4 and 5, l_4 = 4 ft (1.22 m)
- Distance between axle 5 and 6, l_5 = 4 ft (1.22 m)

At truck position 1, the truck was centered over the damage at 3.5 ft (1.07 m) from the barrier, see Figure 4-3. To compute the load it has been considered that the axle number six was 1 ft (0.3 m) from support ant the axle number 1 at 43 ft (13.11 m) from the southernmost support.

To obtain the load transmitted for each axle to the damaged girder, it has been used the lever rule. The final loads to be applied to the girder models are calculated by applying the distribution factor given by this method to the total axle's load. According to NCHRP Report 592, (2007):

> "the lever rule is defined as an approximate distribution factor method that assumes no transverse deck moment continuity at interior beams, which renders the transverse deck cross section statically determinate."

This is equivalent to establish a hinge in the interior beam doing the bending moment zero at this point. Hence it is possible to take moment about this point and determine a distribution factor.

For truck position 1 the distribution factor obtained applying the lever rule is determined as follows:

Case 1: Truck positioned over damaged girder at 3.5 ft (1.07 m) from barrier:

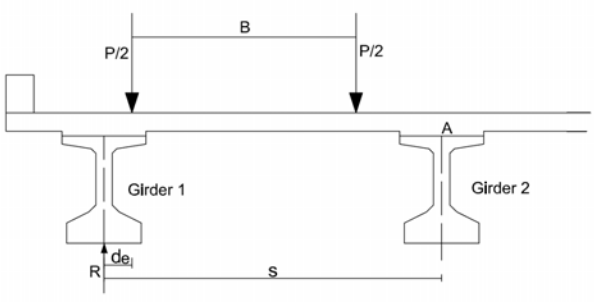

Figure 5-21 Lever Rule. Case 1

Taking moment about point A the distribution factor is:

$$\sum M_A = 0 = \frac{P}{2} \cdot (s - d_e) + \frac{P}{2} \cdot (s - d_e - B) - R \cdot s$$

$$\frac{P}{2} \cdot (2s - 2de - B) = R \cdot s$$

$$DF_1 = \frac{R}{P} = 1 - \frac{d_e}{s} - \frac{B}{2s} \quad (26)$$

For truck position 1, at 3.5 ft (1.07 m) from barrier:

$$d_e = 1\ ft\ (0.3\ m)$$

$$s = 11.45\ ft\ (3.5\ m)$$

$$B = 8\ ft\ (2.44\ m)$$

$$DF_1 = 0.563$$

Applying this distribution factor, the live loads transmitted for each axle are:

For axles 1, 2 and 3, P_1 = 18,000 lbs (80,068 N)

$$P_{g1} = DF_1 \cdot P_1 = 10{,}139\ lbs\ (45{,}101\ N)$$

For axles 4, 5 and 6, P_2 = 12,000 lbs (53,379 N)

$$P_{g2} = DF_1 \cdot P_2 = 6{,}759.37\ lbs\ (30{,}067\ N)$$

To introduce the live loads into ABAQUS, these loads have been applied on a surface equivalent to the tire contact area of the wheel over the girder. This contact area

has been taken as 360 in^2 (232,257 mm^2). Table 5-6 shows the value of the live load introduced for each axle and the center location of each load.

Table 5-6 Live Load. Truck Position 1

	Live Load, psi (MPa)		z, ft (m)	
Axle 1	28.16	(0.19)	43	(13.11)
Axle 2	28.16	(0.19)	31	(9.45)
Axle 3	28.16	(0.19)	27	(8.23)
Axle 4	18.78	(0.13)	9	(2.74)
Axle 5	18.78	(0.13)	5	(1.52)
Axle 6	18.78	(0.13)	1	(0.3)

5.2.5.4.- Live Load: Truck Position 2

At truck position 2, the truck was over girder 2, at 10.95 ft (3.34 m) from barrier, see Figure 4-4

For this position the distribution factor is:

Case 2: Truck positioned over next undamaged girder at 10.95 ft (3.34 m) from barrier:

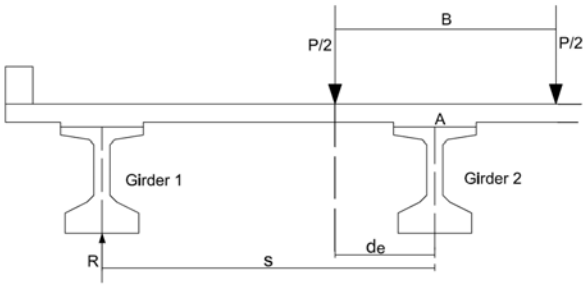

Figure 5-22 Lever Rule. Case 2

Taking moment about point A the distribution factor is:

$$\sum M_A = 0 = \frac{P}{2} \cdot d_e - R \cdot s$$

$$\frac{P}{2} \cdot d_e = R \cdot s$$

$$DF_2 = \frac{R}{P} = \frac{d_e}{2s} \quad (27)$$

The distribution factor that has been applied for truck position 2 is:

$$d_e = 3\ ft\ (0.91\ m)$$

$$s = 11.45\ ft\ (3.5\ m)$$

$$B = 8\ ft\ (2.44\ m)$$

$$DF_2 = 0.131$$

For this distribution factor, the live loads transmitted for each axle are:

For axles 1, 2 and 3, P_1 = 18,000 lbs (80,068 N)

$$P_{g1} = DF_2 \cdot P_1 = 2{,}358.3\ lbs\ (10{,}490\ N)$$

For axles 4, 5 and 6, P_2 = 12,000 lbs (53,379 N)

$$P_{g2} = DF_2 \cdot P_2 = 1{,}572.2\ lbs\ (6{,}993\ N)$$

The live loads introduced into ABAQUS on an area of 360 in^2 (232,257 mm^2) can be shown in Table 5-7.

Table 5-7 Live Load. Truck Position 2

	Live Load, psi (MPa)		z, ft (m)	
Axle 1	6.55	(0.05)	43	(13.11)
Axle 2	6.55	(0.05)	31	(9.45)
Axle 3	6.55	(0.05)	27	(8.23)
Axle 4	4.37	(0.03)	9	(2.74)
Axle 5	4.37	(0.03)	5	(1.52)
Axle 6	4.37	(0.03)	1	(0.3)

5.2.6.- Mesh

This module is used to define the size and type of elements that form the mesh. Smaller elements lead to more accurate results. However the use of smaller elements

involves greater computational cost. Therefore it is important to balance the computational cost with the element size.

In order to obtain a structured mesh the element type used has been the 3D solid tetrahedral elements, C3D4, for concrete elements and 3D truss elements, T3D2, for the wires.

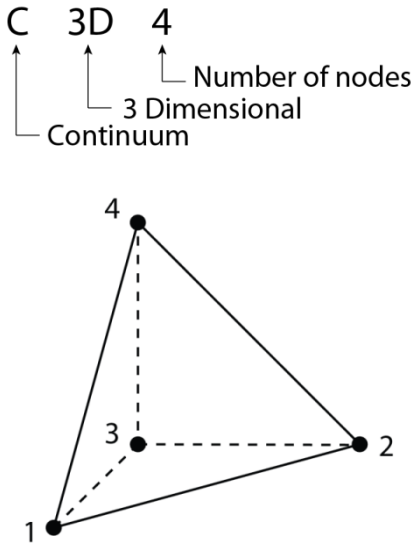

Figure 5-23 Tetrahedral Elements

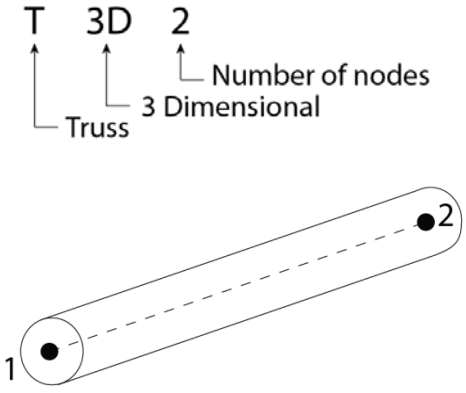

Figure 5-24 3D Truss Elements

The computation was performed first using 15 in (381 mm) elements size. After checking that the model did not have errors, the size of the elements was gradually reduced to 3 in (76.2 mm). Size elements smaller than 3 in (76.2 mm) had a great computational cost that overcame the capacity of the computer used. Therefore, the element used for the mesh had a maximum size of 3 in (76.2 mm), Figure 5-25.

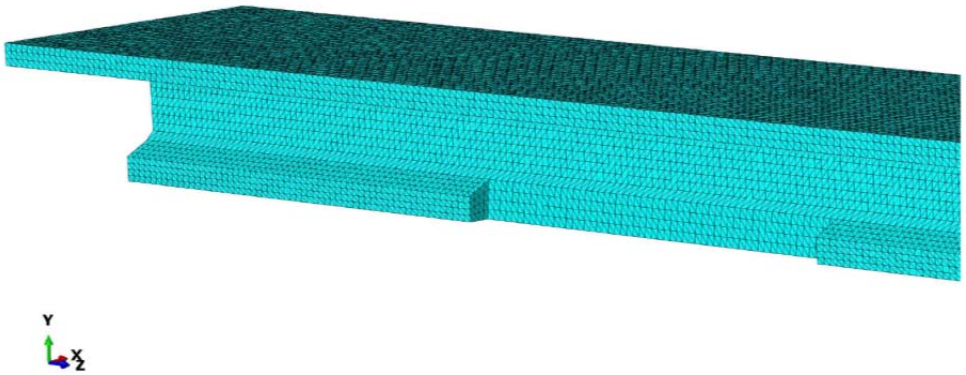

Figure 5-25 Damaged Girder Mesh

This size element was used for modeling not only phase 1 but also Phase 2.

The definition of the mesh was the last step needed to compute the model. The results obtained from the model developed with ABAQUS are explained in Chapter 6.

5.3.- Phase 2: Repaired Girder Model

To model the Phase 2 of the field test four different loading cases corresponding with truck position 3 to 6 have been analyzed. The model was performed following the same steps than for the Phase 1 model.

5.3.1.- Geometry

To model the Phase 2, five different parts were introduced:

1) Concrete girder section
2) Concrete slab and haunch section
3) Steel reinforcement
4) Concrete repaired section
5) Fiber glass rebar

Three of these parts, part 1 through part 3, were the same parts defined for the Phase 1 model. The geometry of the two news parts is defined below.

5.3.1.1.- Concrete Repaired Section

This part was defined as a 3D deformable extrusion solid. It has the same length than the damage. Its dimensions and position into the ABAQUS model are shown in Figures 5-26 and 5-27.

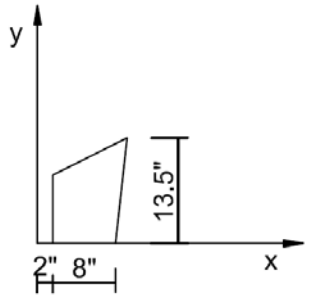

Note: 1 in = 25.4 mm

Figure 5-26 Concrete Repaired Section

Figure 5-27 ABAQUS Concrete Repaired Section

5.3.1.2.- Fiber Glass Rebar

The fiber glass rebar have been defined as a 3D deformable wire with a truss section. The dimensions of the fiber glass rebar used are defined by Table 5-8.

Table 5-8 Fiber Glass Rebar

Type	Nominal Diameter, ϕ, in (mm)	Nominal Area, A_n, in^2(mm^2)
#4	0.5 (12.7 mm)	0.1963 (127)

The rebar were placed according to the repair sketch shown in Figure 5-28.

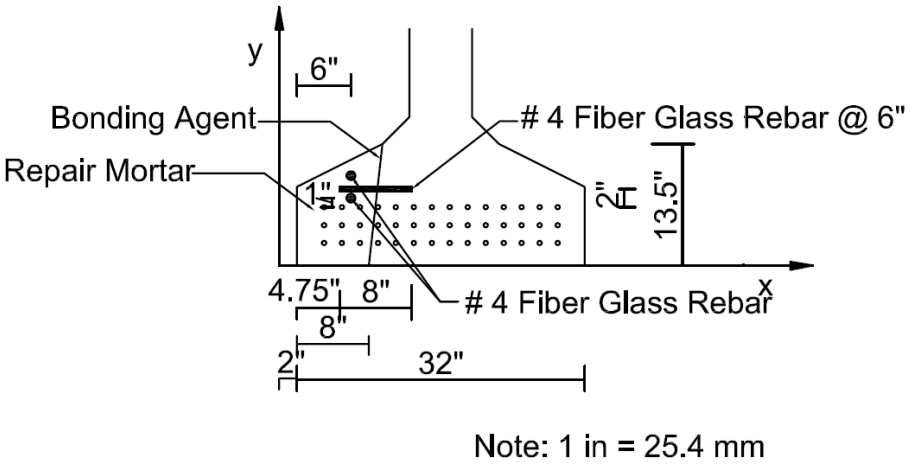

Figure 5-28 Fiber Glass Rebar Sketch

5.3.2.- Material Properties

The material properties for parts 1, 2 and 3 are the same than the ones used for the same parts in the Phase 1 model.

5.3.2.1.- Concrete Repaired Section

To model the concrete repaired section the material properties were defined following the same criteria used for the concrete girder section. Therefore, the concrete damaged plasticity model was used. The data introduced into ABAQUS are described below.

For elastic behavior:

- $f'_c = 6{,}000\ psi\ (41.4\ MPa)$
- $E_c = 43.25 \cdot 10^5\ psi\ (29{,}822\ MPa)$
- $\nu = 0.2$

For concrete damaged plasticity:

Default parameters:

- Dilatation angle: 36
- Eccentricity: 0.1
- $f_{b0}/f_{c0} = 1.16$
- k = 0
- Viscosity parameter: 0

Compressive stress-strain relationship: From Equation 6 the stress - strain values are given by Table 5-9. Figure 5-29 shows the stress-strain diagram.

Table 5-9 Concrete Repaired Section: Compressive Stress-Strain Values

k	ε_c	σ, psi (Mpa)	
1	0	0.00	(0.00)
1	0.00025	1080.72	(7.45)
1	0.0005	2151.42	(14.83)
1	0.00075	3183.05	(21.95)
1	0.001	4126.90	(28.45)
1	0.00125	4923.20	(33.94)
1	0.0015	5517.01	(38.04)
1	0.00175	5875.74	(40.51)
1	0.002	5999.49	(41.37)
1.34	0.00225	5643.58	(38.91)
1.34	0.0025	5060.29	(34.89)
1.34	0.00275	4390.60	(30.27)
1.34	0.003	3729.00	(25.71)
1.34	0.00325	3129.29	(21.58)
1.34	0.0035	2612.50	(18.01)
1.34	0.00375	2179.94	(15.03)
1.34	0.004	1823.47	(12.57)
1.34	0.00425	1531.77	(10.56)
1.34	0.0045	1293.47	(8.92)

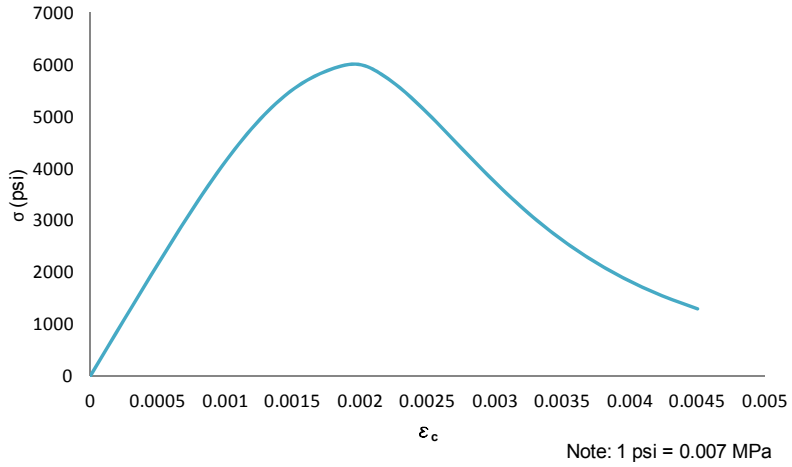

Figure 5-29 Concrete Repaired Section. Compressive Stress-Strain Diagram

The inelastic behavior for compression has been assumed to begin at $0.5 \cdot \sigma_{cu} = 0.5 \cdot f'_c = 0.5 \cdot 6{,}000 = 3{,}000\ psi\ (20.7\ MPa)$.

The tensile stress-strain values are given by Table 5-10. The diagram is shown in Figure 5-30.

Table 5-10 Concrete Repaired Section: Tensile Stress-Strain Values

σ_t, psi (MPa)	ε^{ela}_{cr}	ε^{ine}_{cr}
587.88 (4.05)	1.36E-04	0.00E+00
452.67 (3.12)	1.05E-04	6.52E-05
264.54 (1.82)	6.12E-05	4.82E-04
58.79 (0.41)	1.36E-05	1.17E-03

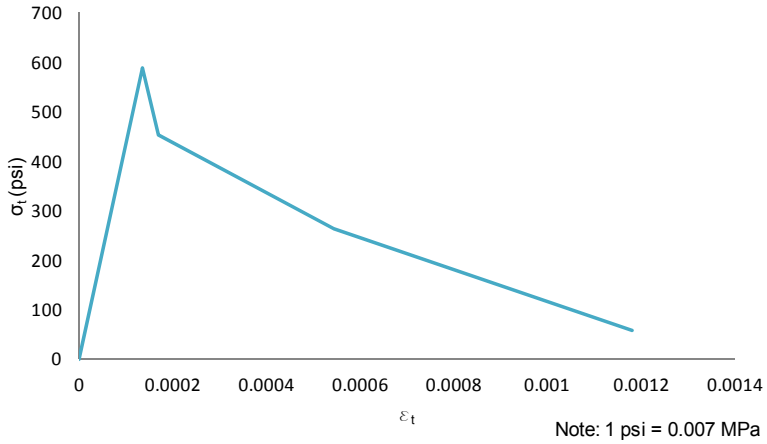

Figure 5-30 Concrete Repaired Section. Tensile Stress -Average Tensile Strain Diagram

From Equations 8 and 10 the damage parameters for the concrete repaired section are shown in Figures 5-31 and 5-32.

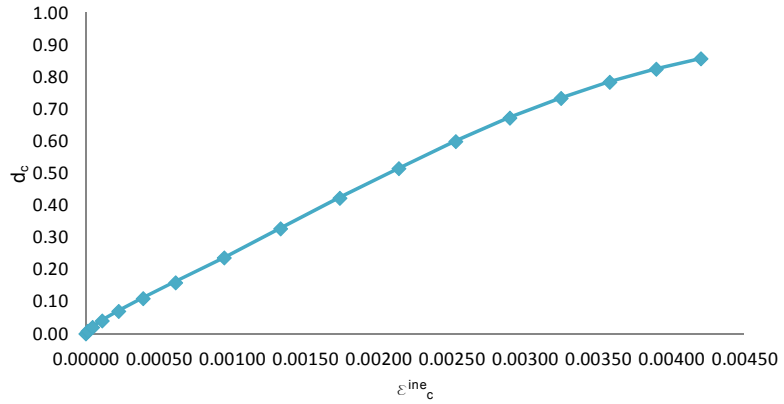

Figure 5-31 Concrete Repaired Section. Compressive Inelastic Strain - Compressive Damage Diagram

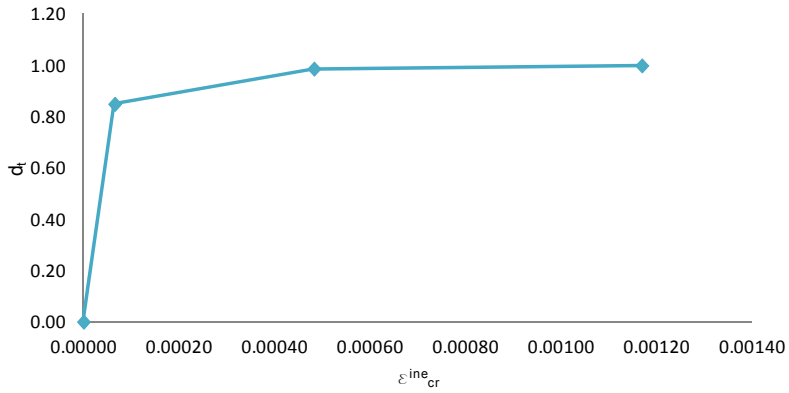

Figure 5-32 Concrete Repaired Section. Tensile Inelastic Strain - Tensile Damage Diagram

5.3.2.2.- Fiber Glass Rebar

The behavior considered for the fiber glass rebar was elastic. The stress-strain diagram is shown in Figure 5-33.

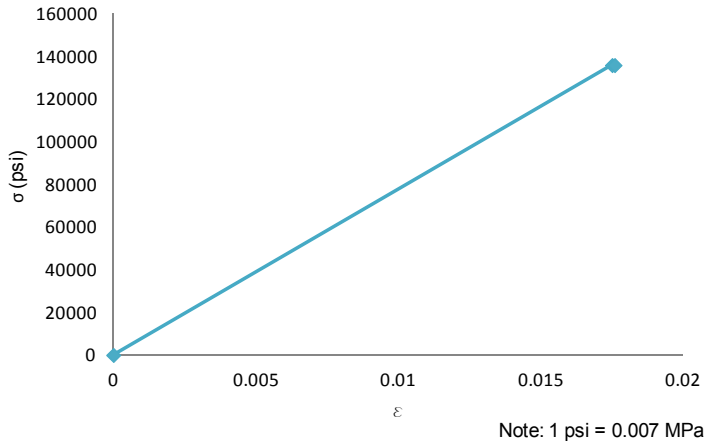

Figure 5-33 Fiber Glass Rebar. Stress-Strain Diagram

For the elastic behavior it has been introduced the following modulus of elasticity and Poisson's ratio:

$$E_s = 77.68 \cdot 10^5\ psi\ (53{,}558\ MPa)$$

$$\nu = 0.26$$

5.3.3.- Assembly

The same criteria and procedures followed in the development of the Phase 1 model have been used. The two new parts were incorporated into their final position. The fiber glass rebar were embedded into the girder and the repaired sections.

5.3.4.- Step

It was defined a new step, step 1, in which the loads were introduced. The problem type was static general. The variables defined were stresses, strains and displacements.

5.3.5.- Load

For Phase 2 the dead loads and the prestress force used have been the same than the loads obtained for Phase 1.

Similarly to the live loads obtained for Phase 1, the live loads for Phase 2 have been computed using the lever rule.

5.3.5.1.- Live Load: Truck Position 3

At truck position 3, the truck was at end of the damaged girder at 3.5 ft (1.07 m) from the barrier, see Figure 4-8. The axle number six was 1 ft (0.3 m) from support and the axle number 1 at 43 ft (13.11 m) from the southernmost support.

Using the case 1 of the lever rule the distribution factor applied for truck position 3, at 3.5 ft from barrier is:

$$DF_1 = 0.563$$

Therefore, the live loads transmitted for each axle are:

For axles 1, 2 and 3, P_1 = 18,000 lbs (80,068 N)

$$P_{g1} = DF_1 \cdot P_1 = 10{,}139\ lbs\ (45{,}101\ N)$$

For axles 4, 5 and 6, P_2 = 12,000 lbs (53,379 N)

$$P_{g2} = DF_1 \cdot P_2 = 6{,}759.37\ lbs\ (30{,}067\ N)$$

The values of the live loads introduced for each axle applied over a contact area of 360 in^2 (232,257 mm^2) are shown in Table 5-11. This table also includes the center location of each live load.

Table 5-11 Live Load. Truck Position 3

	Live Load, psi (MPa)		z, ft (m)	
Axle 1	28.16	(0.19)	43	(13.11)
Axle 2	28.16	(0.19)	31	(9.45)
Axle 3	28.16	(0.19)	27	(8.23)
Axle 4	18.78	(0.13)	9	(2.74)
Axle 5	18.78	(0.13)	5	(1.52)
Axle 6	18.78	(0.13)	1	(0.3)

5.3.5.2.- Live Load: Truck Position 4

For truck position 4, the truck was at 3.5 ft (1.07 m) from the barrier, Figure 4-9. In this case the axle number six was at 21.33 ft (6.50 m) from support and the axle number 1 at 63.33 ft (19.30 m) from the southernmost support.

The distribution factor applied was the same that the distribution factor for truck position 3, DF_1, case 1 of the lever rule. Although the live load values obtained are the same than those for truck position 3, the points of application are different. Table 5-12 gives the values and the center location of each live load.

Table 5-12 Live Load. Truck Position 4

	Live Load, psi (MPa)		z, ft (m)	
Axle 1	28.16	(0.19)	63.33	(19.30)
Axle 2	28.16	(0.19)	51.33	(15.65)
Axle 3	28.16	(0.19)	47.33	(14.43)
Axle 4	18.78	(0.13)	29.33	(8.94)
Axle 5	18.78	(0.13)	25.33	(7.72)
Axle 6	18.78	(0.13)	21.33	(6.50)

5.3.5.3.- Live Load: Truck Position 5

In this case to obtain the live loads, case 2 of the lever rule has been used. For truck position 5 the truck was at 10.95 ft (3.34 m) from the barrier, Figure 4-10.

The distribution factor used was:

$$DF_2 = 0.131$$

The live loads transmitted for each axle are:

For axles 1, 2 and 3, P_1 = 18,000 lbs (80,068 N)

$$P_{g1} = DF_2 \cdot P_1 = 2{,}358.3\ lbs\ (10{,}490\ N)$$

For axles 4, 5 and 6, P_2 = 12,000 lbs (53,379 N)

$$P_{g2} = DF_2 \cdot P_2 = 1{,}572.2\ lbs\ (6{,}993\ N)$$

Table 5-13 shows the live loads introduced into ABAQUS.

Table 5-13 Live Load. Truck Position 5

	Live Load, psi (MPa)		z, ft (m)	
Axle 1	6.55	(0.05)	43	(13.11)
Axle 2	6.55	(0.05)	31	(9.45)
Axle 3	6.55	(0.05)	27	(8.23)
Axle 4	4.37	(0.03)	9	(2.74)
Axle 5	4.37	(0.03)	5	(1.52)
Axle 6	4.37	(0.03)	1	(0.3)

5.3.5.4.- Live Load: Truck Position 6

The last live load computed was the live load for truck position 6, Figure 4-11. At this position the truck was located at 10.95 ft (3.34 m) from the barrier, case 2 lever rule. Therefore the distribution factor applied has been the same than the distribution factor used for truck position 5.

The values of the live loads are given by Table 5-14.

Table 5-14 Live Load. Truck Position 6

	Live Load, psi (MPa)		z, ft (m)	
Axle 1	6.55	(0.05)	63.33	(19.30)
Axle 2	6.55	(0.05)	51.33	(15.65)
Axle 3	6.55	(0.05)	47.33	(14.43)
Axle 4	4.37	(0.03)	29.33	(8.94)
Axle 5	4.37	(0.03)	25.33	(7.72)
Axle 6	4.37	(0.03)	21.33	(6.50)

5.3.6.- Mesh

The mesh used to model the Phase 2 has the same characteristic than the mesh used to model the damaged girder. That is:

Size of element: 3 in (76.2 mm)

Type of element:

- Tetrahedral, C3D4, for concrete elements
- 3D truss element, T3D2, for wires.

With these characteristics the mesh created for Phase 2 have been the same for the different truck positions considered. Figure 5-34 shows the mesh generated using these elements:

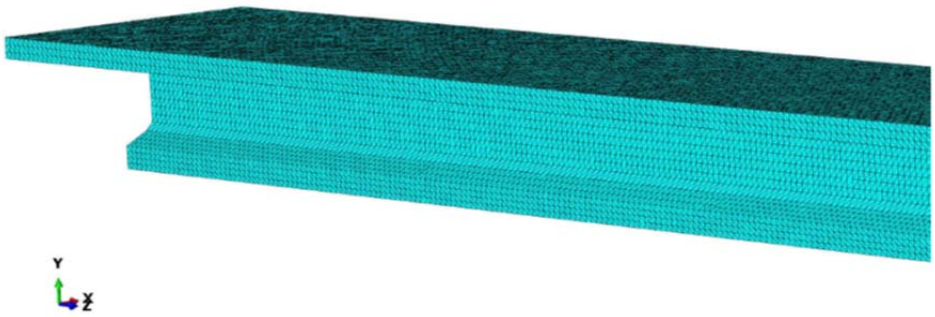

Figure 5-34 Repaired Girder Mesh

The results obtained for Phase 2 are explained in Chapter 6.

Chapter 6

RESULTS

This chapter analyzes the results obtained from the finite element models generated using ABAQUS. It is divided in two parts. The first part studies the strains given by the model for each phase and compares these values to the strains measured by the gauges in the field testing. This comparison also serves to validate the finite element model. The second part of this chapter discusses the stresses obtained from ABAQUS at a section located at the center of the repaired section.

6.1.- Strains

To compare the strains given by ABAQUS to the average strains measured from the field testing the strains values of the closer nodes to the location of the strain gauges have been used. The coordinates of each strain gauge and its corresponding node refer to the models coordinate systems are given by Table 6-1.

Table 6-1 Strain Gauges Coordinates & Nodes

Gauge	Coordinate, in (mm)						Node
	x		y		z		
SG 01	18	(457.2)	0	(0.0)	516	(13106.4)	22424
SG 02	23	(584.2)	15	(381.0	516	(13106.4)	4334
SG 03	21.5	(546.1)	22	(558.8)	312	(7924.8)	15006
SG 04	21.5	(546.1)	22	(558.8)	288	(7315.2)	14998
SG 05	18	(457.2)	0	(0.0)	264	(6705.6)	17870
SG 06	13	(330.2)	15	(381.0)	264	(6705.6)	3008
SG 07	6	(152.4)	0	(0.0)	264	(6705.6)	303

As explained before, the strain values to be compared to the strains measured by the gauges have been obtained by the difference of two strains. The first strain was the strain corresponding to the state 0, where only dead loads and prestress force were

applied. The second strain was the strain obtained from a state with dead loads, prestress force and its corresponding live load, state 1. This was due to the fact that the strain measured in the field test did not include the deformation of the girder once in place and subjected to the self-weight of the rest of the bridge superstructure elements.

6.1.1.- Phase 1

As mentioned before, Phase 1 includes two loading cases. These two loading cases correspond to the two truck positions of the field testing for Phase 1.

The strain values from the field test for each strain gauge are shown in Table 6-2.

Table 6-2 Strains Phase 1 Field Testing

Gauge	Strain	
	Truck Position 1	Truck Position 2
SG 01	5.567E-05	1.346E-05
SG 02	3.138E-05	9.400E-06
SG 03	2.265E-05	3.480E-06
SG 04	2.083E-05	3.120E-06
SG 05	6.635E-05	1.215E-05
SG 06	5.591E-05	1.121E-05

For this phase the strains obtained for the state 0 are shown in Figure 6-1.

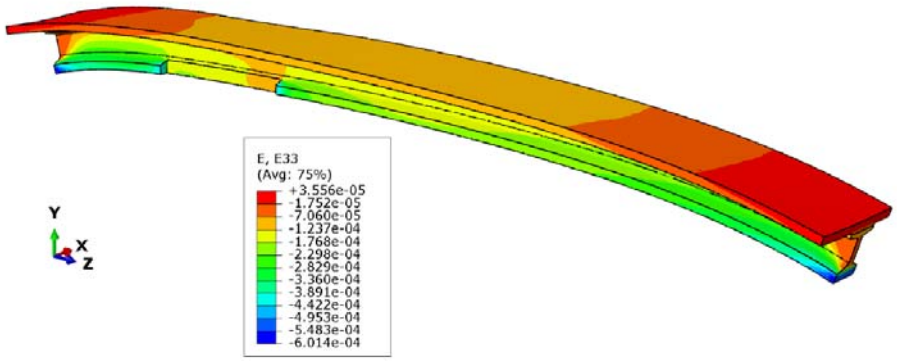

Figure 6-1 Strains. State 0

Figure 6-1 shows the maximum and minimum strain values that have been obtained for the damaged girder. However the values that have been used are those corresponding with the nodes given by Table 6-1. Table 6-3 gives the strains of these nodes for state 0.

Table 6-3 Strains. State 0 Phase 1

Gauge	Node	Strain
		State 0
SG 01	22424	-1.785E-04
SG 02	4334	-1.637E-04
SG 03	15006	-1.266E-04
SG 04	14998	-1.298E-04
SG 05	17870	-1.653E-04
SG 06	3008	-1.431E-04

6.1.1.1.- Truck Position 1

Figure 6-2 shows the strains obtained from ABAQUS for state 1.

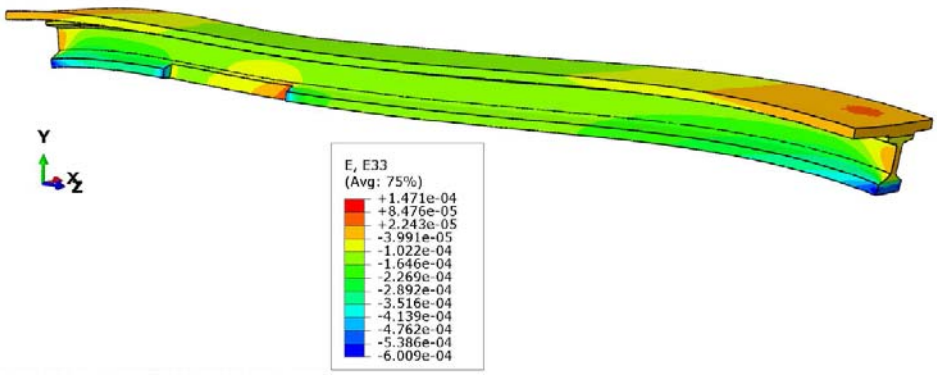

Figure 6-2 Strains. Truck Position 1

The values of the strains given by this model and their difference with respect to state 0 for each gauge are given by Table 6-4.

Table 6-4 Strains. Truck Position 1

Gauge	Node	Strain	
		State 1	Difference
SG 01	22424	-1.059E-04	7.262E-05
SG 02	4334	-1.182E-04	4.558E-05
SG 03	15006	-9.181E-05	3.477E-05
SG 04	14998	-9.741E-05	3.243E-05
SG 05	17870	-8.568E-05	7.961E-05
SG 06	3008	-9.625E-05	4.681E-05

State 1: Truck Position 1

In this case the maximum value of strain is 79.61 με, for the node closer to the position of the strain gauge number 5. The lower value is obtained for the node close to gauge 3, 34.77 με.

The comparison between the strains from the model and the field test is shown in Figure 6.3.

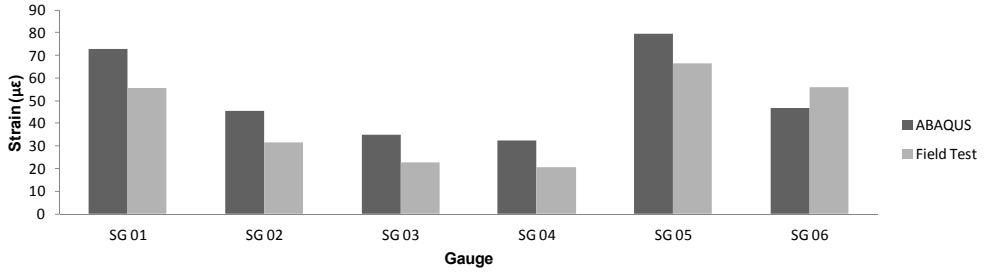

Figure 6-3 Comparison Model-Field Testing Truck Position 1

Looking at Figure 6-3 it can be observed that most of the values obtained from ABAQUS are slightly higher than those given by Table 6-2. Although for the strain gauge number six the strain given by ABAQUS is lower than the strain measured in the field

test, the difference between the values is less than 9.5 με. Therefore for this loading case the model is conservative.

6.1.1.2.- Truck Position 2

At this position the live loads applied were lower than those from position 1, then the strains values were lower, Figure 6-4.

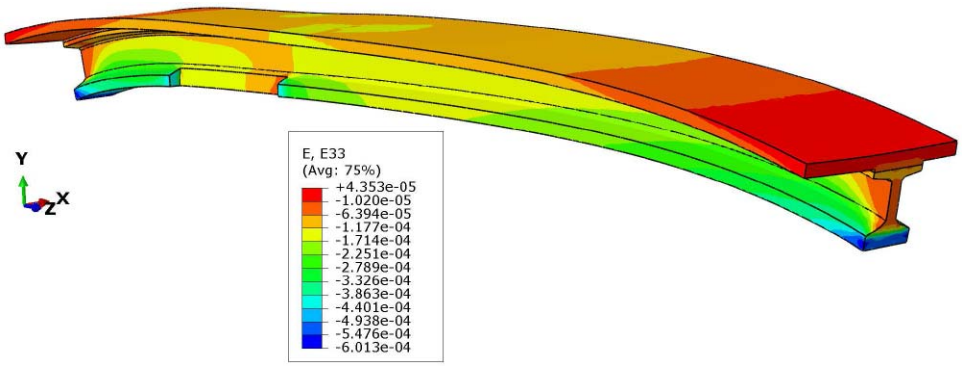

Figure 6-4 Strains. Truck Position 2

From Table 6-5 it can be observed that the strains are lower than those from truck position 1 as a result of a lower load.

Table 6-5 Strains. Truck Position 2

Gauge	Node	Strain	
		State 1	Difference
SG 01	22424	-1.616E-04	1.691E-05
SG 02	4334	-1.531E-04	1.060E-05
SG 03	15006	-1.185E-04	8.102E-06
SG 04	14998	-1.223E-04	7.554E-06
SG 05	17870	-1.468E-04	1.852E-05
SG 06	3008	-1.322E-04	1.089E-05

State 1: Truck Position 2

Figure 6-5 shows the strains obtained from ABAQUS and the strains from the field testing.

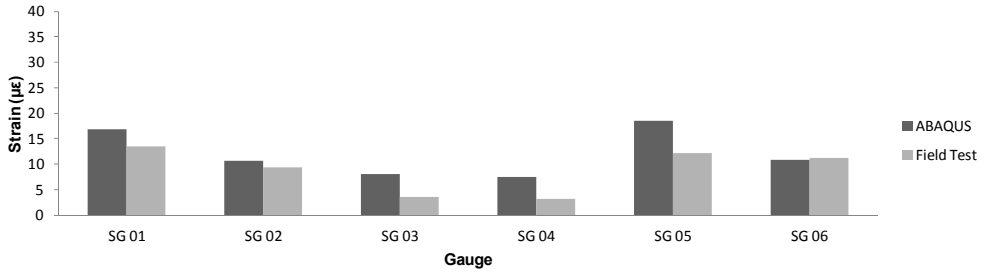

Figure 6-5 Comparison Model-Field Testing Truck Position 2

Looking at Figure 6-5 and comparing the values from Table 6-5 to those from Table 6-2 for this position it can be observed that in this case the model is more accurate. The differences between the model and the field testing are minimum; the greatest difference is about 6.3 με.

The fact that for the second loading case the 3D model was closer to the measurements suggests that the model for Phase 1 is valid. The greater differences obtained from the first loading case can be due to inaccuracies in the truck position considered. Since the position of the truck was not controlled using topographical equipment it is possible that the position of the truck was not the one indicated by the field testing.

6.1.2.- Phase 2

For Phase 2 the number of loading cases were four, corresponding to truck position 3 to truck position 6.

The data obtained from the field testing for this phase is given by Table 6-6.

Table 6-6 Strains Phase 2 Field Testing

Gauge	Strain			
	Truck Position 3	Truck Position 4	Truck Position 5	Truck Position 6
SG 01	2.884E-05	3.650E-05	1.368E-05	1.818E-05
SG 02	1.919E-05	2.370E-05	1.043E-05	1.257E-05
SG 03	1.321E-05	1.438E-05	5.320E-06	6.600E-06
SG 04	6.560E-06	1.004E-05	3.210E-06	4.800E-06
SG 05	3.069E-05	3.913E-05	1.298E-05	1.616E-05
SG 06	1.773E-05	2.241E-05	1.045E-05	1.293E-05
SG 07	2.924E-05	3.448E-05	1.289E-05	1.671E-05

Table 6-7 gives the strain values obtained for the state 0 for Phase 2.

Table 6-7 Strains. State 0 Phase 2

Gauge	Node	Strain
		State 0
SG 01	22424	-1.786E-04
SG 02	4334	-1.646E-04
SG 03	15006	-1.677E-04
SG 04	14998	-1.715E-04
SG 05	17870	-2.437E-04
SG 06	3008	-1.998E-04
SG 07	303	-2.503E-04

6.1.2.1.- Truck Position 3

Figure 6-6 shows the strains given by ABAQUS for this loading case.

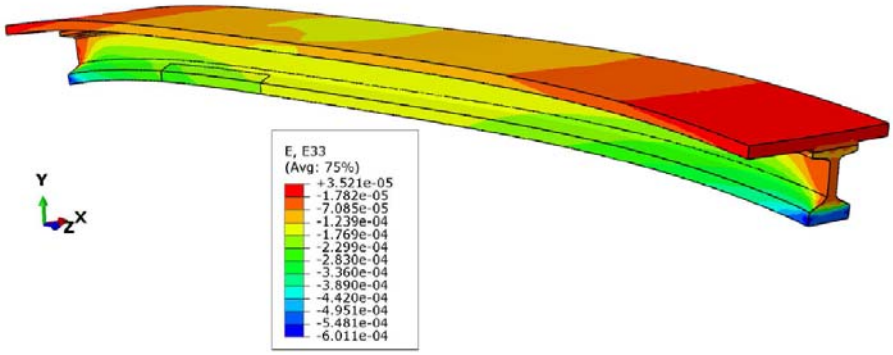

Figure 6-6 Strains. Truck Position 3

The differences between the strains given by this model and the strains from state 0 at the position of the gauges are given by Table 6-8.

Table 6-8 Strains. Truck Position 3

Gauge	Node	Strain	
		State 1	Difference
SG 01	22424	-1.466E-04	3.200E-05
SG 02	4334	-1.451E-04	1.959E-05
SG 03	15006	-1.541E-04	1.364E-05
SG 04	14998	-1.592E-04	1.230E-05
SG 05	17870	-2.109E-04	3.278E-05
SG 06	3008	-1.812E-04	1.856E-05
SG 07	303	-2.163E-04	3.401E-05

State 1: Truck Position 3

For this case the strains values have decreased with respect to the values obtained for the position 1 of the Phase 1. For this loading case the strain obtained for the node closer to gauge number 5 is about 32 με while for the same node the value was about 79 με for position 1. The lower value given for position 3 is 12.3 με.

The comparison between the strains from the field testing and the ABAQUS model is shown in Figure 6-7.

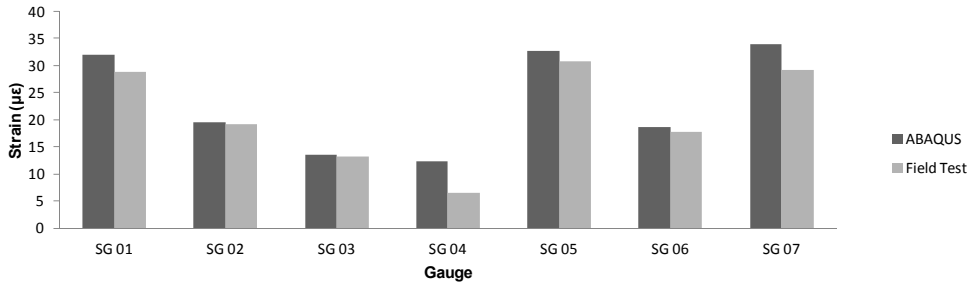

Figure 6-7 Comparison Model-Field Testing Truck Position 3

From Figure 6-7 it can be observed that the values are almost the same. The greatest difference is obtained for the strain gauge number 4. In this case the value from the field test was 6.56 με while the value obtained from the ABAQUS model was 12.30 με. Looking at the position of the strains gauges, Figure 4-7, it can be observed that the strain gauges 3 and 4 are located at the same height in the girder cross section and separated 2 ft (0.61 m) longitudinally. Therefore it is expected that the values from both strain were similar. However for the strain gauge number 3 the value measured was 12.21 με, which differs from 6.56 με. On the other hand the strain given by ABAQUS for the node closer to the strain gauge 3 was 13.64 με, which is a very similar value to 12.30 με. Based on the results obtained, it can be concluded for this position the strain gauge number 4 was not placed appropriately or did not work properly. It can be said that the model is adequate for this case.

6.1.2.2.- Truck Position 4

At this position the loads were applied at midspan and the strains values obtained were greater than those for the truck position 3, Figure 6-8.

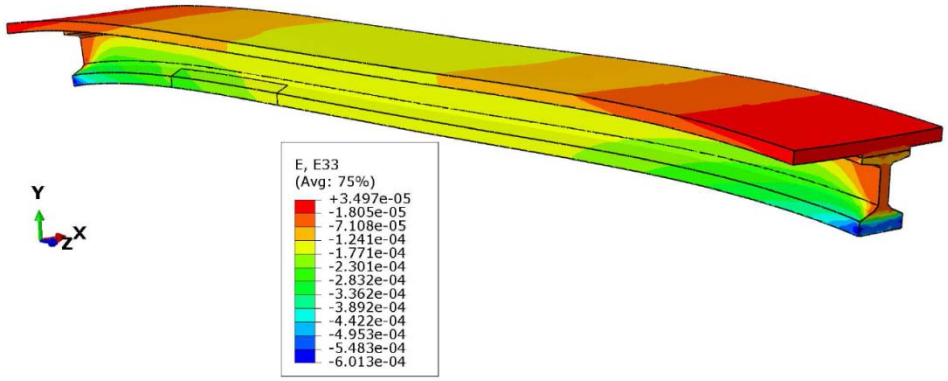

Figure 6-8 Strains. Truck Position 4

The data obtained for each node and their difference with the state 0 are given by Table 6-9.

Table 6-9 Strains. Truck Position 4

Gauge	Node	Strain	
		State 1	Difference
SG 01	22424	-1.242E-04	5.444E-05
SG 02	4334	-1.296E-04	3.502E-05
SG 03	15006	-1.507E-04	1.708E-05
SG 04	14998	-1.555E-04	1.592E-05
SG 05	17870	-2.004E-04	4.325E-05
SG 06	3008	-1.760E-04	2.375E-05
SG 07	303	-2.053E-04	4.500E-05

State 1: Truck Position 4

From this table it can be observed that the maximum value is obtained for the node 22424 and it is 54.4 με. The minimum value, 17 με, is given by the node closer to the strain gauge number 3.

The comparison between these values and the values obtained from the field testing is shown by Figure 6-9

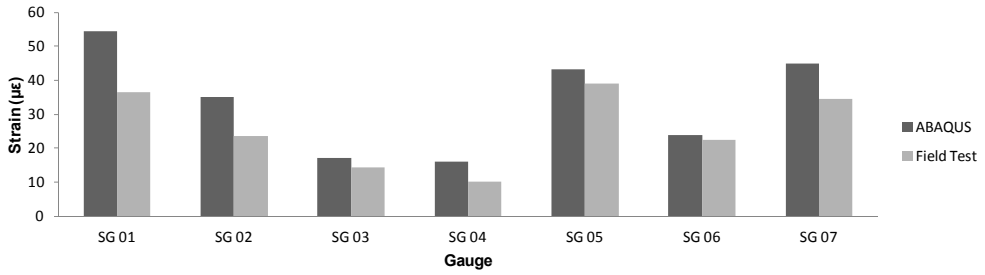

Figure 6-9 Comparison Model-Field Testing Truck Position 4

For this case the values obtained from ABAQUS are greater than those obtained from the field test. The greater difference is obtained for the gauge number 1 and it is about 17 με. Then the 3D model is conservative for this truck position.

6.1.2.3.- Truck Position 5

The strains obtained from ABAQUS are shown in Figure 6-10.

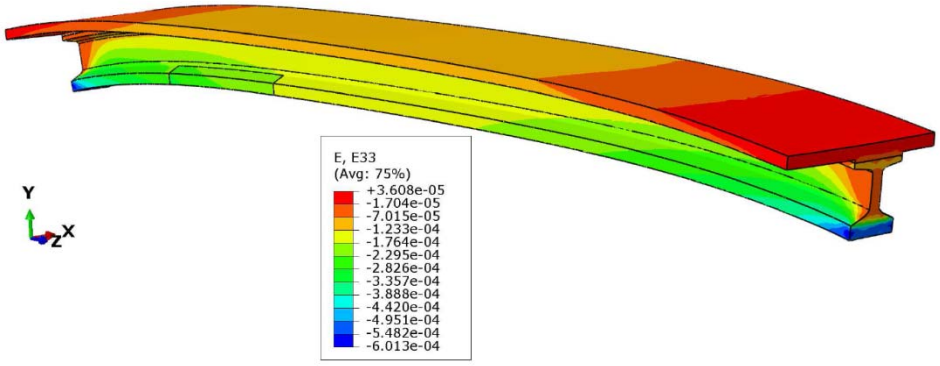

Figure 6-10 Strains. Truck Position 5

Since the loads applied for this position are lower than those for position 3 and 4, the strains values are lower. The values obtained for each node and their difference with the state 0 are given by Table 6-10.

Table 6-10 Strains. Truck Position 5

Gauge	Node	Strain	
		State 1	Difference
SG 01	22424	-1.617E-04	1.690E-05
SG 02	4334	-1.541E-04	1.058E-05
SG 03	15006	-1.616E-04	6.144E-06
SG 04	14998	-1.658E-04	5.685E-06
SG 05	17870	-2.284E-04	1.526E-05
SG 06	3008	-1.912E-04	8.591E-06
SG 07	303	-2.344E-04	1.587E-05

State 1: Truck Position 5

In general the values are low; the maximum strain value was about 17 με. When comparing this data to the data obtained from the field, Figure 6-11, it can be observed that the difference is minimum. Therefore the 3D model for this truck position is accurate.

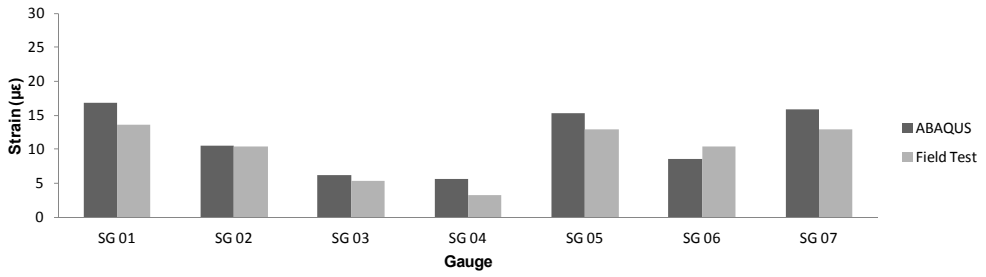

Figure 6-11 Comparison Model-Field Testing Truck Position 5

6.1.2.4.- Truck Position 6

For this case the strains values, Figure 6-12, were a little higher than those obtained for the position 5 but lower than the values given by the truck position 3 and 4 models.

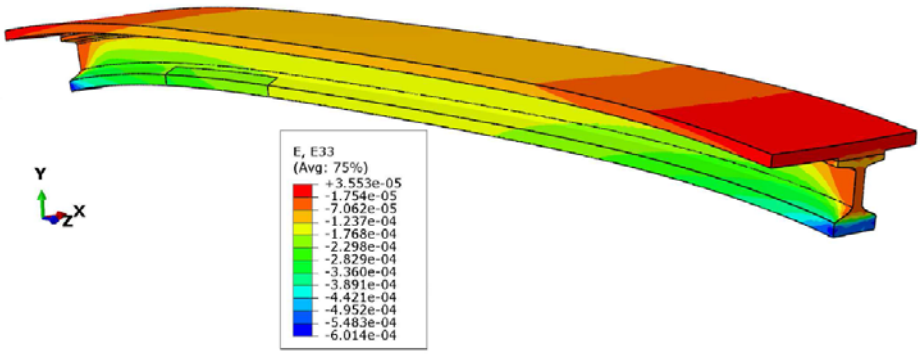

Figure 6-12 Strains. Truck Position 6

Table 6-11 gives the differences between the strain values from state 0 and the state 1 for each node studied.

Table 6-11 Strains. Truck Position 6

Gauge	Node	Strain	
		State 1	Difference
SG 01	22424	-1.565E-04	2.212E-05
SG 02	4334	-1.505E-04	1.416E-05
SG 03	15006	-1.608E-04	6.950E-06
SG 04	14998	-1.649E-04	6.527E-06
SG 05	17870	-2.260E-04	1.770E-05
SG 06	3008	-1.900E-04	9.799E-06
SG 07	303	-2.319E-04	1.842E-05

State 1: Truck Position 6

The maximum strain value is obtained for the node closer to the strain gauge number 5 and it is 17.7 με.

Looking at the graph given below, Figure 6-13, it can be observed that the strains values obtained from the finite element model and the field testing are almost the same. Therefore the 3D model is accurate.

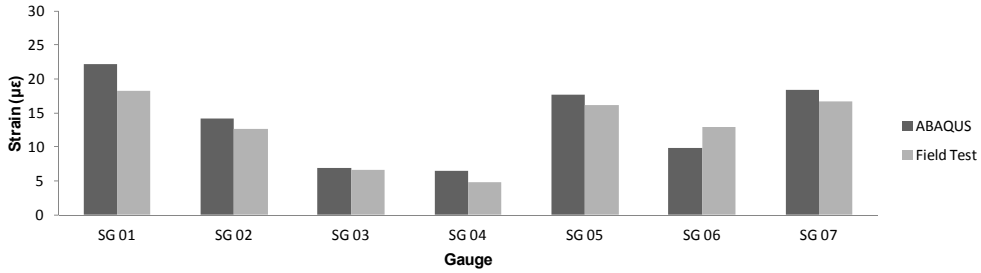

Figure 6-13 Comparison Model-Field Testing Truck Position 6

Finally it can be observed that for all cases the finite element model is accurate or conservative, therefore the model has been validated and it can be used to study similar problems.

6.2.- Stresses

Once the finite element model has been validated, the stresses were analyzed.

In a general case, for a prestressed girder under dead and live load the stresses at the bottom fiber can be obtained as the summation of the compressive stress caused by the prestress force and the tensile stress due to the gravity loads. Figure 6-14 shows the effects of a prestress force and a distributed load on a rectangular beam.

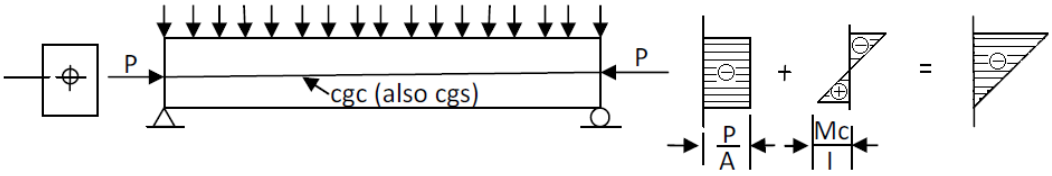

Figure 6-14 Concrete Fiber Stress Distribution in a Rectangular Beam with Concentric Straight Tendon (Nawy, 2010)

The prestress force produces a compression on the girder, the stress, σ_c, is given by:

$$\sigma_c = \frac{P}{A}$$

Where:

σ_c = Compressive stress

P = Prestress force

A = Area of the section

The dead and live loads, gravity loads, generate tensions on the girder bottom fiber. The tensile stress, σ_t, obtained is:

$$\sigma_t = \frac{M \cdot y}{I}$$

Where:

M = Flexural moment produced by the gravity load, w

y = c = Distance from the neutral axis to the fiber investigated.

I = Moment of inertia of the section.

The total stress, σ, is given by the following equation:

$$\sigma = \sigma_t + \sigma_c = \frac{M \cdot y}{I} - \frac{P}{A}$$

The main objective of the repair procedure presented is recovering the section capacity lost by increasing its moment of inertia. By doing so, based on the previous equation, the tensile stresses caused by the gravity loads are reduced. Consequently higher compressive stresses at the bottom fiber are expected to be obtained for the repaired girder model compared to the ones obtained for the damaged girder model.

6.2.1. Stresses: Concrete Sections

The stresses analyzed were the stresses at the section bottom fiber given by the 3D model at a section located 22 ft (6.71 m) from the southernmost support. This section corresponds to the center of the damage.

For Phase 1, the values obtained are the values from the nodes closer to the following coordinates, (10, 0, 264), (18, 0, 264), and (34, 0, 264). These coordinates correspond to points 1, 2 and 3 of Figure 6-15.

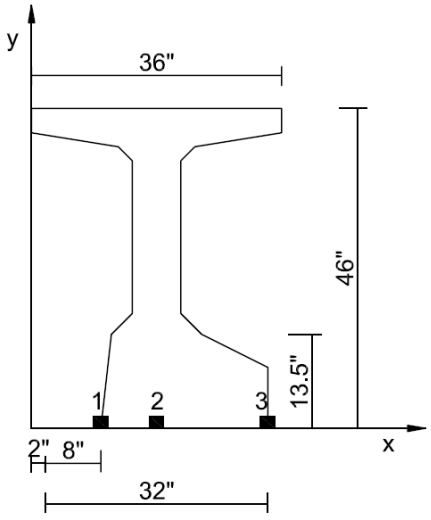

Figure 6-15 Phase 1: Stress Points Analyzed

For Phase 2 the points analyzed were the same ones that those for Phase 1. Additionally, two new points, 4, (8, 0, 264), and 5, (2, 0, 264) located at the repaired section have been checked, Figure 6-16.

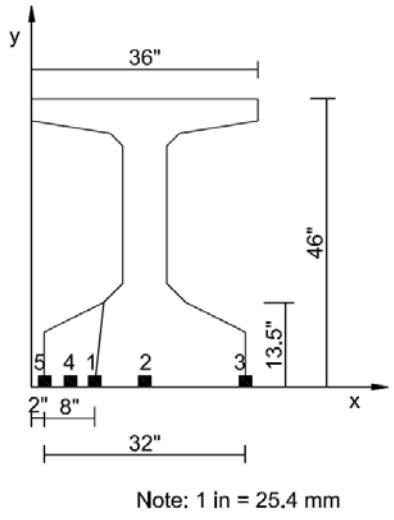

Figure 6-16 Phase 2: Stress Points Analyzed

The nodes corresponding to these points are shown in Table 6-12.

Table 6-12 Stresses. Nodes

Point	Coordinate, in (mm)						Node
	x		y		z		
1	10	(254)	0	(0)	264	(6,705)	3997
2	18	(457)	0	(0)	264	(6,705)	17870
3	34	(863)	0	(0)	264	(6,705)	4758
4	8	(203)	0	(0)	264	(6,705)	303
5	2	(50.8)	0	(0)	264	(6,705)	38

At these nodes the stresses obtained for Phase 1 are given by Table 6-13

Table 6-13 Stresses. Phase 1

Node	Stress, psi (MPa)	
	Truck Position 1	Truck Position 2
3997	-431.28 (-2.97)	-781.97 (-5.39)
17870	-478.28 (-3.3)	-820.33 (-5.66)
4758	-590.95 (-4.07)	-916.73 (-6.32)

The maximum compression is obtained for point 3. For both truck positions the minimum compression value is obtained for the point closer to the damage, point 1.

As expected, for Phase 2 the compressive stress values are greater than those obtained for Phase 1, Table 6-14.

Table 6-14 Stresses. Phase 2

Node	Stress, psi (MPa)							
	Truck Position 3		Truck Position 4		Truck Position 5		Truck Position 6	
3997	-1195.91	(-8.25)	-1136.40	(-7.84)	-1294.69	(-8.93)	-1280.86	(-8.83)
17870	-1179.54	(-8.13)	-1120.79	(-7.73)	-1277.61	(-8.81)	-1263.91	(-8.71)
4758	-1165.13	(-8.03)	-1110.90	(-7.66)	-1261.61	(-8.7)	-1248.43	(-8.61)
303	-935.12	(-6.45)	-887.60	(-6.12)	-1013.52	(-6.99)	-1002.49	(-6.91)
38	-933.04	(-6.43)	-886.96	(-6.12)	-1073.52	(-7.4)	-999.23	(-6.89)

For this phase when the truck was at positions 5 and 6 the compressive values were greater than for positions 3 and 4. This was because for position 3 and 4 the loads applied on the girder were greater, therefore the flexural moment was greater too resulting in higher tensile stress σ_t.

From Tables 6-13 and 6-14, it can be observed that for points 1, 2 and 3, the compressive values are greater for truck positions 3 and 5 than for truck positions 1 and 2, similar positions for both phases. This means that as was expected the compressive stresses increased once the girder was repaired. As explain before, the increase in the moment of inertia resulted in lower tensile stresses due to the bending action.

It can be said that once the girder was repaired the compressive stress at the bottom fiber increased.

For both phases the stress values obtained indicated that the girder was under elastic behavior. From Tables 6-13 and 6-14 the maximum compressive stress for the concrete girder section was 1,294.69 psi, (8.93 MPa), that is a value lower than the elastic limit for this section, 4,250 psi, (29.3 MPa). Similarly for the repaired section the maximum compressive stress, 1,073.52 psi, (7.4 MPa), was lower than the yield stress, 3,000 psi, (20.68 MPa).

6.2.2.- Stresses: Fiber Glass Rebar.

The longitudinal fiber glass rebar were placed with the objective of increasing the strength of the repaired section to compensate the use of a material, grout, with a lower strength than the original one, concrete. The maximum stresses developed by the longitudinal fiber glass rebar for each truck position are given by Table 6-15.

Table 6-15 Maximum Stresses. Fiber Glass Rebar

Fiber Glass Rebar	Stress, psi (Mpa)			
	Truck Position 3	Truck Position 4	Truck Position 5	Truck Position 6
1	-2054.4 (-14.16)	-2034.72 (-14.03)	-2142.44 (-14.77)	-2137.89 (-14.74)
2	-1975.7 (-13.62)	-1957.96 (-13.50)	-2056.26 (-14.18)	-2052.19 (-14.15)

The fiber glass rebar number 1 correspond to the rebar placed at 7.5 in (190 mm) from the bottom flange and the rebar placed at 10 in (254 mm) from bottom is the fiber glass rebar number 2.

From Table 6-15 it can be observed that the minimum compressive stress value is obtained for the positions 3 and 4. This is the expected result since for these truck positions the loads applied on the girder were greater than those applied for the other two positions. The tensile stresses transmitted by the live loads were greater making the compressive stress values lower.

For the fiber glass rebar all the stresses values were under the elastic limit considered for the rebar. Therefore the rebar had an elastic behavior.

Chapter 7

SUMMARY AND CONCLUSIONS

This chapter is divided into two parts. The first part includes a brief summary of what has been studied in this thesis. The second part contains the conclusions that have been derived after performing the study.

7.1.- Summary

This thesis has analyzed the strains and stresses generated in a girder damaged by a truck and repaired with fiber glass rebar.

The damaged girder was located in the bridge number 54 of the LBJ project. The girder hit by a truck was the girder number 1 of the span 2 in the southbound structure. The damage was 14 ft (4.27 m) long at the bottom flange of the beam. It had several strands exposed but none of them was severed. The solution adopted by the company was based on the use of three materials: bonding agent, fiber glass rebar, and repair mortar.

To study the behavior of the girder the developer conducted two field tests. On both field test several strains gauges were placed at different positions. The first test was performed before repairing the girder and the second test was conducted once the girder was repaired. For both phases the data given by the strains gauges were recorded.

For this thesis two different finite element models were generated to analyze de behavior of both the damaged and the repaired girder. This allowed the comparison between the results from the model and the data from the field tests. The software ABAQUS was used in the development of the finite element models.

To model the two phases the following considerations were taken into account:

1) The concrete damaged plasticity model was used to model the concrete behavior of the elements. This model performed the inelastic behavior of the concrete both in compression and tension.
2) The prestress force was modeled using the balancing method. This method allows modeling the effect of depressing a strand by the introduction of a vertical reaction at the hold down points.
3) The live loads applied on the studied girder were calculated using the lever rule. The lever rule provided a distribution factor to apply on the live loads transmitted by the truck resulting in the live load applied on the girder studied.

Once the model was performed the comparison between the strains given by the ABAQUS model and the average strains given by the strain gauges was done. This comparison allowed the validation of the model.

7.2.- Conclusions

Once the results have been analyzed the following conclusions can be drawn:

1) The strain comparison between the model and the field test showed that the values given by ABAQUS were similar to those given by the strain gauges. The small differences found between some measurements may be due to the fact that the truck was not placed on the position indicated by the field test or that some strain gauge did not work properly. Then the 3D model is adequate. It can be concluded that the software ABAQUS can be used to model this kind of problem.

2) The concrete damaged plasticity model, the balancing method and the lever rule, were good approximations of the structural behavior of the girder. Therefore these considerations can be used for future modeling.
3) Both the field test and the 3D model gave lower strain values for the repaired girder than those obtained for the damaged girder. This is one indication that the repair method used worked.
4) The stresses given by ABAQUS were the expected. Greater compression stresses for the repair girder than for the damage girder were expected. It can be said that once the girder was repaired the strength of the girder increased due to the repair technique used.
5) From the stress values obtained from the model it can be observed that all the values were lower than the elastic limit considered for each material. Then it can be concluded that the model could have been made only by defining elastic behavior to reduce the computational cost.
6) It can be said that the use of the provisions given by AASHTO to obtain the composite section of bridge girder is conservative and it can be used in the development of finite element models.
7) The behavior of the interface between the concrete of the girder and the repair mortar in the repaired section has been modeled using a tie interaction from ABAQUS. This type of interaction constrains the degrees of freedoms of the nodes in contact and guarantees the compatibility in the deformation of the different elements and, therefore an adequate stress transmission. Since the results from the model are similar to the measurements from the field test it can be concluded that the solution consisting of applying a bonding agent and using transverse fiber glass

rebar is adequate to guarantee the adherence between the two materials.

8) The longitudinal fiber glass rebar were under an elastic behavior, having greater compressive values when the load were low, truck position 5 and 6, and decreasing these values for the other two positions. These rebar contributed to increase the strength of the girder.

9) The objectives of this study have been achieved. A better understanding of the structural behavior of the repaired girder has been provided. Also, an adequate modeling technique for beams repaired with GFRP rebar has been proposed that will help to establish adequate repair procedures and to anticipate the structural behavior of damaged girders prior to the repair process.

Appendix A

Drawings

STATE OF TEXAS
DEPARTMENT OF TRANSPORTATION

PLANS OF PROPOSED
STATE HIGHWAY IMPROVEMENT

FEDERAL AID PROJECT
CSJ: 2374-01-068, ETC.

IH 635 MANAGED LANES PROJECTS
IH 635
DALLAS COUNTY
SEGMENT 3
IFC SUBMITTAL BRIDGE 54

DESIGN	FED.RD. DIV.NO.	FEDERAL AID PROJECT NO.		HIGHWAY NO.
JRL				
GRAPHICS	6	XX-XXXX-XXX		IH 635
DNA	STATE	DISTRICT	COUNTY	SHEET NO.
CHECK	TEXAS	DALLAS	DALLAS	S3-B540001
MAH	CONTROL	SECTION	JOB	
CHECK	2374	01	068, ETC	
JFG				

NO.	DATE	REVISION	APPROV.
0	11/30/11	IFC SUBMITTAL SEGMENT 3 B54	JFG
1	6/18/12	REVISED AS NOTED	JFG
2	7/12/12	REVISED AS NOTED	JFG
3	10/26/12	REVISED AS NOTED	JFG
4	12/05/12	REVISED AS NOTED	JFG

PROJECTS DESIGN SPEEDS

ROADWAY	DESIGN SPEED
GENERAL PURPOSE LANES	60 MPH
SURFACE & DEPRESSED HOV / MANAGED LANES	60 MPH
DIRECT CONNECTORS	50 MPH
ELEVATED CONNECTORS	50 MPH
FRONTAGE ROADS	45 MPH
RAMPS AND BYPASSES	45 MPH
ARTERIALS	40 MPH
COLLECTORS	30 MPH

PROJECT LOCATION
IH635
FROM LUNA ROAD TO WEST OF COIT ROAD
STA 10533+63.00 TO STA 413+71.78
STA EQ: 10607+23.68 (BK) =40+00.00 (AH)

PROJECT LOCATION
IH35E
FROM IH35E/IH635 INTERCHANGE TO
VALWOOD PKWY
STA 711+49.20 TO STA 823+00.00

PROJECT LOCATION
IH 635
FROM WEST OF ROSSER RD. TO WEST OF
COIT RD.
STA. 162+05 TO STA. 413+71.78

PROJECT LOCATION
IH35E
FROM JOE'S CREEK TO
IH35E/IH635 INTERCHANGE
STA 984+18.40 TO STA 711+49.20
STA EQ:1153+81.75 (BK) =
684+00.00 (AH)

PROJECT LOCATION
LOOP 12
FROM NORTHWEST HIGHWAY
TO IH35E
STA 1498+60.73 TO STA 1512+42.00

PROJECT LOCATION
IH 635/ US 75 INTERCHANGE
FOR BARRIER & PAVEMENT
MARKINGS IMPROVEMENTS

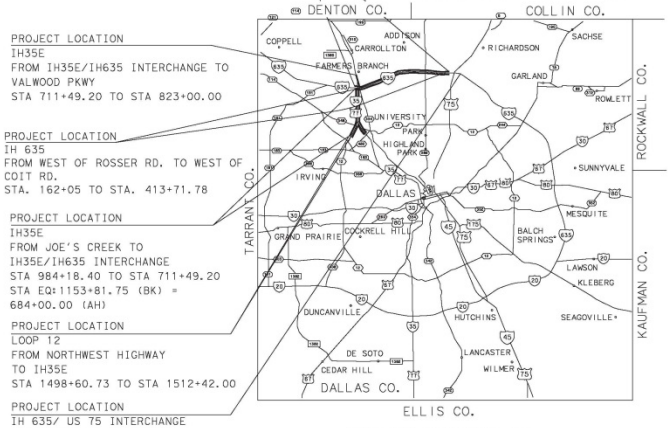

PROJECT LOCATION MAP
N.T.S.

LBJ express
trinity infrastructure, LLC
Improving mobility in Texas

Texas Department of Transportation
© 2012

JANSSEN & SPAANS ENGINEERING
CONSULTING ENGINEERS
FIRM REGISTRATION NUMBER: F-11319

STATE OF TEXAS
JAVIER F. GAUTHIER
106475
LICENSED
PROFESSIONAL ENGINEER
12/05/12

© 2012 by Texas Department of Transportation; all rights reserved

SN 136
IFC-S3-B54-R4

$TIME$
$DATE$
$USER$
$FILE$

BRIDGE APPROACH SLAB CONCRETE PAVEMENT

1. ALL STRUCTURAL DESIGN ELEMENTS SHALL CONFORM TO THE REQUIREMENTS AND CRITERIA CONTAINED IN COMPREHENSIVE DEVELOPMENT AGREEMENT (CDA), TECHNICAL PROVISIONS BOOK 2A & BOOK 2B (BOOK 2).
2. REFERENCE SHALL BE MADE TO THE FOLLOWING DOCUMENTS FOR APPLICABLE DESIGN CRITERIA AND GUIDELINES THAT MAY NOT BE SPECIFICALLY ADDRESSED IN THE DOCUMENTS LISTED ABOVE:
   A. AASHTO LRFD BRIDGE DESIGN SPECIFICATIONS, 5TH EDITION.
   B. TXDOT BRIDGE DETAILING MANUAL. DATED AUGUST 2001.
3. BOOK 2A AND BOOK 2B SHALL PREVAIL IF A CONFLICT IS DISCOVERED BETWEEN CRITERIA CONTAINED IN THE DOCUMENTS LISTED ABOVE. THE DESIGNER SHALL NOTIFY THE DESIGN MANAGER OF ANY ERRONEOUS CRITERIA CONTAINED IN BOOK 2 THAT IF USED WILL BE DETRIMENTAL TO THE PROJECT OR CAUSE AN UNSAFE CONDITION.
4. SEE UTILITY PLANS FOR IDENTIFICATION AND RELOCATION OF EXISTING UTILITIES.
5. SEE ROWY PLAN AND PROFILE SHEETS FOR HORIZONTAL AND VERTICAL GEOMETRY.
6. SEE GEOTECHNICAL REPORT FOR BORING LOG INFORMATION.
7. TRINITY INFRASTRUCTURE, LLC WILL VERIFY LOCATIONS OF ALL UTILITIES PRIOR TO CONSTRUCTION, EXCAVATION OR DRILLING.
8. SEE RETAINING WALL SHEETS FOR LIMITS AND DETAILS.
9. SEE GENERAL ARRANGEMENT DRAWINGS AND FOUNDATION SHEETS FOR ADDITIONAL INFORMATION ON FOUNDATIONS.
10. ALL DIMENSIONS ARE HORIZONTAL OR VERTICAL AND MUST BE CORRECTED FOR VERTICAL GRADE AND SUPERELEVATION WHERE APPLICABLE.
11. IN CASE OF CONFLICT BETWEEN THE DESIGN AND TXDOT STANDARD DRAWINGS, DESIGN DRAWING INFORMATION PREVAILS.

GENERAL STRUCTURAL DESIGN REQUIREMENTS

1. PRESTRESSED CONCRETE I-GIRDERS
   1.1 THE MAXIMUM CONCRETE STRENGTH AT RELEASE OF PRESTRESS SHALL BE: 8000 PSI(SPAN1 NB), 7000 PSI (SPAN1 SB), 6300 PSI (SPAN 2 NB), 6300 PSI (SPAN 2 SB), 6800 PSI (SPAN 3 NB), 6800 PSI (SPAN 3 EXCEPT GIRDER 1) AND 8000 PSI (SPAN 3 SB GIRDER 1)
   1.2 THE MAXIMUM 28-DAY COMPRESSIVE STRENGTH FOR PRESTRESSED CONCRETE SHALL BE: 10000 PSI(SPAN1 NB), 9000 PSI (SPAN1 SB), 8500 PSI (SPAN 2 NB), 8500 PSI (SPAN 2 SB), 8500 PSI (SPAN 3 NB), 8500 PSI (SPAN 3 EXCEPT GIRDER 1) AND 10000 PSI (SPAN 3 SB GIRDER 1)
   1.3 USE 0.5" LOW-RELAXATION STRANDS OR 0.6" LOW-RELAXATION STRANDS.
   1.4 CONCRETE CLASS H.
2. CONCRETE COMPRESSIVE STRENGTH (SEE TXDOT STD SPEC ITEM 421. TABLE 5)
   2.1 DECK SLABS-CLASS S. 4000 PSI.
   2.2 SUBSTRUCTURE-CLASS C. 3600 PSI, UNLESS NOTED OTHERWISE (UNO).
   2.3 DRILLED SHAFTS-CLASS C. 3600 PSI, PER TXDOT STD SPEC ITEM 421.4.A.1. UNO.
3. REINFORCING STEEL
   3.1 ALL REINFORCING STEEL SHALL BE GRADE 60.
   3.2 DIMENSIONS TO THE REINFORCING BARS ARE OUT TO OUT, UNLESS NOTED OTHERWISE.
4. CONSTRUCTION JOINTS OTHER THAN THOSE SHOWN ON THE PLANS WILL NOT BE PERMITTED WITHOUT PRIOR APPROVAL BY THE ENGINEER.
5. ALL EXPOSED EDGES SHALL BE CHAMFERED ¾" UNLESS NOTED OTHERWISE.
6. DECK SLAB
   6.1 MINIMUM DECK THICKNESS IS 8".
   6.2 SEE TxDOT STANDARD DRAWING IGMS FOR MISCELLANEOUS DETAILS.
   6.3 SEE TxDOT STANDARD DRAWING IGTS FOR THICKENED SLAB END DETAILS.
   6.4 PRECAST CONCRETE DECK PANELS, PER TxDOT STANDARD DRAWING PCP AND PCP (MOD). SHALL BE USED FOR ALL CONCRETE I-GIRDERS, UNLESS NOTED OTHERWISE.
   6.5 SEE BRIDGE LAYOUTS. TYPICAL SECTIONS AND PERMANENT ILLUMINATION PLANS FOR LOCATION OF CONDUITS AND LIGHTING FIXTURES ON BRIDGE STRUCTURES.
   6.6 THE SURFACE TREATMENT FOR THE BRIDGE DECKS SHALL BE SURFACE TREATMENT CLASS 1, PER TxDOT STD SPEC ITEM 428. (1)
7. DESIGN LOADS
   7.1 DEAD LOADS
      7.1.1 REFER TO BOOK 2.
      7.1.2 ALL GIRDERS DESIGNED FOR 2" FUTURE WEARING SURFACE AT 25 PSF BETWEEN BARRIER RAILS, DISTRIBUTED EQUALLY TO ALL GIRDERS.
      7.1.3 GIRDER DESIGN INCLUDES LOAD FOR HAUNCH.
      7.1.4 TRAFFIC BARRIER RAIL SHALL BE TXDOT STD TYPE C221
   7.2 LIVE LOADS
      7.2.1 ALL BRIDGES DESIGNED FOR HL93 LOADING.
      7.2.2 LIVE LOAD DISTRIBUTION FACTORS CALCULATED PER AASHTO LRFD BRIDGE DESIGN SPECIFICATIONS. 5TH EDITION.

GENERAL STRUCTURAL DESIGN REQUIREMENTS CONT' D

8. SUBSTRUCTURES
   8.1 SEE GIRDER LAYOUT SHEETS FOR GIRDER ANGLES.
   8.2 SEE BENT SHEETS FOR DOWEL LOCATIONS AND BEARING SEAT DETAILS.
   8.3 SEE COLUMN AND FOUNDATION DETAILS SHEET FOR COLUMN CHAMFERS.
   8.4 DRILLED SHAFT VERTICAL REBAR SPLICES:

CLASS C, 3600 psi CONCRETE GRADE 60 REINFORCING STEEL		
REBAR SIZE	SPLICE LENGTH (BARS SPACED LESS THAN THAN 6" C-C)	SPLICE LENGTH (BARS SPACED 6" C-C OR MORE)
# 3	1'-4"	1'-1"
# 4	1'-9"	1'-5"
# 5	2'-2"	1'-9"
# 6	2'-7"	2'-1"
# 7	3'-5"	2'-9"
# 8	4'-6"	3'-7"
# 9	5'-8"	4'-7"
# 10	7'-3"	5'-9"
# 11	8'-11"	7'-2"

   8.5 TOP AND BOTTOM OF BENT CAPS ARE LEVELED. PEDESTAL HEIGHTS SHALL BE ADJUSTED TO MEET BEARING SEAT ELEVATIONS.
   8.6 WHERE THE DRILLED SHAFT EXTENDS OUTSIDE THE PERIMETER OF THE COLUMN, THE TOP OF THE DRILLED SHAFT SHALL RECEIVE A WOOD FLOAT FINISH OUTSIDE THE REBAR DOWELS TO THE EDGE OF THE DRILLED SHAFT.

NO.	DATE	REVISION	APPROV.
1	6/18/12	NOTE ADDED	JFG
0	11/30/11	FC SUBMITTAL SEGMENT 3 B54	JFG

LBJ express

trinity infrastructure, LLC
Improving mobility in Texas

JANSSEN & SPAANS ENGINEERING CONSULTING ENGINEERS
FIRM REGISTRATION NUMBER: F-1019

Texas Department of Transportation
© 2011

LBJ CROSS STREET BRIDGE NO. 54 PRESTON ROAD BRIDGE GENERAL NOTES

SHEET 1 OF 1

STATE OF TEXAS — JAMES F. GAITHER — 106475 — LICENSED PROFESSIONAL ENGINEER
06/18/12

DESIGN	FED.RD. DIV.NO.	FEDERAL AID PROJECT NO.		HIGHWAY NO.
JRL	6	XX-XXXX-XXX		IH 635
DRAWN	STATE	DISTRICT	COUNTY	SHEET NO.
DNA	TEXAS	DALLAS	DALLAS	S3-B540004
CHECK	CONTROL	SECTION	JOB	
MAH	2374	01	068, ETC	
CHECK				
JFG				

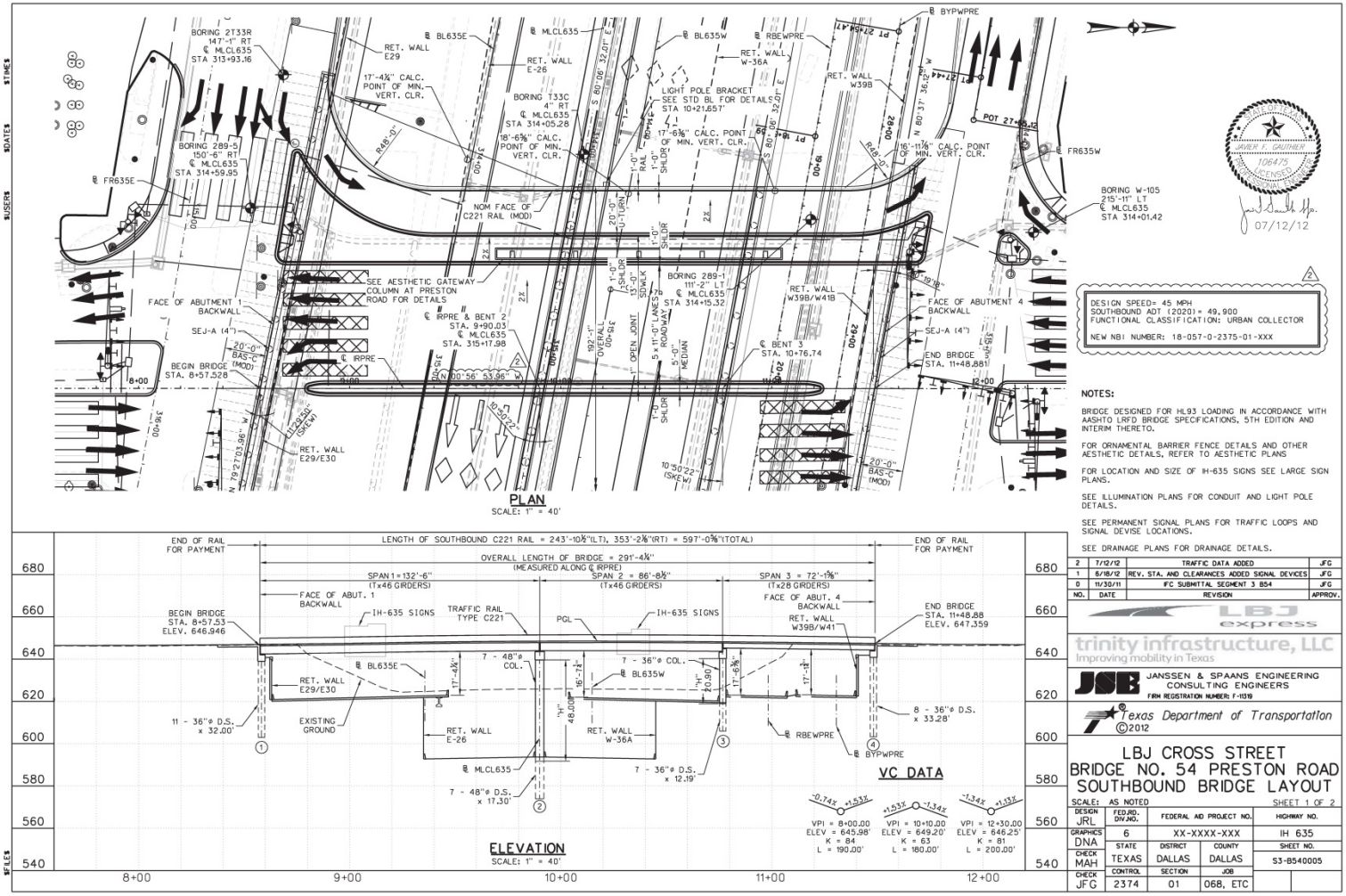

DESIGN SPEED= 45 MPH
SOUTHBOUND ADT (2020) = 49,900
FUNCTIONAL CLASSIFICATION: URBAN COLLECTOR

NEW NBI NUMBER: 18-057-0-2375-01-XXX

NOTES:

BRIDGE DESIGNED FOR HL93 LOADING IN ACCORDANCE WITH AASHTO LRFD BRIDGE SPECIFICATIONS, 5TH EDITION AND INTERIM THERETO.

FOR ORNAMENTAL BARRIER FENCE DETAILS AND OTHER AESTHETIC DETAILS, REFER TO AESTHETIC PLANS

FOR LOCATION AND SIZE OF IH-635 SIGNS SEE LARGE SIGN PLANS.

SEE ILLUMINATION PLANS FOR CONDUIT AND LIGHT POLE DETAILS.

SEE PERMANENT SIGNAL PLANS FOR TRAFFIC LOOPS AND SIGNAL DEVISE LOCATIONS.

SEE DRAINAGE PLANS FOR DRAINAGE DETAILS.

NO.	DATE	REVISION	APPROV.
2	7/12/12	TRAFFIC DATA ADDED	JFG
1	6/18/12	REV. STA. AND CLEARANCES ADDED SIGNAL DEVICES	JFG
0	11/30/11	IFC SUBMITTAL SEGMENT 3 B54	JFG

LBJ express

trinity infrastructure, LLC
Improving mobility in Texas

JANSSEN & SPAANS ENGINEERING CONSULTING ENGINEERS
FIRM REGISTRATION NUMBER: F-11319

Texas Department of Transportation ©2012

LBJ CROSS STREET BRIDGE NO. 54 PRESTON ROAD SOUTHBOUND BRIDGE LAYOUT

SCALE: AS NOTED — SHEET 1 OF 2

DESIGN	FED.RD. DIV.NO.	FEDERAL AID PROJECT NO.		HIGHWAY NO.
JRL				
GRAPHICS	6	XX-XXXX-XXX		IH 635
DNA				
CHECK	STATE	DISTRICT	COUNTY	SHEET NO.
MAH	TEXAS	DALLAS	DALLAS	S3-B540005
CHECK	CONTROL	SECTION	JOB	
JFG	2374	01	068, ETC	

07/12/12

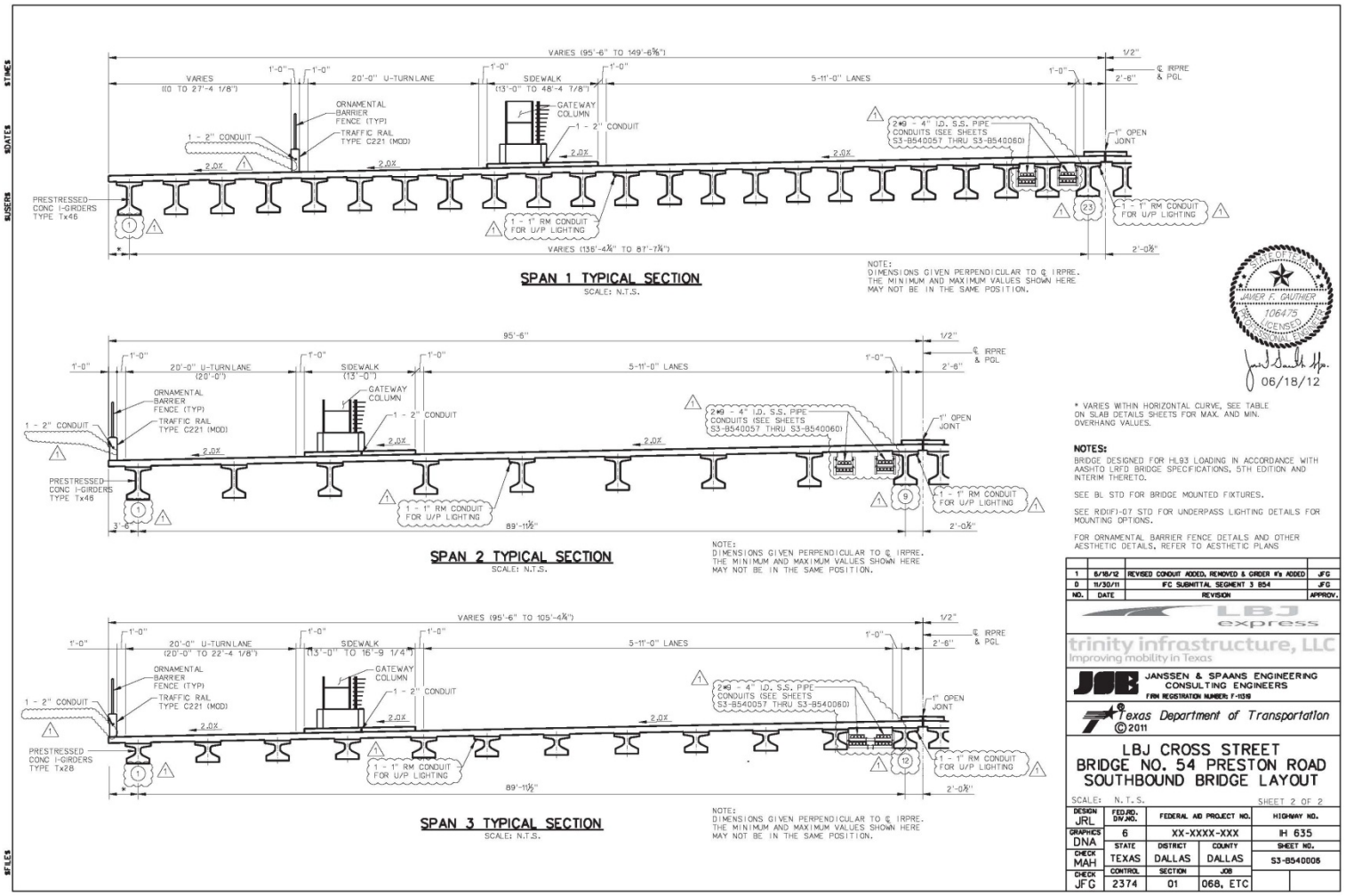

STATE OF TEXAS
JAMES F. GAITHER
106475
LICENSED
PROFESSIONAL ENGINEER
06/18/12

* VARIES WITHIN HORIZONTAL CURVE, SEE TABLE ON SLAB DETAILS SHEETS FOR MAX. AND MIN. OVERHANG VALUES.

NOTES:

BRIDGE DESIGNED FOR HL93 LOADING IN ACCORDANCE WITH AASHTO LRFD BRIDGE SPECIFICATIONS, 5TH EDITION AND INTERIM THERETO.

SEE BL STD FOR BRIDGE MOUNTED FIXTURES.

SEE RDI(IF)-07 STD FOR UNDERPASS LIGHTING DETAILS FOR MOUNTING OPTIONS.

FOR ORNAMENTAL BARRIER FENCE DETAILS AND OTHER AESTHETIC DETAILS, REFER TO AESTHETIC PLANS

NO.	DATE	REVISION	APPROV.
1	6/18/12	REVISED CONDUIT ADDED, REMOVED & GIRDER #'s ADDED	JFG
0	11/30/11	IFC SUBMITTAL SEGMENT 3 854	JFG

LBJ express

trinity infrastructure, LLC
Improving mobility in Texas

JANSSEN & SPAANS ENGINEERING CONSULTING ENGINEERS
FIRM REGISTRATION NUMBER: F-1519

Texas Department of Transportation ©2011

LBJ CROSS STREET BRIDGE NO. 54 PRESTON ROAD SOUTHBOUND BRIDGE LAYOUT

SCALE: N.T.S. SHEET 2 OF 2

DESIGN	FED.RD. DIV.NO.	FEDERAL AID PROJECT NO.	HIGHWAY NO.
JRL	6	XX-XXXX-XXX	IH 635
GRAPHICS DNA	STATE	DISTRICT	COUNTY	SHEET NO.
CHECK MAH	TEXAS	DALLAS	DALLAS	S3-B540006
CHECK JFG	CONTROL	SECTION	JOB	
	2374	01	068, ETC	

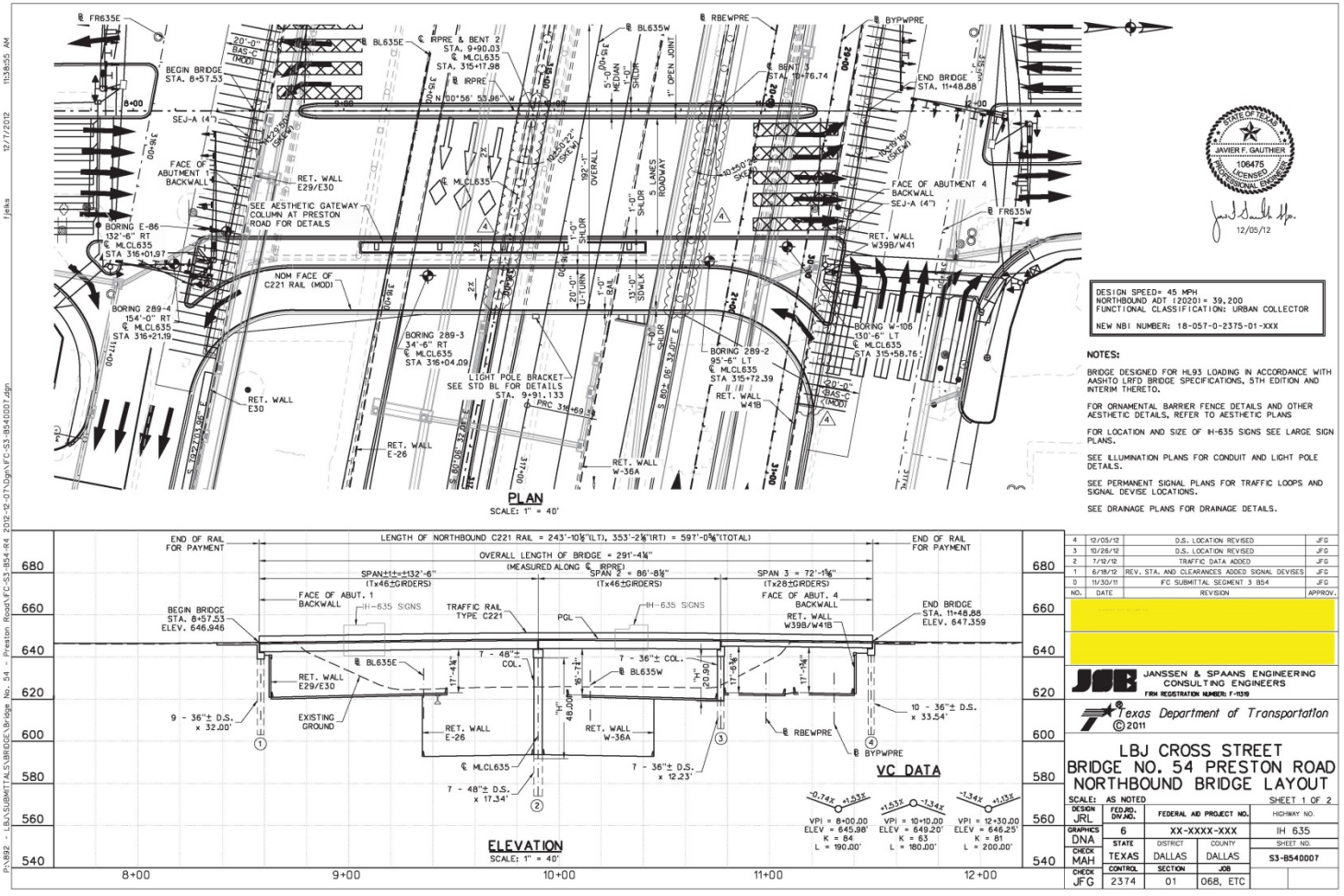
PLAN
SCALE: 1" = 40'
ELEVATION
SCALE: 1" = 40'
VC DATA
DESIGN SPEED= 45 MPH
NORTHBOUND ADT (2020) = 39,200
FUNCTIONAL CLASSIFICATION: URBAN COLLECTOR
NEW NBI NUMBER: 18-057-0-2375-01-XXX
NOTES:
BRIDGE DESIGNED FOR HL93 LOADING IN ACCORDANCE WITH AASHTO LRFD BRIDGE SPECIFICATIONS, 5TH EDITION AND INTERIM THERETO.
FOR ORNAMENTAL BARRIER FENCE DETAILS AND OTHER AESTHETIC DETAILS, REFER TO AESTHETIC PLANS
FOR LOCATION AND SIZE OF IH-635 SIGNS SEE LARGE SIGN PLANS.
SEE ILLUMINATION PLANS FOR CONDUIT AND LIGHT POLE DETAILS.
SEE PERMANENT SIGNAL PLANS FOR TRAFFIC LOOPS AND SIGNAL DEVISE LOCATIONS.
SEE DRAINAGE PLANS FOR DRAINAGE DETAILS.
JANSSEN & SPAANS ENGINEERING CONSULTING ENGINEERS
FIRM REGISTRATION NUMBER: F-1319
Texas Department of Transportation
© 2011
LBJ CROSS STREET
BRIDGE NO. 54 PRESTON ROAD
NORTHBOUND BRIDGE LAYOUT
SCALE: AS NOTED
SHEET 1 OF 2
DESIGN JRL
FED.RD. DIV.NO. 6
FEDERAL AID PROJECT NO. XX-XXXX-XXX
HIGHWAY NO. IH 635
GRAPHICS DNA
STATE TEXAS
DISTRICT DALLAS
COUNTY DALLAS
SHEET NO. S3-8540007
CHECK MAH
CONTROL 2374
SECTION 01
JOB 068, ETC
CHECK JFG

124

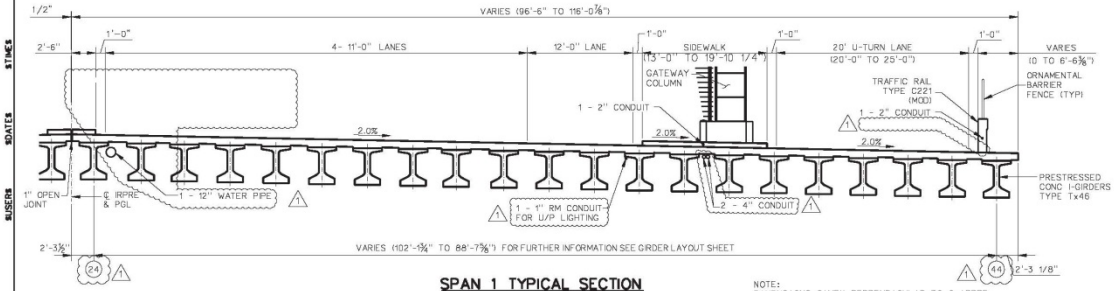

SPAN 1 TYPICAL SECTION
SCALE: N.T.S.

NOTE:
DIMENSIONS GIVEN PERPENDICULAR TO ℄ IRPRE. THE MINIMUM AND MAXIMUM VALUES SHOWN HERE MAY NOT BE IN THE SAME POSITION.

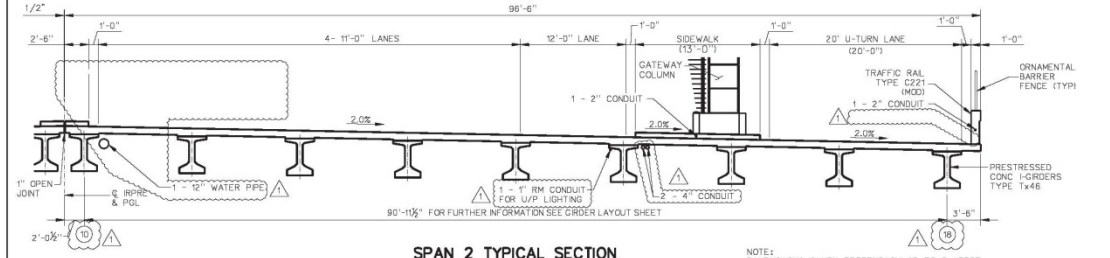

SPAN 2 TYPICAL SECTION
SCALE: N.T.S.

NOTE:
DIMENSIONS GIVEN PERPENDICULAR TO ℄ IRPRE. THE MINIMUM AND MAXIMUM VALUES SHOWN HERE MAY NOT BE IN THE SAME POSITION.

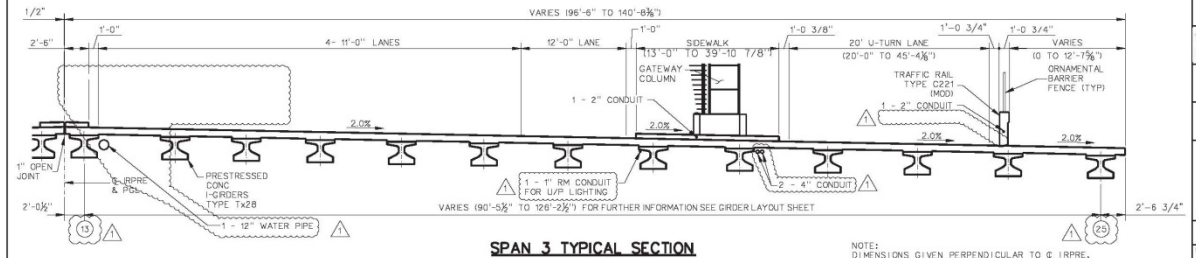

SPAN 3 TYPICAL SECTION
SCALE: N.T.S.

NOTE:
DIMENSIONS GIVEN PERPENDICULAR TO ℄ IRPRE. THE MINIMUM AND MAXIMUM VALUES SHOWN HERE MAY NOT BE IN THE SAME POSITION.

* VARIES WITHIN HORIZONTAL CURVE. SEE TABLE ON SLAB DETAILS SHEETS FOR MAX. AND MIN. OVERHANG VALUES.

NOTES:

BRIDGE DESIGNED FOR HL93 LOADING IN ACCORDANCE WITH AASHTO LRFD BRIDGE SPECIFICATIONS, 5TH EDITION AND INTERIM THERETO.

SEE BL STD FOR BRIDGE MOUNTED FIXTURES.

SEE RIDIF1-07 STD FOR UNDERPASS LIGHTING DETAILS FOR MOUNTING OPTIONS.

FOR ORNAMENTAL BARRIER FENCE DETAILS AND OTHER AESTHETIC DETAILS, REFER TO AESTHETIC PLANS

NO.	DATE	REVISION	APPROV.
1	6/18/12	REVISED CONDUIT, REMOVED PHASE JT., ADDED WATER PIPE & GIRDER NUMBERS ADDED	JFG
0	11/30/11	IFC SUBMITTAL SEGMENT 3 854	JFG

LBJ express

trinity infrastructure, LLC
Improving mobility in Texas

JANSSEN & SPAANS ENGINEERING CONSULTING ENGINEERS
FIRM REGISTRATION NUMBER: F-1518

Texas Department of Transportation
©2011

LBJ CROSS STREET
BRIDGE NO. 54 PRESTON ROAD
NORTHBOUND BRIDGE LAYOUT

SCALE: N.T.S. SHEET 2 OF 2

DESIGN	FED.RD. DIV.NO.	FEDERAL AID PROJECT NO.		HIGHWAY NO.
JRL				
GRAPHICS	6	XX-XXXX-XXX		IH 635
DNA				
CHECK	STATE	DISTRICT	COUNTY	SHEET NO.
MAH	TEXAS	DALLAS	DALLAS	S3-8540008
CHECK	CONTROL	SECTION	JOB	
JFG	2374	01	068, ETC	

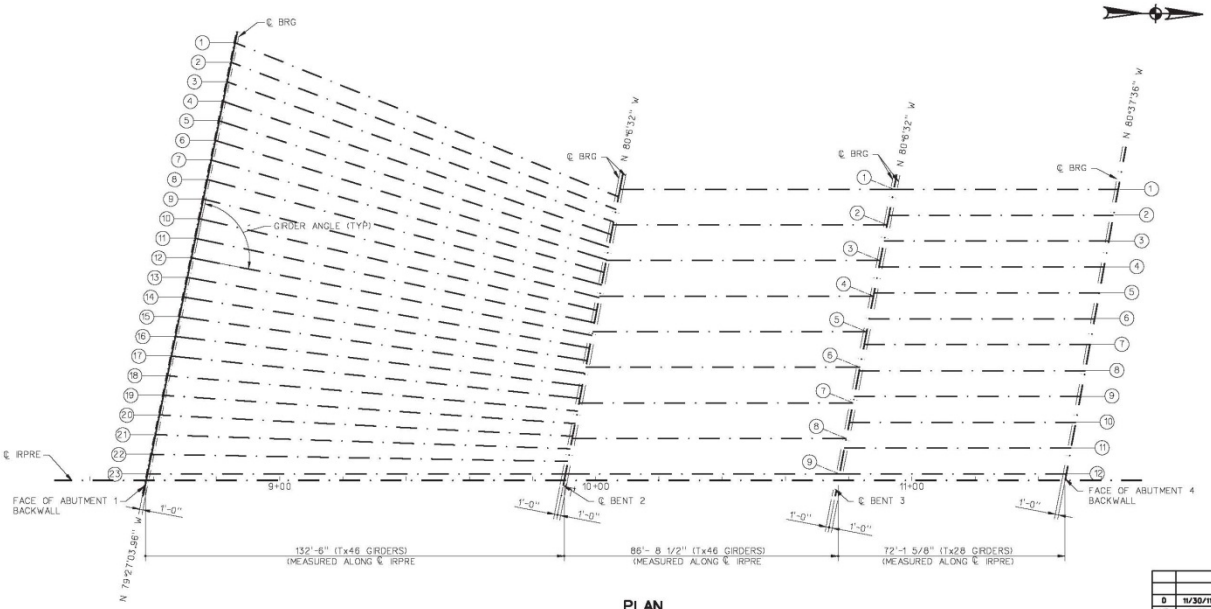

PLAN
N.T.S.

NO.	DATE	REVISION	APPROV.
0	11/30/11	IFC SUBMITTAL SEGMENT 3 B54	JFG

LBJ express

trinity infrastructure, LLC
Improving mobility in Texas

JANSSEN & SPAANS ENGINEERING
CONSULTING ENGINEERS
FIRM REGISTRATION NUMBER: F-1518

Texas Department of Transportation
©2011

STATE OF TEXAS
JAVIER F. GAUTHIER
106475
LICENSED
PROFESSIONAL ENGINEER
11/30/11

LBJ CROSS STREET
BRIDGE NO. 54 PRESTON ROAD
SOUTHBOUND GIRDER LAYOUT

SCALE: AS NOTED — SHEET 1 OF 2

DESIGN	FED.RD. DIV.NO.	FEDERAL AID PROJECT NO.		HIGHWAY NO.
JRL				
GRAPHICS	6	XX-XXXX-XXX		IH 635
DNA				
CHECK	STATE	DISTRICT	COUNTY	SHEET NO.
MAH	TEXAS	DALLAS	DALLAS	S3-B540031
CHECK	CONTROL	SECTION	JOB	
JFG	2374	01	068, ETC	

BENT REPORT

ABUTMENT NO. 1 (N 79°27'4" W)
DISTANCE BETWEEN ℄ IRPRE AND GIRDER 1 = 141.443' LT ⚠1

		GIRDER SPAC. (C.L. ABUT.)	GIRDER ANGLE D	M	S
SPAN 1	GIRDER 1	0.000	100	29	36
	GIRDER 2	6.325'	99	30	16
	GIRDER 3	6.325'	98	30	37
	GIRDER 4	6.325'	97	30	42
	GIRDER 5	6.325'	96	30	33
	GIRDER 6	6.325'	95	30	13
	GIRDER 7	6.325'	94	29	43
	GIRDER 8	6.325'	93	29	5
	GIRDER 9	6.325'	92	28	22
	GIRDER 10	6.325'	91	27	36
	GIRDER 11	6.325'	90	26	50
	GIRDER 12	6.325'	89	26	5
	GIRDER 13	6.325'	88	25	25
	GIRDER 14	6.325'	87	24	50
	GIRDER 15	6.325'	86	24	24
	GIRDER 16	6.325'	85	24	8
	GIRDER 17	6.325'	84	24	5
	GIRDER 18	6.325'	83	24	17
	GIRDER 19	6.325'	82	24	46
	GIRDER 20	6.325'	81	25	34
	GIRDER 21	5.325'	80	26	42
	GIRDER 22	6.325'	79	28	14
	GIRDER 23	6.325'	78	30	10
	TOTAL	139.147'			

BENT NO. 2 (N 80°6'32" W)
DISTANCE BETWEEN ℄ IRPRE AND GIRDER 1 = 91.478' LT ⚠1

		GIRDER SPAC. (C.L. BENT)	GIRDER ANGLE D	M	S
SPAN 1	GIRDER 1	0.000	78	50	56
	GIRDER 2	4.054'	79	50	16
	GIRDER 3	4.054'	80	49	55
	GIRDER 4	4.054'	81	49	50
	GIRDER 5	4.054'	82	49	59
	GIRDER 6	4.054'	83	50	19
	GIRDER 7	4.054'	84	50	49
	GIRDER 8	4.054'	85	51	27
	GIRDER 9	4.054'	86	52	10
	GIRDER 10	4.054'	87	52	56
	GIRDER 11	4.054'	88	53	42
	GIRDER 12	4.054'	89	54	27
	GIRDER 13	4.054'	90	55	8
	GIRDER 14	4.054'	91	55	42
	GIRDER 15	4.054'	92	56	9
	GIRDER 16	4.054'	93	56	24
	GIRDER 17	4.054'	94	56	27
	GIRDER 18	4.054'	95	56	15
	GIRDER 19	4.054'	96	55	46
	GIRDER 20	4.054'	97	54	59
	GIRDER 21	4.054'	98	53	50
	GIRDER 22	4.054'	99	52	18
	GIRDER 23	4.054'	100	50	22
	TOTAL	89.188'			

BENT NO. 2 (N 80°6'32" W)
DISTANCE BETWEEN ℄ IRPRE AND GIRDER 1 = 93.882' LT ⚠1

		GIRDER SPAC. (C.L. BENT)	GIRDER ANGLE D	M	S
SPAN 2	GIRDER 1	0.000	79	9	37
	GIRDER 2	11.449'	79	9	37
	GIRDER 3	11.449'	79	9	37
	GIRDER 4	11.449'	79	9	37
	GIRDER 5	11.449'	79	9	37
	GIRDER 6	11.449'	79	9	38
	GIRDER 7	11.449'	79	9	38
	GIRDER 8	11.449'	79	9	38
	GIRDER 9	11.449'	79	9	38
	TOTAL	91.592'			

BENT NO. 3 (N 80°6'32" W)
DISTANCE BETWEEN ℄ IRPRE AND GIRDER 1 = 93.882' LT ⚠1

		GIRDER SPAC. (C.L. BENT)	GIRDER ANGLE D	M	S
SPAN 2	GIRDER 1	0.000	100	50	23
	GIRDER 2	11.449'	100	50	23
	GIRDER 3	11.449'	100	50	23
	GIRDER 4	11.449'	100	50	23
	GIRDER 5	11.449'	100	50	22
	GIRDER 6	11.449'	100	50	22
	GIRDER 7	11.449'	100	50	22
	GIRDER 8	11.449'	100	50	22
	GIRDER 9	11.449'	100	50	22
	TOTAL	91.592'			

BENT NO. 3 (N 80°6'32" W)
DISTANCE BETWEEN ℄ IRPRE AND GIRDER 1 = 93.887' LT ⚠1

		GIRDER SPAC. (C.L. BENT)	GIRDER ANGLE D	M	S
SPAN 3	GIRDER 1	0.000	79	9	37
	GIRDER 2	8.327'	79	9	37
	GIRDER 3	8.327'	79	9	38
	GIRDER 4	8.327'	79	9	38
	GIRDER 5	8.327'	79	9	38
	GIRDER 6	8.327'	79	9	38
	GIRDER 7	8.327'	79	9	38
	GIRDER 8	8.327'	79	9	38
	GIRDER 9	8.327'	79	9	38
	GIRDER 10	8.327'	79	9	38
	GIRDER 11	8.327'	79	9	38
	GIRDER 12	8.327'	79	9	38
	TOTAL	91.592'			

ABUTMENT NO. 4 (N 80°37'38" W)
DISTANCE BETWEEN ℄ IRPRE AND GIRDER 1 = 93.730' LT ⚠1

		GIRDER SPAC. (C.L. ABUT.)	GIRDER ANGLE D	M	S
SPAN 3	GIRDER 1	0.000	100	19	19
	GIRDER 2	8.313'	100	19	19
	GIRDER 3	8.313'	100	19	18
	GIRDER 4	8.313'	100	19	18
	GIRDER 5	8.313'	100	19	18
	GIRDER 6	8.313'	100	19	18
	GIRDER 7	8.313'	100	19	18
	GIRDER 8	8.313'	100	19	18
	GIRDER 9	8.313'	100	19	18
	GIRDER 10	8.313'	100	19	18
	GIRDER 11	8.313'	100	19	18
	GIRDER 12	8.313'	100	19	18
	TOTAL	91.438'			

GIRDER REPORT

BENT REPORT SPAN 1

GIRDER No.	HORIZONTAL C-C BENT* ⚠1	DISTANCE C-C BRG ⚠1	TRUE GIRDER LENGTH BOTTOM FLANGE ⚠1
GIRDER 1	130.982'	128.945'	130.473'
GIRDER 2	130.631'	128.601'	130.124'
GIRDER 3	130.319'	128.295'	129.813'
GIRDER 4	130.047'	128.028'	129.542'
GIRDER 5	129.814'	127.800'	129.311'
GIRDER 6	129.622'	127.611'	129.119'
GIRDER 7	129.469'	127.462'	128.967'
GIRDER 8	129.356'	127.352'	128.855'
GIRDER 9	128.284'	127.281'	128.784'
GIRDER 10	129.252'	127.251'	128.752'
GIRDER 11	129.261'	127.260'	128.761'
GIRDER 12	129.310'	127.309'	128.810'
GIRDER 13	129.399'	127.398'	128.899'
GIRDER 14	129.528'	127.526'	129.028'
GIRDER 15	129.698'	127.694'	129.197'
GIRDER 16	129.908'	127.902'	129.406'
GIRDER 17	130.157'	128.148'	129.655'
GIRDER 18	130.446'	128.434'	129.943'
GIRDER 19	130.774'	128.758'	130.270'
GIRDER 20	131.141'	129.120'	130.636'
GIRDER 21	131.547'	129.521'	131.041'
GIRDER 22	131.991'	129.959'	131.483'
GIRDER 23	132.474'	130.435'	131.964'

BENT REPORT SPAN 2

GIRDER No.	HORIZONTAL C-C BENT ⚠1	DISTANCE C-C BRG ⚠1	TRUE GIRDER LENGTH BOTTOM FLANGE ⚠1
GIRDER 1	86.704'	84.667'	86.195'
GIRDER 2	86.704'	84.667'	86.195'
GIRDER 3	86.704'	84.667'	86.195'
GIRDER 4	86.704'	84.667'	86.195'
GIRDER 5	86.704'	84.667'	86.195'
GIRDER 6	86.704'	84.667'	86.195'
GIRDER 7	86.704'	84.667'	86.195'
GIRDER 8	86.704'	84.667'	86.195'
GIRDER 9	86.704'	84.667'	86.195'

BENT REPORT SPAN 3

GIRDER No.	HORIZONTAL C-C BENT* ⚠1	DISTANCE C-C BRG ⚠1	TRUE GIRDER LENGTH BOTTOM FLANGE ⚠1
GIRDER 1	71.287'	69.253'	70.778'
GIRDER 2	71.364'	69.330'	70.855'
GIRDER 3	71.440'	69.406'	70.931'
GIRDER 4	71.516'	69.483'	71.008'
GIRDER 5	71.593'	69.559'	71.084'
GIRDER 6	71.669'	69.636'	71.161'
GIRDER 7	71.746'	69.712'	71.237'
GIRDER 8	71.822'	69.789'	71.314'
GIRDER 9	71.899'	69.865'	71.390'
GIRDER 10	71.975'	69.942'	71.467'
GIRDER 11	72.052'	70.018'	71.543'
GIRDER 12	72.128'	70.095'	71.620'

* MEASURED FROM FRONT FACE OF BACKWALL TO ℄ OF BENT.

NOTES:
BRIDGE DESIGNED FOR HL93 LOADING IN ACCORDANCE WITH AASHTO LRFD BRIDGE SPECIFICATIONS, 5TH EDITION AND INTERIM THERETO.

THE DIRECTION OF OFFSETS FOR END OF GIRDER AND ℄ OF BEARING IS MEASURED PERPENDICULAR TO THE ℄ OF SUPPORT

NO.	DATE	REVISION	APPROV.
1	6/18/12	REVISED AS NOTED	JFG
0	11/30/11	FC SUBMITTAL SEGMENT 3 B54	JFG

LBJ express
trinity infrastructure, LLC
Improving mobility in Texas
JANSSEN & SPAANS ENGINEERING CONSULTING ENGINEERS
FIRM REGISTRATION NUMBER: F-1319
Texas Department of Transportation ©2011

STATE OF TEXAS — JAMES F. GAUTHIER — 106475 — LICENSED PROFESSIONAL ENGINEER
06/18/12

LBJ CROSS STREET BRIDGE NO. 54 PRESTON ROAD SOUTHBOUND GIRDER LAYOUT

SCALE: AS NOTED — SHEET 2 OF 2

DESIGN	FED.RD. DIV.NO.	FEDERAL AID PROJECT NO.		HIGHWAY NO.
JRL				
GRAPHICS	6	XX-XXXX-XXX		IH 635
DNA				
CHECK	STATE	DISTRICT	COUNTY	SHEET NO.
MAH	TEXAS	DALLAS	DALLAS	S3-B540032
CHECK	CONTROL	SECTION	JOB	
JFG	2374	01	068, ETC	

STATE | STATES | BORDERS | SHEET

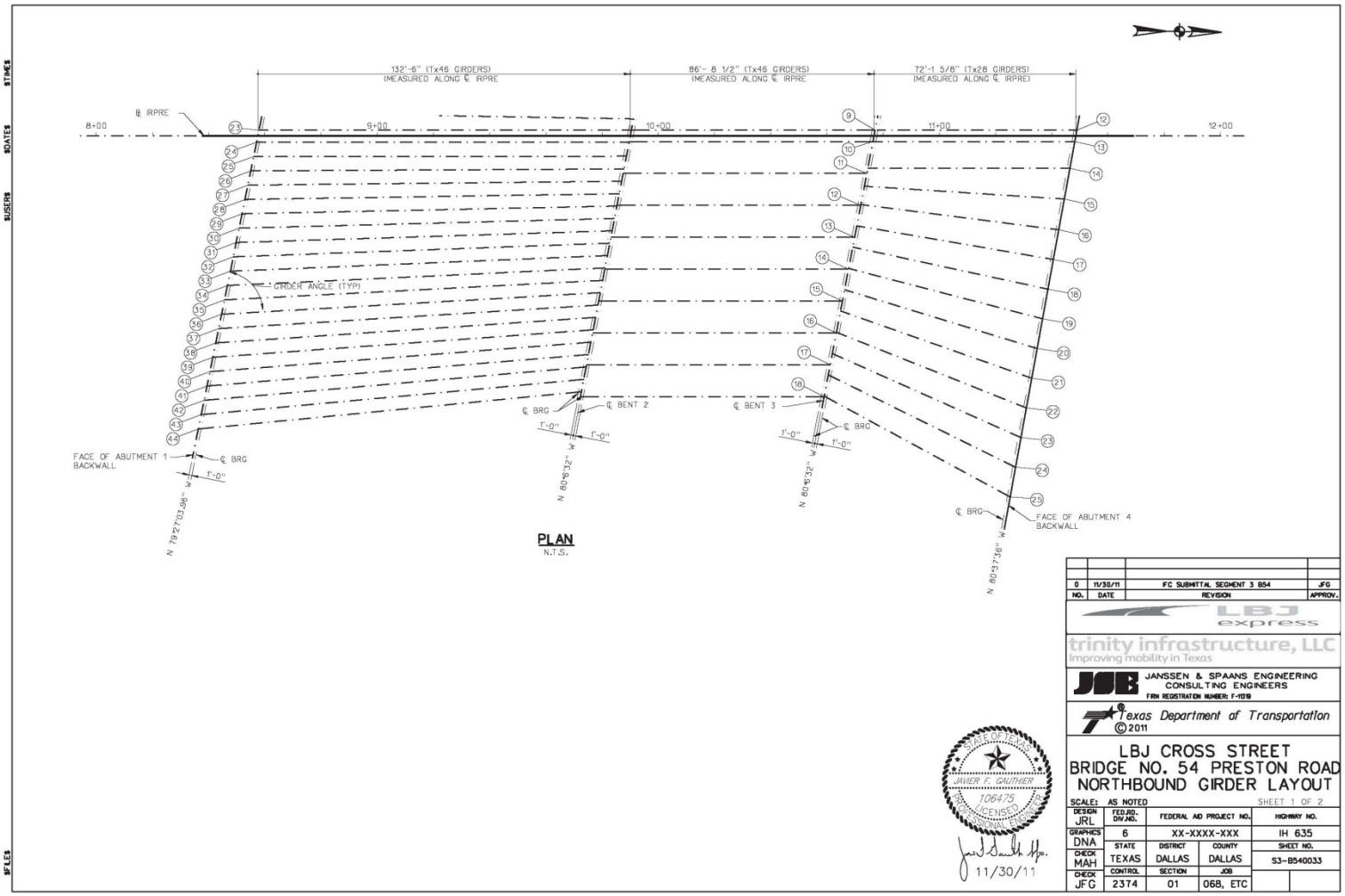

NO.	DATE	REVISION	APPROV.
0	11/30/11	FC SUBMITTAL SEGMENT 3 B54	JFG

LBJ express

trinity infrastructure, LLC
Improving mobility in Texas

JANSSEN & SPAANS ENGINEERING
CONSULTING ENGINEERS
FIRM REGISTRATION NUMBER: F-1019

Texas Department of Transportation
©2011

STATE OF TEXAS
JAMES F. GAUTHIER
106475
LICENSED
PROFESSIONAL ENGINEER
11/30/11

LBJ CROSS STREET
BRIDGE NO. 54 PRESTON ROAD
NORTHBOUND GIRDER LAYOUT

SCALE: AS NOTED — SHEET 1 OF 2

DESIGN	FED.RD. DIV.NO.	FEDERAL AID PROJECT NO.		HIGHWAY NO.
JRL	6	XX-XXXX-XXX		IH 635
GRAPHICS DNA	STATE	DISTRICT	COUNTY	SHEET NO.
CHECK MAH	TEXAS	DALLAS	DALLAS	S3-B540033
CHECK JFG	CONTROL 2374	SECTION 01	JOB 068, ETC	

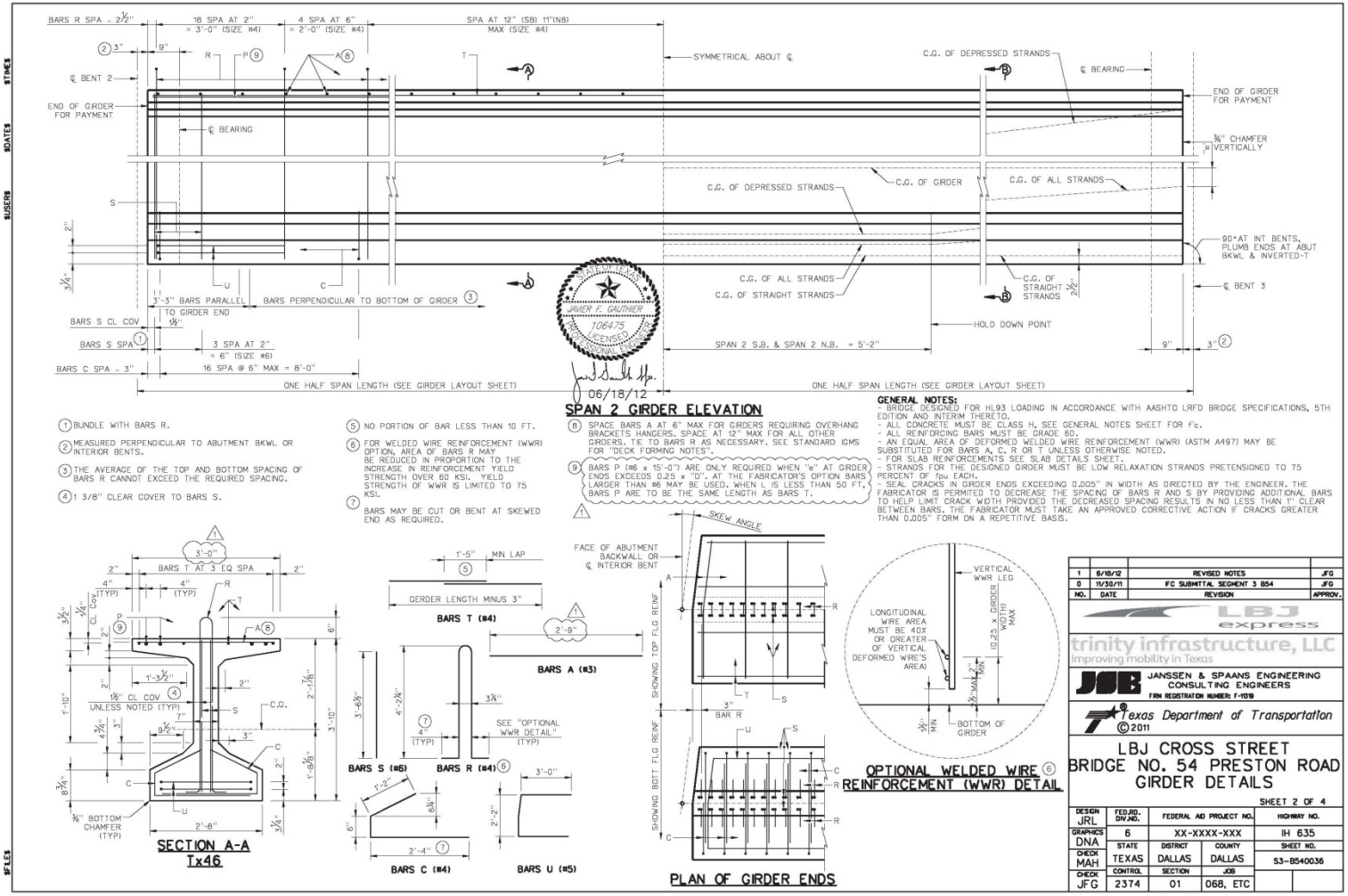

SPAN 2 GIRDER ELEVATION

(1) BUNDLE WITH BARS R.

(2) MEASURED PERPENDICULAR TO ABUTMENT BKWL OR INTERIOR BENTS.

(3) THE AVERAGE OF THE TOP AND BOTTOM SPACING OF BARS R CANNOT EXCEED THE REQUIRED SPACING.

(4) 1 3/8" CLEAR COVER TO BARS S.

(5) NO PORTION OF BAR LESS THAN 10 FT.

(6) FOR WELDED WIRE REINFORCEMENT (WWR) OPTION, AREA OF BARS R MAY BE REDUCED IN PROPORTION TO THE INCREASE IN REINFORCEMENT YIELD STRENGTH OVER 60 KSI. YIELD STRENGTH OF WWR IS LIMITED TO 75 KSI.

(7) BARS MAY BE CUT OR BENT AT SKEWED END AS REQUIRED.

(8) SPACE BARS A AT 6" MAX FOR GIRDERS REQUIRING OVERHANG BRACKETS HANGERS. SPACE AT 12" MAX FOR ALL OTHER GIRDERS. TIE TO BARS R AS NECESSARY. SEE STANDARD IGMS FOR "DECK FORMING NOTES".

(9) BARS P (#6 x 15'-0") ARE ONLY REQUIRED WHEN "e" AT GIRDER ENDS EXCEEDS 0.25 x "D". AT THE FABRICATOR'S OPTION BARS LARGER THAN #6 MAY BE USED. WHEN L IS LESS THAN 50 FT, BARS P ARE TO BE THE SAME LENGTH AS BARS T.

GENERAL NOTES:

- BRIDGE DESIGNED FOR HL93 LOADING IN ACCORDANCE WITH AASHTO LRFD BRIDGE SPECIFICATIONS, 5TH EDITION AND INTERIM THERETO.
- ALL CONCRETE MUST BE CLASS H, SEE GENERAL NOTES SHEET FOR f'c.
- ALL REINFORCING BARS MUST BE GRADE 60.
- AN EQUAL AREA OF DEFORMED WELDED WIRE REINFORCEMENT (WWR) (ASTM A497) MAY BE SUBSTITUTED FOR BARS A, C, R OR T UNLESS OTHERWISE NOTED.
- FOR SLAB REINFORCEMENTS SEE SLAB DETAILS SHEET.
- STRANDS FOR THE DESIGNED GIRDER MUST BE LOW RELAXATION STRANDS PRETENSIONED TO 75 PERCENT OF f_{pu} EACH.
- SEAL CRACKS IN GIRDER ENDS EXCEEDING 0.005" IN WIDTH AS DIRECTED BY THE ENGINEER. THE FABRICATOR IS PERMITTED TO DECREASE THE SPACING OF BARS R AND S BY PROVIDING ADDITIONAL BARS TO HELP LIMIT CRACK WIDTH PROVIDED THE DECREASED SPACING RESULTS IN NO LESS THAN 1" CLEAR BETWEEN BARS. THE FABRICATOR MUST TAKE AN APPROVED CORRECTIVE ACTION IF CRACKS GREATER THAN 0.005" FORM ON A REPETITIVE BASIS.

SECTION A-A
Tx46

PLAN OF GIRDER ENDS

OPTIONAL WELDED WIRE (6) REINFORCEMENT (WWR) DETAIL

NO.	DATE	REVISION	APPROV.
1	6/18/12	REVISED NOTES	JFG
0	11/30/11	FC SUBMITTAL SEGMENT 3 B54	JFG

LBJ express

trinity infrastructure, LLC
Improving mobility in Texas

JANSSEN & SPAANS ENGINEERING CONSULTING ENGINEERS
FIRM REGISTRATION NUMBER: F-1019

Texas Department of Transportation ©2011

LBJ CROSS STREET BRIDGE NO. 54 PRESTON ROAD GIRDER DETAILS

SHEET 2 OF 4

DESIGN	FED.RD. DIV.NO.	FEDERAL AID PROJECT NO.		HIGHWAY NO.
JRL				
GRAPHICS	6	XX-XXXX-XXX		IH 635
DNA				
CHECK	STATE	DISTRICT	COUNTY	SHEET NO.
MAH	TEXAS	DALLAS	DALLAS	S3-B540036
CHECK	CONTROL	SECTION	JOB	
JFG	2374	01	068, ETC	

DESIGNED GIRDERS (DEPRESSED STRANDS)

STRUCTURE	SPAN LENGTH	GIRDER NO.	GIRDER TYPE	NON-STD STRAND PATTERN	PRESTRESSING STRANDS TOTAL NO.	TOTAL SIZE (in)	TOTAL STRGTH fpu (ksi)	TOTAL "e" @ ℄ (in)	TOTAL "e" END (in)	DEPRESSED NO.	DEPRESSED TO (in)	CONCRETE RELEASE STRGTH f'ci (ksi)	CONCRETE MINIMUM 28 DAY COMP STRGTH f'c (ksi)
SPAN 1	132'-6"	1	Tx46	1	48	0.6	270K	15.1	9.43	8	42.5	6.425	8.031
		2 TO 22	Tx46	1	48	0.6	270K	15.1	9.43	8	42.5	6.425	8.031
		23	Tx46	1	48	0.6	270K	15.1	9.43	8	42.5	6.452	9.025
		24	Tx46	5	48	0.6	270K	15.1	9.43	8	42.5	7.102	8.877
		25 TO 43	Tx46	5	48	0.6	270K	15.1	9.43	8	42.5	7.102	8.877
		44	Tx46	5	48	0.6	270K	15.1	9.43	8	42.5	7.102	8.877
SPAN 2	86'-8½"	1	Tx46	2	42	0.5	270K	15.6	12.17	4	42.5	5.023	6.279
		2 TO 8	Tx46	2	42	0.5	270K	15.6	12.17	4	42.5	5.023	6.815
		9	Tx46	2	42	0.5	270K	15.6	12.17	4	42.5	5.023	6.279
		10	Tx46	2	42	0.5	270K	15.6	12.17	4	42.5	5.023	6.279
		11 TO 17	Tx46	2	42	0.5	270K	15.6	12.17	4	42.5	5.023	6.834
		18	Tx46	2	42	0.5	270K	15.6	12.17	4	42.5	5.023	6.279
SPAN 3	72'-1⅞"	1	Tx28	3	38	0.6	270K	8.69	5.85	6	24.5	7.722	9.652
		2 TO 11	Tx28	4	42	0.5	270K	8.38	6.86	4	24.5	6.585	8.231
		12	Tx28	4	42	0.5	270K	8.38	6.86	4	24.5	6.585	8.231
		13	Tx28	6	34	0.6	270K	8.95	6.83	4	24.5	6.755	8.444
		14 TO 24	Tx28	6	34	0.6	270K	8.95	6.83	4	24.5	6.755	8.444
		25	Tx28	6	34	0.6	270K	8.95	6.83	4	24.5	6.755	8.444

OPTIONAL DESIGN

DESIGN LOAD COMP STRESS (TOP @ SERVICE I) fct(ksi)	DESIGN LOAD TENSILE STRESS (BOTT @ SERVICE III) fcb(ksi)	REQUIRED MINIMUM ULTIMATE MOMENT CAPACITY (STRENGTH I) (ft-k/ga)	LIVE LOAD DISTRIB FACTOR MOMENT	LIVE LOAD DISTRIB FACTOR (SHEAR)
5.867	5.478	8265.5	0.519	0.519
5.836	5.459	8152.5	0.492	0.646
5.925	5.591	8719.4	0.600	0.600
6.055	5.659	8799.3	0.600	0.600
5.824	5.341	7857.3	0.454	0.598
5.988	5.519	8270.3	0.509	0.509
3.234	3.656	6539.8	0.944	0.944
3.384	3.792	6608.4	0.918	1.063
3.104	3.447	6146.6	0.886	0.886
3.104	3.447	6146.6	0.886	0.886
3.384	3.792	6608.4	0.918	1.063
3.234	3.656	6539.8	0.944	0.944
4.845	5.911	4543.9	0.887	0.887
3.682	4.634	3615.3	0.691	0.848
3.682	4.634	3615.6	0.767	0.767
3.772	4.925	4060.7	0.825	0.825
4.078	5.023	4088.3	0.760	0.937
3.814	4.823	3823.5	0.731	0.731

NON-STANDARD STRAND PATTERNS

PATTERN	STRAND ARRANGEMENT AT ℄ OF GIRDER
1	SPAN 1 SOUTHBOUND
2	SPAN 2 SOUTHBOUND & NORTHBOUND
3	SPAN 3 GIRDER 1 SOUTHBOUND
4	SPAN 3 SOUTHBOUND
5	SPAN 1 NORTHBOUND
6	SPAN 3 NORTHBOUND

GIRDER SECTION PROPERTIES

Girder Type	Area (in.²)	"Ix" (in.⁴)	"Iy" (in.⁴)	Weight (plf)
Tx28	585	55,772	40,559	610
Tx46	761	198,089	46,478	793

GENERAL NOTES:

DESIGNED FOR HL93 LOADING IN ACCORDANCE WITH AASHTO LRFD BRIDGE SPECIFICATIONS, 5TH EDITION.

ALL CONCRETE SHALL BE CLASS H. ALL REINFORCING BARS SHALL BE GRADE 60.

WHEN SHOWN ON THIS SHEET, THE FABRICATOR HAS THE OPTION OF FURNISHING EITHER THE DESIGNED DEPRESSED STRAND GIRDER OR AN APPROVED OPTIONAL DESIGN. ALL OPTIONAL DESIGN SUBMITTALS SHALL BE SIGNED, SEALED AND DATED BY A REGISTERED PROFESSIONAL ENGINEER.

PRESTRESS LOSSES FOR THE DESIGNED GIRDERS HAVE BEEN CALCULATED FOR A RELATIVE HUMIDITY OF 70 PERCENT. OPTIONAL DESIGNS SHALL LIKEWISE CONFORM.

SEAL CRACKS IN GIRDER ENDS EXCEEDING 0.005" IN WIDTH AS DIRECTED BY THE ENGINEER. THE FABRICATOR IS PERMITTED TO DECREASE THE SPACING OF BARS R AND S BY PROVIDING ADDITIONAL BARS TO HELP LIMIT CRACK WIDTH PROVIDED THE DECREASED SPACING RESULTS IN NO LESS THAN 1" CLEAR BETWEEN BARS. THE FABRICATOR MUST TAKE AN APPROVED CORRECTIVE ACTION IF CRACKS GREATER THAN 0.005" FORM ON A REPETITIVE BASIS.

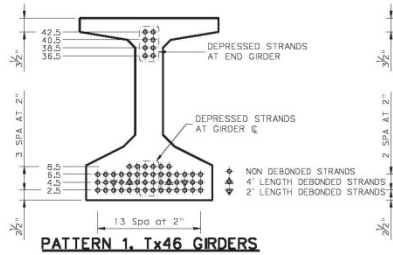

PATTERN 1, Tx46 GIRDERS

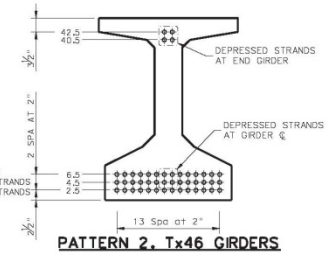

PATTERN 2, Tx46 GIRDERS

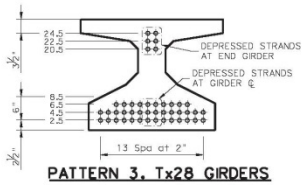

PATTERN 3, Tx28 GIRDERS

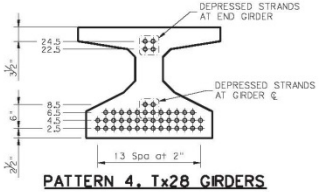

PATTERN 4, Tx28 GIRDERS

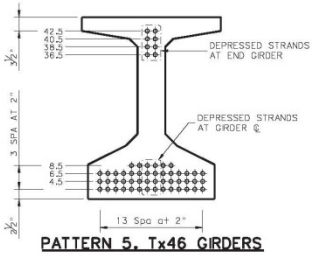

PATTERN 5, Tx46 GIRDERS

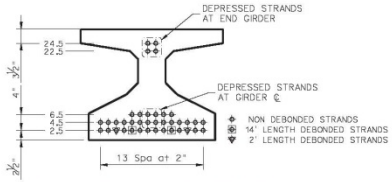

PATTERN 6, Tx28 GIRDERS

NO.	DATE	REVISION	APPROV.
0	10/28/11	IFC SUBMITTAL SEGMENT 3 854	JFG

LBJ express

trinity infrastructure, LLC
Improving mobility in Texas

JANSSEN & SPAANS ENGINEERING
CONSULTING ENGINEERS
FIRM REGISTRATION NUMBER: F-11518

Texas Department of Transportation
©2011

LBJ CROSS STREET
BRIDGE NO. 54 PRESTON ROAD
GIRDER DETAILS

SHEET 4 OF 4

DESIGN	FED.RD. DIV.NO.	FEDERAL AID PROJECT NO.		HIGHWAY NO.
JRL	6	XX-XXXX-XXX		IH 635
GRAPHICS: DNA	STATE	DISTRICT	COUNTY	SHEET NO.
CHECK: MAH	TEXAS	DALLAS	DALLAS	S3-8540038
CHECK: JFG	CONTROL	SECTION	JOB	
	2374	01	068, ETC	

$FILE$ $USER$ $DATE$ $TIME$

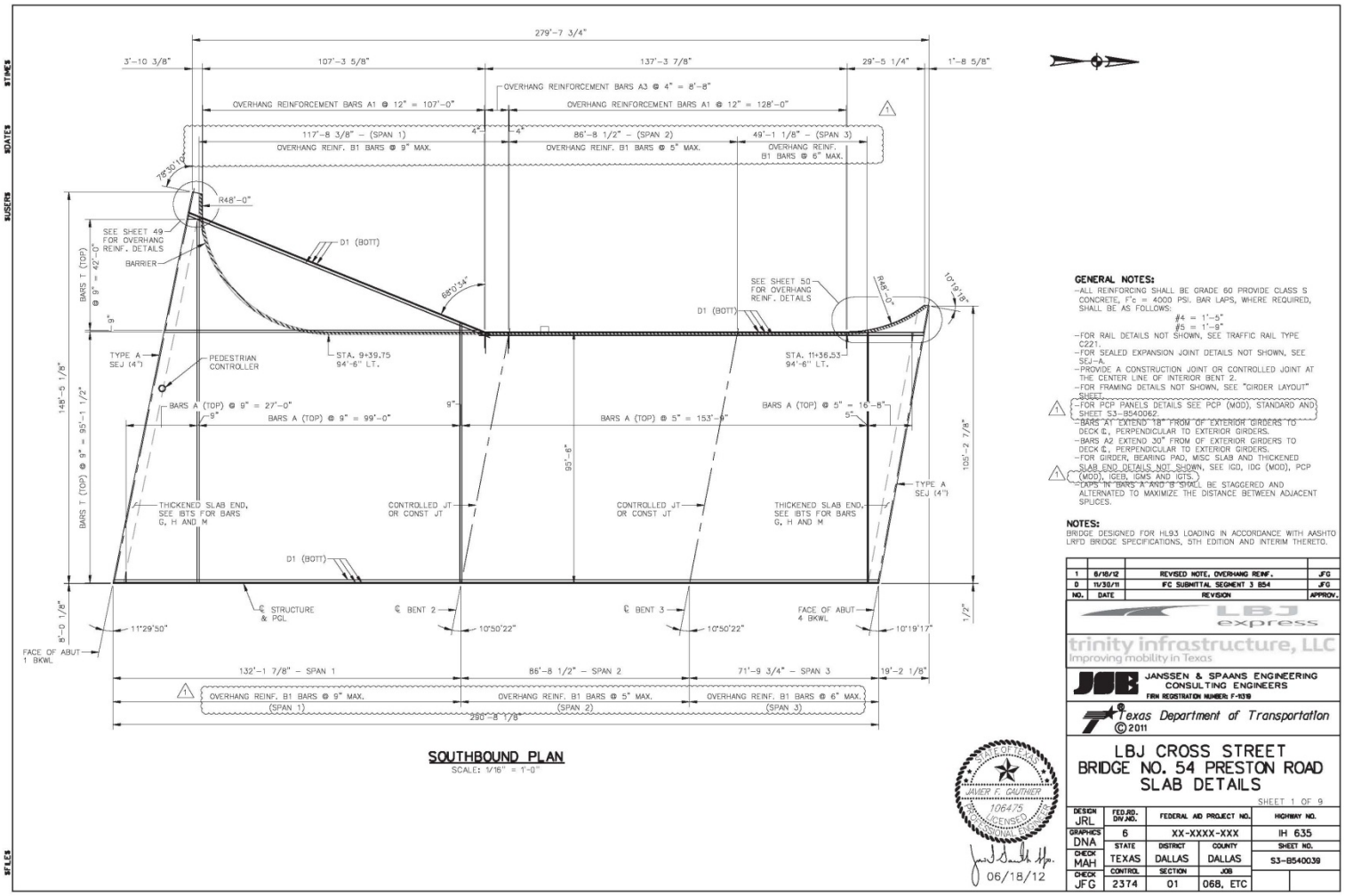

SOUTHBOUND PLAN
SCALE: 1/16" = 1'-0"

GENERAL NOTES:

- ALL REINFORCING SHALL BE GRADE 60 PROVIDE CLASS S CONCRETE, F'c = 4000 PSI. BAR LAPS, WHERE REQUIRED, SHALL BE AS FOLLOWS:
  #4 = 1'-5"
  #5 = 1'-9"
- FOR RAIL DETAILS NOT SHOWN, SEE TRAFFIC RAIL TYPE C221.
- FOR SEALED EXPANSION JOINT DETAILS NOT SHOWN, SEE SEJ-A.
- PROVIDE A CONSTRUCTION JOINT OR CONTROLLED JOINT AT THE CENTER LINE OF INTERIOR BENT 2.
- FOR FRAMING DETAILS NOT SHOWN, SEE "GIRDER LAYOUT" SHEET.
- 1 FOR PCP PANELS DETAILS SEE PCP (MOD), STANDARD AND SHEET S3-8540062.
- BARS A1 EXTEND 18" FROM OF EXTERIOR GIRDERS TO DECK ℄, PERPENDICULAR TO EXTERIOR GIRDERS.
- BARS A2 EXTEND 30" FROM OF EXTERIOR GIRDERS TO DECK ℄, PERPENDICULAR TO EXTERIOR GIRDERS.
- FOR GIRDER, BEARING PAD, MISC SLAB AND THICKENED SLAB END DETAILS NOT SHOWN, SEE IGD, IDG (MOD), PCP (MOD), IGEB, IGMS AND IGTS.
- 1 LAPS IN BARS A AND B SHALL BE STAGGERED AND ALTERNATED TO MAXIMIZE THE DISTANCE BETWEEN ADJACENT SPLICES.

NOTES:
BRIDGE DESIGNED FOR HL93 LOADING IN ACCORDANCE WITH AASHTO LRFD BRIDGE SPECIFICATIONS, 5TH EDITION AND INTERIM THERETO.

NO.	DATE	REVISION	APPROV.
1	6/18/12	REVISED NOTE, OVERHANG REINF.	JFG
0	11/30/11	FC SUBMITTAL SEGMENT 3 B54	JFG

LBJ express
trinity infrastructure, LLC
Improving mobility in Texas
JANSSEN & SPAANS ENGINEERING CONSULTING ENGINEERS
FIRM REGISTRATION NUMBER: F-1319
Texas Department of Transportation ©2011

LBJ CROSS STREET BRIDGE NO. 54 PRESTON ROAD SLAB DETAILS

SHEET 1 OF 9

DESIGN	FED.RD. DIV.NO.	FEDERAL AID PROJECT NO.		HIGHWAY NO.
JRL				
GRAPHICS	6	XX-XXXX-XXX		IH 635
DNA				
CHECK	STATE	DISTRICT	COUNTY	SHEET NO.
MAH	TEXAS	DALLAS	DALLAS	S3-8540039
CHECK	CONTROL	SECTION	JOB	
JFG	2374	01	068, ETC	

STATE OF TEXAS
JAMES F. CAUTHEN
106475
LICENSED
PROFESSIONAL ENGINEER
06/18/12

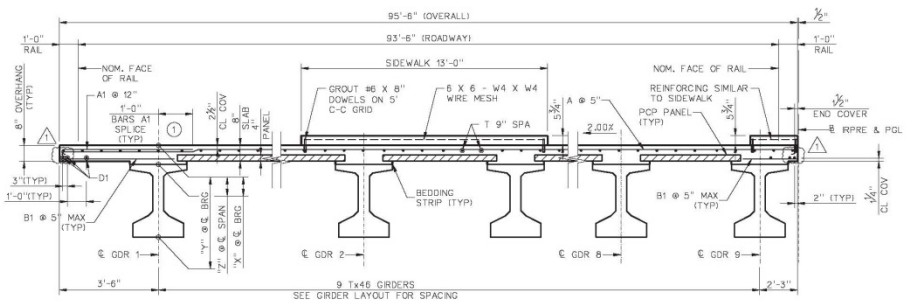

SPAN 2 SOUTHBOUND SLAB SECTION

SCALE: 1"= 5'

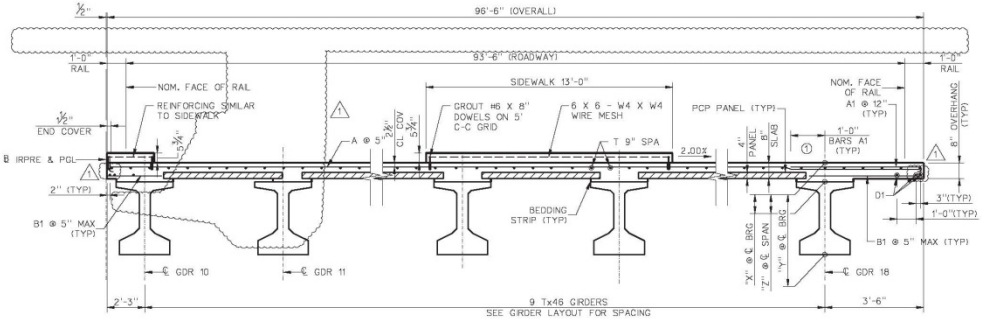

SPAN 2 NORTHBOUND SLAB SECTION

SCALE: 1"= 5'

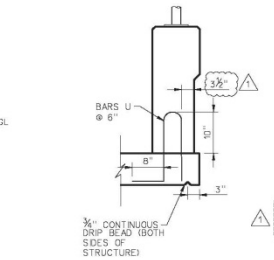

END SLAB DETAIL

N.T.S.

BAR TABLE	
BAR	SIZE
A	#5
A1	#4
A3	#6
B	#5
B1	#5
D	#5
D1	#5
H	#5
J	#5
K	#5
M	#5
T	#6
U	#4

GENERAL NOTES:

-ALL REINFORCING SHALL BE GRADE 60
PROVIDE CLASS S CONCRETE, F'c = 4000 PSI.
BAR LAPS, WHERE REQUIRED, SHALL BE AS FOLLOWS:
#4 = 1'-5"
#5 = 2'-2"
-FOR RAIL DETAILS NOT SHOWN, SEE TRAFFIC RAIL TYPE SSTR..
-FOR SEALED EXPANSION JOINT DETAILS NOT SHOWN, SEE SEJ-A.
-PROVIDE A CONSTRUCTION JOINT OR CONTROLLED JOINT AT THE CENTER LINE OF INTERIOR BENTS 2 AND 3.
-FOR FRAMING DETAILS NOT SHOWN, SEE "GIRDER LAYOUT" SHEET.
1 -FOR PCP PANELS DETAILS SEE PCP (MOD), STANDARD AND SHEET S3-8540062.
2 BARS A1 EXTEND 4'-0" FROM ℄ OF EXTERIOR GIRDERS TO DECK E
-FOR, BEARING PAD, MISC SLAB AND THICKENED SLAB END DETAILS NOT SHOWN, SEE, PCP (MOD), IGEB, IGMS, AND IGTS.
1 -BARS "A" BARS "A" AND "B" SHALL BE STAGGERED AND ALTERNATED TO MAXIMIZE THE DISTANCE BETWEEN ADJACENT SPLICES.
-FOR GIRDER DETAILS NOT SHOWN SEE GIRDER DETAILS SHEETS.
-E1 & E2 BARS, FIELD DRILLED HOLES IN CONCRETE SHALL EXTEND A DEPTH REQUIRED TO EMBED BAR 4" WITH AN APPROVED ANCHOR SYSTEM HAVING A MINIMUM PULLOUT EQUAL TO 12000 LBS FOR #4 BAR.

NO.	DATE	REVISION	APPROV.
1	6/18/12	REVISED NOTE, OVERHANG REINF. &	JFG
		REMOVE PHASED CONSTR. JT.	
0	11/30/11	IFC SUBMITTAL SEGMENT 3 B54	JFG

LBJ express

trinity infrastructure, LLC
Improving mobility in Texas

JANSSEN & SPAANS ENGINEERING CONSULTING ENGINEERS
FIRM REGISTRATION NUMBER: F-1518

Texas Department of Transportation ©2011

TABLE OF OVERHANG				
SPAN No.	LEFT		RIGHT	
	MIN	MAX	MIN	MAX
2	3.500'	3.500'	3.500"	3.500"

TABLE OF SECTION DEPTHS				
SPAN No.	"Z" @ MIDSPAN	"X" @ C/L BRG	"Y" @ C/L BRG
2 SOUTHBOUND	9⅜"	9"	4'-7"
2 NORTHBOUND	9⅜"	9"	4'-7"

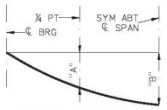

DEAD LOAD DEFLECTION DIAGRAM

SPAN NO.	"A" in	"B" in
2 SOUTHBOUND	0.885	1.277
2 NORTHBOUND	0.885	1.277

CALCULATED DEFLECTIONS SHOWN ARE DUE TO THE CONCRETE SLAB ON INTERIOR GIRDERS ONLY (E = 5589 KSI). ADJUST VALUES AS REQUIRED FOR EXTERIOR GIRDERS AND IF OPTIONAL SLAB FORMING IS USED. THESE VALUES MAY REQUIRE FIELD VERIFICATION.

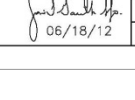

LBJ CROSS STREET BRIDGE NO. 54 PRESTON ROAD SLAB DETAILS

SHEET 5 OF 9

DESIGN	FED.RD. DIV.NO.	FEDERAL AID PROJECT NO.		HIGHWAY NO.
JRL				
GRAPHICS	6	XX-XXXX-XXX		IH 635
DNA				
CHECK	STATE	DISTRICT	COUNTY	SHEET NO.
MAH	TEXAS	DALLAS	DALLAS	S3-8540044
CHECK	CONTROL	SECTION	JOB	
JFG	2374	01	068, ETC	

132

Appendix B

Field Testing

PHASE 1 MONITORING. TRUCK POSITION 1

TIME (seconds)	Strain ($\mu\varepsilon$)					
	SG 01	SG 02	SG 03	SG 04	SG 05	SG 06
0	54.73	32.61	23.8	19.54	66.12	54.75
10	54.25	31.65	22.85	20.02	65.65	54.27
20	55.21	31.17	23.8	20.02	65.65	54.27
30	55.69	30.69	23.33	19.54	65.65	54.27
40	56.17	32.13	22.85	20.5	65.65	54.75
50	56.17	32.61	22.85	20.5	65.65	54.75
60	55.69	32.61	22.37	18.59	64.7	56.19
70	56.17	32.13	22.37	19.07	65.65	55.23
80	58.09	31.17	22.37	20.5	66.12	55.23
90	56.17	31.17	23.33	18.59	65.65	55.71
100	57.13	30.69	21.9	20.5	65.65	54.75
110	54.25	31.17	23.8	19.54	66.12	54.75
120	56.17	31.17	22.85	19.07	66.6	54.75
130	55.69	30.69	23.33	19.54	66.6	54.27
140	56.17	30.21	22.85	20.02	65.17	56.19
150	56.17	31.17	23.33	20.5	66.12	55.23
160	56.17	30.69	22.37	20.02	65.65	55.71
170	55.69	31.65	23.8	19.54	66.12	53.79
180	55.21	30.69	22.85	19.54	66.12	54.27
190	56.17	29.73	23.8	20.02	66.6	55.23
200	55.69	30.69	22.37	19.54	66.6	55.71
210	56.17	31.17	21.9	20.5	66.12	55.23
220	54.73	31.17	23.8	20.5	65.65	54.75
230	56.17	32.13	20.94	20.5	66.12	56.19
240	56.17	32.61	22.37	20.02	65.65	55.71
250	56.17	31.17	22.37	19.07	66.6	55.71
260	56.65	31.17	23.33	19.54	65.65	55.71
270	56.65	31.17	21.9	20.5	66.6	55.23
280	56.17	30.69	22.85	20.5	65.65	55.23
290	56.17	29.73	22.85	19.54	65.17	56.19
300	55.21	30.69	22.85	20.5	66.12	55.71
310	57.61	29.73	22.85	19.54	66.12	56.19
320	55.69	30.69	22.85	19.54	65.65	55.71
330	54.73	31.65	22.85	20.5	66.12	55.71
340	56.17	30.69	21.9	20.02	66.12	55.71
350	56.17	32.13	21.9	19.54	66.6	56.19
360	55.21	31.65	21.42	20.5	66.6	56.19
370	55.69	30.21	22.85	19.54	67.07	54.75
380	56.17	31.65	22.85	19.54	67.07	55.71
390	57.13	31.65	23.8	20.02	66.12	54.75
400	55.21	31.65	22.85	19.07	66.6	54.27
410	56.65	31.65	22.37	19.54	66.12	55.71
420	56.17	31.17	22.85	24.79	66.6	54.75
430	57.61	31.65	22.85	24.31	65.65	56.19

440	55.69	32.61	20.94	22.88	66.6	55.71
450	55.69	32.13	21.9	22.41	65.65	56.19
460	55.21	32.13	22.37	22.88	66.6	55.71
470	57.61	30.69	21.9	22.88	65.65	55.71
480	56.17	29.25	23.8	22.88	66.12	55.71
490	55.21	32.13	20.94	22.88	65.65	56.19
500	56.17	31.65	20.47	21.93	65.65	56.67
510	54.73	32.61	21.9	21.45	65.65	55.23
520	56.65	30.69	22.85	21.45	67.07	55.23
530	55.21	31.17	22.85	22.41	68.5	57.63
540	55.21	31.17	23.8	22.41	67.55	57.63
550	54.25	31.65	21.9	22.41	67.07	58.11
560	54.73	31.65	23.8	22.88	67.55	57.63
570	55.69	30.69	22.85	23.36	67.55	59.55
580	54.73	31.65	22.37	21.45	67.55	59.07
590	53.29	31.65	23.33	21.45	67.07	58.11
600	55.21	32.61	21.9	22.41	67.55	58.11
610	52.81	32.61	22.37	22.41	68.5	58.59
620	54.25	31.65	22.85	22.41	68.5	58.11
630	53.77	32.61	22.37	22.88	67.55	58.11
640	53.77	32.61	22.85	22.41	67.55	57.63
650	54.73	31.17	21.9	21.93	66.6	58.11

Average Strain (με)					
SG 01	SG 02	SG 03	SG 04	SG 05	SG 06
55.67	31.38	22.65	20.83	66.35	55.91

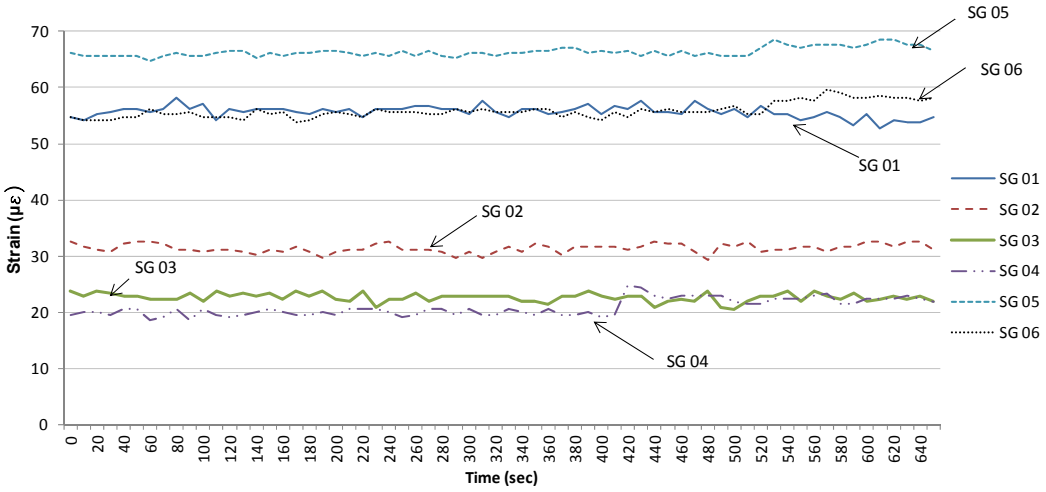

PHASE 1 MONITORING. TRUCK POSITION 2

TIME (seconds)	Strain ($\mu\varepsilon$)					
	SG 01	SG 02	SG 03	SG 04	SG 05	SG 06
783	14.88	9.11	2.86	4.29	11.89	11.04
793	12	9.11	3.81	2.38	12.37	11.04
803	12.96	10.55	2.86	2.38	12.37	10.08
813	12.96	10.07	3.33	3.81	12.37	11.53
823	14.88	9.59	3.81	3.81	12.37	10.56
833	14.4	8.63	3.81	2.38	12.37	11.53
843	12	8.63	4.28	2.38	12.84	10.56
853	13.44	10.55	3.81	2.38	11.89	12.49
863	12.96	10.07	2.86	4.29	11.89	11.53
873	14.4	8.15	3.81	2.38	12.84	10.56
883	12	9.11	3.81	4.29	12.37	10.08
893	13.92	10.07	2.38	3.81	12.37	10.56
903	12.96	10.55	3.33	2.38	12.37	10.56
913	14.88	8.15	2.86	3.81	11.42	11.04
923	12.96	8.15	4.28	2.38	11.89	9.6
933	12.96	10.07	2.86	2.38	11.42	10.56
943	14.88	8.63	3.33	4.29	11.89	12.49
953	13.92	10.07	2.86	3.81	11.89	13.93
963	12.96	9.11	4.76	2.38	12.84	12.97
973	12.96	9.59	3.81	2.38	11.42	11.53

Average Strain ($\mu\varepsilon$)					
SG 01	SG 02	SG 03	SG 04	SG 05	SG 06
13.46	9.40	3.48	3.12	12.15	11.21

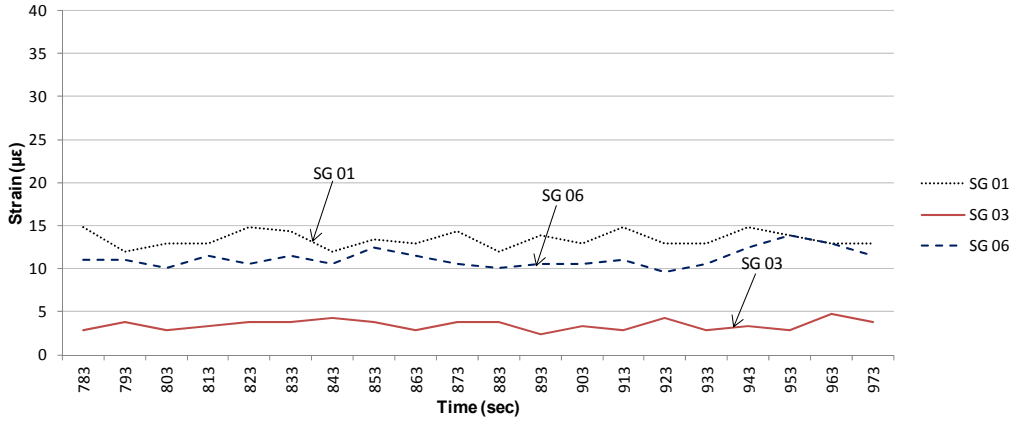

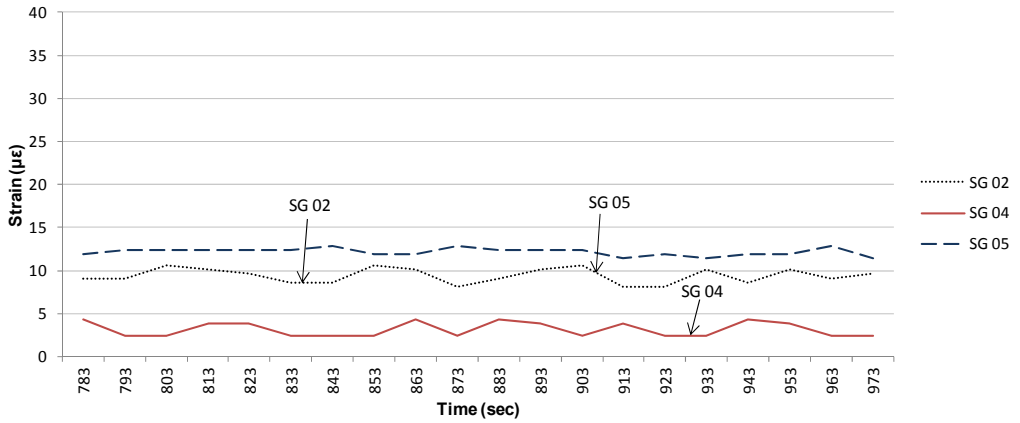

PHASE 2 MONITORING. TRUCK POSITION 3

TIME (seconds)	Strain (με)						
	SG 01	SG 02	SG 03	SG 04	SG 05	SG 06	SG 07
0	28.32	19.954	12.37	6.2	32.67	19.69	28.98
10	29.76	19.954	14.28	7.63	29.513	18.25	27.54
20	30.24	18.381	13.32	6.67	31.614	17.29	28.98
30	31.68	18.381	13.32	6.2	30.041	15.37	28.98
40	28.32	18.381	13.32	6.2	30.569	17.29	30.43
50	30.24	21.538	11.9	6.67	30.041	18.25	29.95
60	29.76	18.381	13.32	6.2	30.569	16.81	28.98
70	26.4	19.954	13.32	7.63	30.569	16.81	28.98
80	29.28	19.437	12.37	7.15	30.569	18.73	29.95
90	27.36	18.909	13.32	6.67	32.142	17.77	29.47
100	26.4	19.437	12.85	6.67	29.513	16.81	28.98
110	28.8	18.909	14.28	5.24	30.041	18.73	29.95
120	28.32	17.853	13.8	6.2	31.086	18.73	28.98

Average Strain (με)						
SG 01	SG 02	SG 03	SG 04	SG 05	SG 06	SG 07
28.84	19.19	13.21	6.56	30.69	17.73	29.24

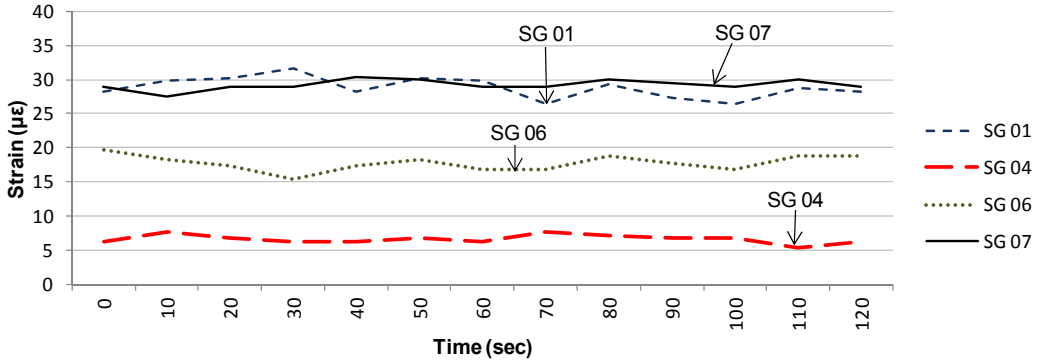
Strain (με)
Time (sec)
SG 01
SG 07
SG 06
SG 04
SG 01
SG 04
SG 06
SG 07

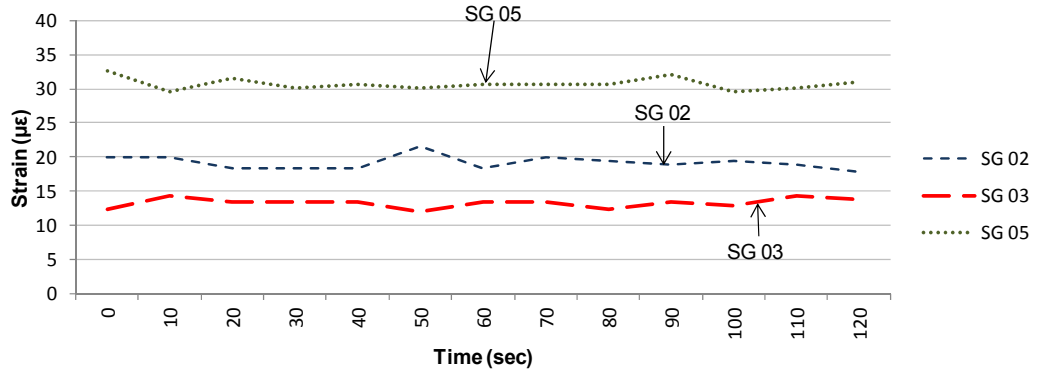
Strain (με)
Time (sec)
SG 05
SG 02
SG 03
SG 02
SG 03
SG 05

PHASE 2 MONITORING. TRUCK POSITION 4

TIME (seconds)	Strain (με)						
	SG 01	SG 02	SG 03	SG 04	SG 05	SG 06	SG 07
130	34.08	24.684	13.32	8.58	35.31	19.21	32.37
140	35.04	24.156	12.85	9.54	39.523	21.13	34.78
150	35.52	22.583	15.23	11.92	40.051	22.09	33.82
160	36	23.639	15.7	9.54	38.467	22.57	35.75
170	37.44	23.639	13.8	9.54	38.995	22.09	35.26
180	36.48	22.583	15.23	10.49	37.411	21.61	34.3
190	35.04	24.684	14.28	9.06	38.467	21.13	34.78
200	38.88	24.684	11.42	9.54	40.579	21.61	34.3
210	34.08	24.684	14.75	10.49	39.523	22.09	34.3
220	36.96	24.156	14.28	9.54	40.051	22.57	35.26
230	37.92	23.639	14.75	9.54	40.051	23.53	34.78
240	36.96	23.639	14.75	10.01	38.995	22.57	34.3
250	36	23.639	14.75	9.54	40.051	23.05	33.82
260	38.88	22.583	14.75	10.97	40.579	22.09	34.78
270	37.92	24.156	14.75	9.54	38.995	22.57	35.75
280	38.88	26.785	13.8	9.54	40.051	23.05	35.26
290	36.96	24.156	14.28	10.97	38.995	22.57	34.78
300	37.92	24.684	14.28	10.97	37.939	21.61	34.78
310	38.88	23.111	13.32	10.01	40.051	23.53	34.78
320	35.52	23.111	15.7	9.54	40.051	24.01	34.3
330	37.92	23.639	14.75	11.92	38.995	22.57	35.26
340	35.52	24.156	13.32	10.49	40.051	23.05	34.3
350	36.96	20.482	15.23	10.97	38.467	23.05	34.3
360	37.44	24.156	14.28	9.54	38.995	23.53	34.78
370	38.88	23.639	13.8	9.54	40.579	22.57	34.78
380	36.96	23.639	14.75	9.54	39.523	23.53	35.26
390	36	25.212	13.32	10.49	40.579	22.09	34.78
400	36.96	22.055	15.23	11.44	41.107	23.53	34.78
410	34.08	24.684	14.75	9.54	39.523	23.53	34.78
420	36	23.639	13.8	10.49	40.051	22.57	34.78
430	36.48	22.583	16.18	10.01	38.467	22.09	34.3
440	29.28	21.538	14.75	8.58	31.614	20.17	28.98

Average Strain (με)						
SG 01	SG 02	SG 03	SG 04	SG 05	SG 06	SG 07
36.50	23.70	14.38	10.04	39.13	22.41	34.48

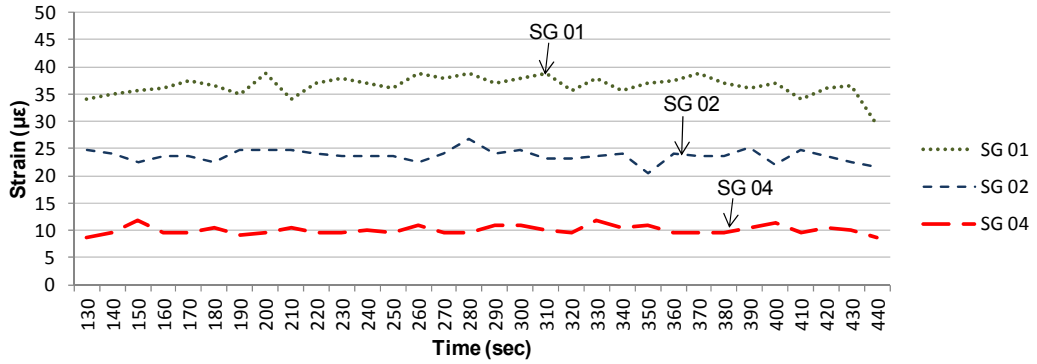

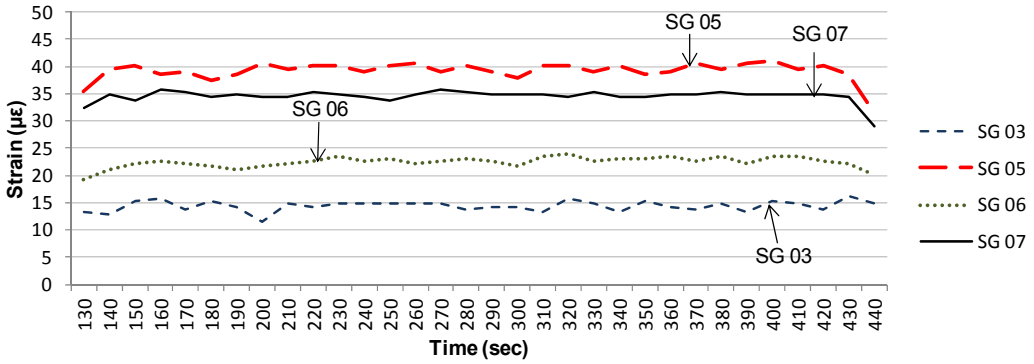

PHASE 2 MONITORING. TRUCK POSITION 5

TIME (seconds)	Strain (με)						
	SG 01	SG 02	SG 03	SG 04	SG 05	SG 06	SG 07
500	12.96	9.977	4.76	2.86	18.447	10.08	12.56
510	12	9.449	4.76	4.29	16.335	9.12	12.56
520	13.44	11.033	5.71	0.95	16.335	11.04	14.01
530	12.48	9.977	4.76	3.81	16.335	10.08	13.04
540	12.48	12.078	5.23	0.95	14.751	10.56	13.53
550	14.88	11.033	5.71	2.86	12.122	11.04	13.53
560	12.96	11.033	4.76	3.81	13.706	10.56	12.56
570	12.96	9.977	4.76	3.81	11.066	10.08	13.04
580	13.44	11.033	4.28	4.29	12.65	10.08	12.56
590	13.92	10.505	5.71	3.34	12.122	9.6	13.04
600	12.96	11.55	6.66	2.38	11.066	10.56	13.04
610	14.88	9.449	4.76	2.86	11.594	11.52	13.04
620	13.92	10.505	5.23	4.77	12.122	10.56	14.01
630	12.48	11.55	6.66	2.86	10.538	12	13.53
640	15.84	11.033	3.81	4.29	12.122	11.04	12.56
650	12.96	9.977	7.14	3.81	10.538	9.12	12.56
660	14.4	9.977	5.23	2.86	12.65	10.08	13.04
670	14.88	9.977	5.71	4.29	11.066	9.12	12.08
680	14.88	9.449	5.71	2.86	12.122	10.56	12.08
690	13.92	10.505	4.76	2.86	13.178	11.04	12.56
700	13.92	9.977	5.23	4.77	12.122	10.08	11.59
710	14.4	9.449	5.71	0.95	12.65	12	13.04

Average Strain (με)						
SG 01	SG 02	SG 03	SG 04	SG 05	SG 06	SG 07
13.68	10.43	5.32	3.21	12.98	10.45	12.89

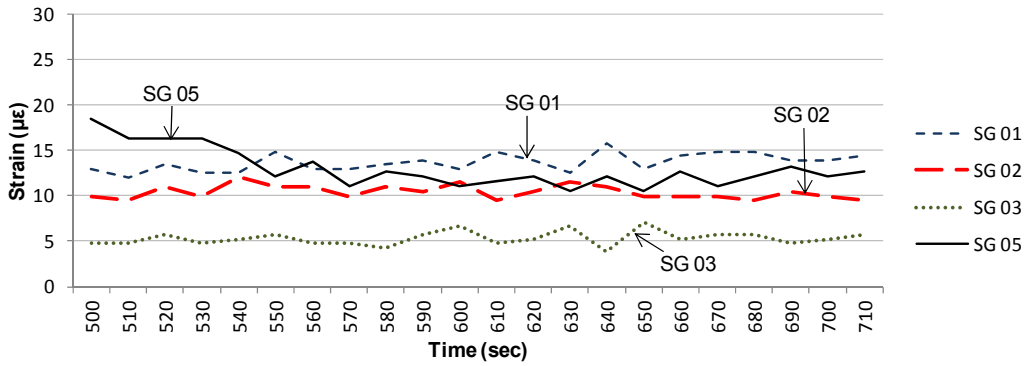
30
25
20
15
10
5
0
Strain (με)
SG 05
SG 01
SG 02
SG 03
500 510 520 530 540 550 560 570 580 590 600 610 620 630 640 650 660 670 680 690 700 710
Time (sec)
SG 01
SG 02
SG 03
SG 05

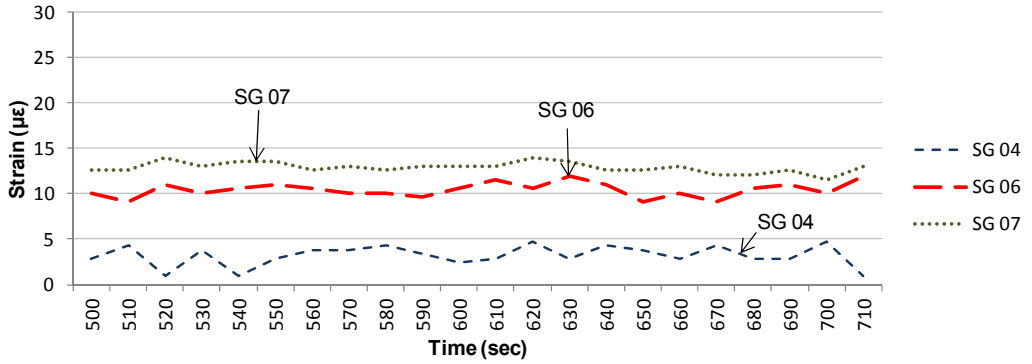
30
25
20
15
10
5
0
Strain (με)
SG 07
SG 06
SG 04
500 510 520 530 540 550 560 570 580 590 600 610 620 630 640 650 660 670 680 690 700 710
Time (sec)
SG 04
SG 06
SG 07

PHASE 2 MONITORING. TRUCK POSITION 6

TIME (seconds)	Strain (με)						
	SG 01	SG 02	SG 03	SG 04	SG 05	SG 06	SG 07
720	17.76	11.55	6.66	3.81	15.807	12.48	15.94
730	16.8	14.707	6.66	5.24	16.335	12.96	16.91
740	16.32	13.651	5.71	4.77	16.863	12.96	16.91
750	18.72	11.033	7.14	4.77	16.863	13.92	15.94
760	18.72	12.078	6.19	4.77	15.807	12.48	16.91
770	19.68	12.078	5.71	5.24	16.863	12.96	16.91
780	17.28	13.134	7.61	6.2	16.863	12.96	16.42
790	19.68	13.134	7.61	4.29	16.863	13.44	16.42
800	18.24	12.078	5.71	5.24	16.863	13.44	17.39
810	18.72	12.078	6.66	3.34	15.279	11.52	17.39
820	19.68	12.078	7.14	5.24	15.807	12.96	16.91
830	18.72	13.651	5.71	4.77	14.751	12.48	16.91
840	18.72	13.651	7.14	4.77	15.807	12.96	16.91
850	17.76	11.55	7.14	3.81	14.751	13.44	16.91
860	15.84	12.078	6.19	5.72	16.863	12.96	15.94

Average Strain (με)						
SG 01	SG 02	SG 03	SG 04	SG 05	SG 06	SG 07
18.18	12.57	6.60	4.80	16.16	12.93	16.71

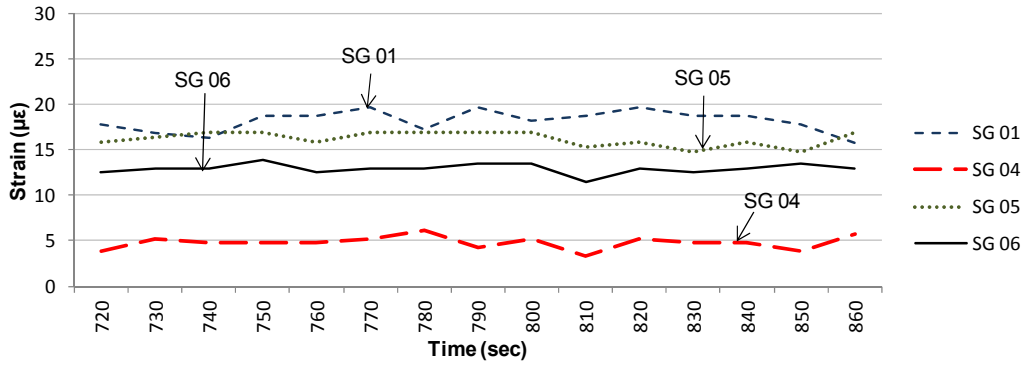

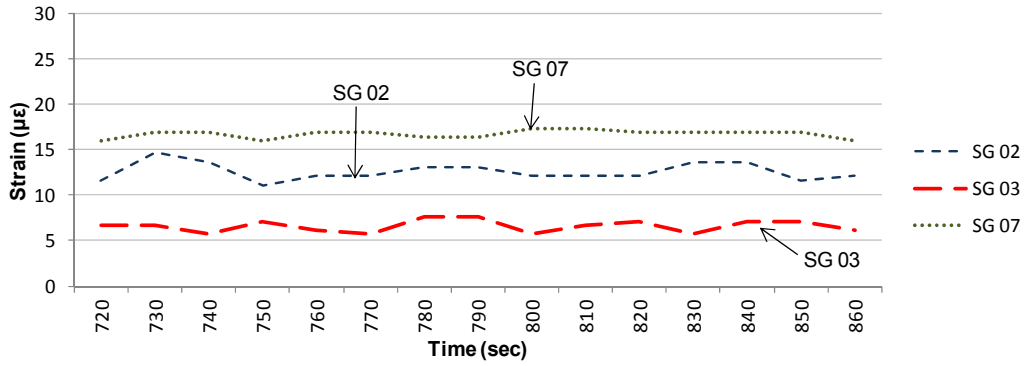
30
25
20
15
10
5
0
Strain (με)
SG 02
SG 07
SG 03
720
730
740
750
760
770
780
790
800
810
820
830
840
850
860
Time (sec)
SG 02
SG 03
SG 07

.

References

AASHTO. (2012). *AASHTO LRFD Bridge Design Specifications.* American Association of State Highway and Transportation Officials.

Abushagur, M. M. (2004). *Enhancement of Flexural Capacity of Steel Beams Using Glass Fiber Reinforced Polymer.* The University of Western Ontario.

Ali, S. M. (2000). *Optimum Design of Precast Bridge Prestressed with Carbon Fiber Reinforced Polymers.* Concordia University Montreal.

B, T. (2010). *Studies on Hydrid Fibre Reinforced Beam-Column Joinst Under Reverse Cyclic Loading.* ANNA University.

Beshah, F. B. (2002). *Performance of Concrete Beams and Slabs Reinforced with FRP Bars.* University of Maryland.

Besser, B. T. (2011). *Precast Lightweight Concrete Panels Reinforced WIth Glass Fiber reinforced Polymer Bars.* The University of Utah.

Birtel, P., & Mark, P. (2006). *Parameterised Finite Element Modelling of RC Beam Shear Failure.* ABAQUS User's Conference.

Bridge Tech, I. (2007). *NCHRP Report 592 Simplified Live Load Distribution Factor Equations.* Transportation Research Board.

Brinkman, R. J. (2012). *Carbon Fiber Reinforced Polymer Repairs of Impact-Damaged Prestressed I-Girders.* University of Cincinnati.

Brown, J. P. (2004). *Strengthening of Unreinforced Masonry Structures with Glass Fiber Reinforced Polymers to Mitigate the Effects of Blast.* The Universtity of New Mexico.

Bullock, W. O., Barnes, R. W., & Schindler, A. K. (2011). *Repair of Cracked Prestressed COncrete Girders, I-565, Huntsville, Alabama.* The Alabama Department of Transportation.

Cha, J. Y. (2001). *Analysis of Prestressed Concrete Beams Strengthened with Carbon Fiber Composites.* The State University of New Jersey.

De, S. (n.d.). *Abaqus handout.* Rensselaer Polytechnic Institute.

DSSIMULIA. (2010). *Abaqus 6.10. Abaqus/CAE User's Manual.* DSSIMULIA.

DSSIMULIA. (2010). *Abaqus 6.10. Example Problems Manual.* DSSIMULIA.

Enchayan, R. (2010). *Repair of Damaged Prestressed Concrete Girder.* Detroit: AASHTO Midwest Bridge Preservation Conference.

Grantham, M. G. (2011). *Concrete Repair. A practical guide.* Routledge. Taylor & Francis Group.

Green, P. S., & Boyd, A. J. (2005). *CFRP Repair of Impact-Damaged Bridge Girders.* The Florida Department of Transportation.

Haque, F. (2014). *Enhancing Effectiveness of AASHTO Type Prestressed Concrete Bridge Girder through Fiber Reinforced Polymer Strengthening.* The University of Texas at Arlington.

Harries, K. A., Kasan, J., & Aktas, C. J. (2009). *Repair Method for Prestressed Girder Bridges.* The Pennsylvania Department of Transportation.

Harries, K. A., Kasan, J., Miller, R., & Brinkman, R. (2012). *Updated Research for Collision Damage and Repair of Prestressed Concrete Beams.* Transportation Research Board of The National Academies.

Hasenlamp, C. J., Badie, S. S., Hanna, K. E., & Tadros, M. K. (2012). *Proposed Evaluation and Repair Procedures for Precast, Prestressed Concrete Girders with End Zone Cracking.* PCI Journal.

Huang, J. (2010). *Durability Design of GFRP Bar Reinforced Concrete Members: A new Approach.* Syracuse University.

Hutchinson, R. I. (1999). *The Use of Externally Bonded CFRP Sheets for Shear Strengthening of I-Shape Prestressed Concrete Bridge Girders.* University of Manitoba.

Johnson, D. T. (2014). *Investigation of Glass Fiber Reinforced Polymer (GFRP) Bars as Internal Reinforcement for Concrete Structures.* University of Toronto.

Jonhnson, D. T. (2014). *Investigation of Glass Fiber Reinforced Polymer (GFRP) Bars as Internal Reinforcement for Concrete Structures.* University of Toronto.

Kasan, J. L. (2009). *Structural Repair of Prestressed Concrete Bridge Girders.* University of Pittsburgh.

Kasan, J. L. (2012). *On the Repair of Impact-Damaged Prestressed Concrete bridge girders.* University of Pittsburgh.

Khoshnoud, H. R., & Marsono, A. K. (2012). *Abaqus For Reinforced Concrete Structures. Workshop Linear Analysis.* University Techologi Malaysia.

Klaiber, F. W., Wipf, T. J., & Kempers, B. J. (2003). *Repair of Damaged Prestressed Concrete Bridges Using CFRP.* Ames, Iowa: Transportation Research Symposium.

Kmiecik, P., & Kamiski, M. (2011). *Modelling of Reinforced Concrete Structures and Composite Structures with Concrete Strength Degradation Taken Into Consideration.* Wroclaw University of Technology.

Laosiriphong, K. (2000). *Development and Evaluation of Glass Fiber Reinforced Composite/Wood Railroad Crossties.* West Virginia University.

Liu, R. (2011). *Precast Concrete Bridge Deck Panels Reinfroced With Glass Fiber Reinforced Polymer Bars.* The University of Utah.

Logan, P. L. (2012). *A first Course In The Finite Element Method.* CENGAGE Learning.

Mahmood, H. (2002). *Cracking of Concrete Members Reinforced with Glass FIber Reinforced Polymer Bars.* The University of Cargary.

Mallick, P. K. (2008). *Fiber-Reinforced Composites. Materials, Manufacturing, and Design.* CRC Press. Taylor & Francis Group.

Manjunath, M. (2009). *Finite-Element Project ABAQUS Tutorial.*

Masuelli, M. A. (2013). *Fiber Reinforced Polymers. Technology Applied for Concrete Repair.* Intech.

Memon, M. S. (2002). *Seismic Behavior of Square Concrete Columns Retrofitted with Glass Fiber Reinforced Polymers (GFRPs).* University of Toronto.

Miller, A. D. (2006). *Repair of Impact-Damaged Prestressed Concrete Bridge Girders Using Carbon FIber Reinforced Polymer (CFRP) materials.* North Carolina State University.

Mohanamurthy, M. (2013). *Finite Element Modeling of Prestressed Girder Strengthening Using Fiber Reinforced Polymer and Codal Comparison.* The University of Texas at Arlington.

Naaman, A. E. (2012). *Prestressed Concrete Analysis and Design.* Techno Press 3000.

Nanni, A., Luca, A. D., & Zadeh, H. J. (2014). *Reinforced Concrete with FRP Bars. Mechanics and Design.* CRC Press. Taylor & Francis Group.

Nawy, E. G. (2010). *Prestressed Concrete A Fundamental Approach.* Prentice Hall.

Pantelides, C. P., Reaveley, L. D., & Burningham, C. A. (2010). *Repair of Prestressed Concrete Girder Ends and Girder Collision Repair.* Utah Department of Transportation.

Ragaby, A. E. (2007). *Fatigue Behavior of Concrete Bridge Deck Slabs Reinforced with Glass FRP Bars.* Universite De Sherbrooke.

Roberts, P. (n.d.). *ABAQUS Lecture Part III.*

Roberts, P. (n.d.). *ABAQUS Lecture Part II.*

Rosenboom, O. A. (2006). *Behavior of FRP Repair/Strengthening Systems for Prestressed Concrete.* North Carolina State University.

Rosenboom, O. A., Miller, A. D., & Rizkalla, S. (n.d.). *Repair of Impact-Damaged Prestressed concrete Bridge Girders Using CFRP Materials.* ACSE Journal of Bridge Engineering.

Saiedi, R. (2007). *Load-deflection response of a prestressed concrete T-beam.* Queen's Univsity, Canada.

Smith, A. W. (2004). *Rehabilitation of Timber Railroad Bridges Using Glass Fiber Reinfroced Polymer Composite Wraps.* West Virginia University.

Soleimani, S. M. (2006). *Sprayed Glass Fiber Reinforced Polymers in Shear Strengthening and Enhancement of Impact Resistance of Reinforced Concrete Beams.* The University of British Columbia.

Tadros, M. K., Badie, S. S., & Tuan, C. Y. (2010). *NCHRP REPORT 654. Evaluation and Repair Procedures for Precast/Prestressed Concrete Girders with Longitudinal Cracking in the Web.* Transportation Research Board.

Wahalathantri, Lankananda, B., Thambiratnam, D.P., Chan, T.H.T., & Fawzia, S. (2011). *A Material Model for Flexural Crack Simulation in Reinforced Concrete Elements Using ABAQUS.* Queensland University of Technology.

Wight, J. K., & Macgregor, J. G. (2012). *Reinforced Concrete Mechanics & Design.* Pearson Education, Inc.

Wikipedia. (2015, May 16). *Interstate 635 (Texas).* Retrieved from http://en.wikipedia.org/w/index.php?title=Interstate_635_(Texas)&oldid=662523556

Yan, A. (2005). *Durability of Glass Fiber/Vinyl Ester Composites as Bridge Deck Subject to Weathering Conditions.* Wayne State University.

Zureick, A. H., Ellingwood, B. R., Nowak, A. S., Mertz, D. R., & Triantafillou, T. C. (2010). *NCHRP REPORT 655. Reccommended Guide Specification for the Design of Externally BOnded FRP Systems for Repair and Strengthening of Concrete Bridge Elements.* Transportation Research Board.

Biographical Information

Maria Angeles De la Flor Montero received her Civil Engineering degree from "Universidad de Granada" in Spain in December of 2008. She joined University of Texas at Arlington as a graduate student in spring of 2013. At which she completed her Master of Science in Civil Engineering in fall of 2015.